



# On-line non-intrusive partial discharges detection in aeronautical systems

Abadie, Cédric

## ► To cite this version:

Abadie, Cédric. On-line non-intrusive partial discharges detection in aeronautical systems. Electronics. Université Toulouse 3 Paul sabatier (UT3), 2017. English. NNT : . tel-01629678

**HAL Id: tel-01629678**

**<https://hal.science/tel-01629678>**

Submitted on 6 Nov 2017

**HAL** is a multi-disciplinary open access archive for the deposit and dissemination of scientific research documents, whether they are published or not. The documents may come from teaching and research institutions in France or abroad, or from public or private research centers.

L'archive ouverte pluridisciplinaire **HAL**, est destinée au dépôt et à la diffusion de documents scientifiques de niveau recherche, publiés ou non, émanant des établissements d'enseignement et de recherche français ou étrangers, des laboratoires publics ou privés.



# THÈSE

En vue de l'obtention du

## DOCTORAT DE L'UNIVERSITÉ DE TOULOUSE

Délivré par :

Université Toulouse 3 Paul Sabatier (UT3 Paul Sabatier)

---

Présentée et soutenue par :

**Cédric ABADIE**

le 03 Avril 2017

Titre :

On-line non-intrusive partial discharges detection in  
aeronautical systems

---

École doctorale et discipline ou spécialité :

ED GEET : Génie Electrique

Unité de recherche :

Laboratoire LAPLACE, UMR 5213 - IRT Saint Exupéry

Directeur/trice(s) de Thèse :

Thierry LEBEY, Directeur de Recherche au CNRS

Thibaut BILLARD, Docteur et Ingénieur de recherche à l'IRT Saint Exupéry

Jury :

**Greg STONE**

**Ian COTTON**

**Juan Manuel MARTINEZ-TARIFA**

**Régine SUTRA-ORUS**

**Olivier LESAINT**

**Xavier ROBOAM**

PhD, Iris Power - Qualitrol, CANADA

Professor at the University of Manchester, UK

Professor at the University of Carlos III of Madrid, Spain

Head of MEA at IRT Saint Exupéry, France

Director of research at CNRS - G2Elab, France

Director of research at CNRS - LAPLACE, France

Président

Rapporteur

Rapporteur

Examineur

Examineur

Examineur



## **Remerciements:**

Ce travail a été réalisé à Toulouse au sein de l'IRT Saint Exupéry, dans le projet Fiabilité du domaine Aéronef plus électrique et dans le laboratoire LAPLACE dans l'équipe MDCE. Je tiens à remercier tous les partenaires industriels du projet intéressés par mon sujet et qui m'ont permis de venir réaliser des essais sur leurs équipements.

Tout d'abord je souhaite remercier Thierry Lebey pour m'avoir encadré ces trois années. Il a su me transmettre sa passion pour la recherche et une partie de ses connaissances et compétences. Grâce à lui j'ai appris à toujours remettre en question mes résultats pour ne pas réaliser de conclusions trop hâtives. Il m'a poussé à aller plus loin dans mon travail et a réussi à m'arrêter malgré ma tête dure lorsque je dérivais sur des pistes trop éloignées ou inutiles pour mon sujet et cela toujours dans la bonne humeur. Il a toujours trouvé un moment, malgré son emploi du temps chargé, pour m'aider sur mes travaux ou sur des sujets plus personnels. Je tiens aussi à le remercier pour avoir continué à m'aider pour l'après thèse.

Je voudrais ensuite remercier Thibaut Billard pour m'avoir encadré à l'IRT. La rigueur dans son travail m'a servi d'exemple tout le long de ma thèse. Ses conseils et ses idées m'ont toujours permis d'avancer sur les points bloquants tout le long de la thèse. Sa culture et sa bonne humeur ont permis de toujours travailler dans une ambiance cordiale et agréable même lors des installations de manip nocturnes. Grâce à lui j'ai appris la règle du ratio 80/20 concernant l'excellence au travail.

Je tiens à remercier sincèrement les membres de mon jury pour leur présence et leurs remarques le jour de ma soutenance.

Je tiens ensuite à remercier toutes les personnes de l'IRT et plus particulièrement les membres de l'équipe Aéronef plus électrique grâce à qui j'ai passé trois années dans les meilleures conditions possibles. Je tiens à remercier ceux qui étaient là au tout début, Régine, Arnaud et André ainsi que ceux qui sont arrivés petit à petit et qui composent l'équipe où il fait bon travailler, Nicolas et son franc-parler, Aurore et sa gentillesse, (gossip) Loïc l'organisateur de nombreux événements hors IRT ainsi que pour ses spécialités (rhum et samoussa), Bouazza le crooner, Gilles, Vincent, Bernardo, Hoan, Ludovic, Laurent, Jean, Gaetan, Pascal, Victor, Anne et Alexandre.

Pour tous les membres du groupe MDCE, merci à vous pour votre aide, votre gentillesse et aussi les moments de détente en pause qui ont permis de travailler dans une atmosphère conviviale tout le long de cette thèse. Merci à Sorin, Pierre, Jean-Pascal, David, Marie-Laure, Nadine, Vincent et Céline. Et aussi à tous les doctorants François, Trung, Thomas, Laurent, Hélène, Zenjebil, Cyril, Ana et Mateusz.

Je ne peux pas continuer sans parler de Guillaume et Simon. Malgré mon insertion légèrement accélérée, ces trois années auraient semblaient beaucoup plus longues sans vous. Merci pour ces trois

années, les pauses et les discussions plus ou moins profondes, pour les mots croisés, les plaisanteries ainsi que nos grandes idées souvent trouvées à notre rendez-vous hebdomadaire (au Mulligans). Je vous souhaite le meilleur pour la suite et ne vous inquiétez pas les dossiers compromettant que j'ai sur vous ne seront pas dévoilés (pour l'instant ...).

Pour tous les anciens qui étaient là avant et notamment Pierre et Céline, merci. Qui aurait pensé que l'on en serait là lorsque l'on s'est rencontré. Merci à vous pour tous les bons moments qui m'ont permis de changer d'ambiance et de décompresser le long de ces années.

Je voudrais maintenant remercier ma belle-famille et plus particulièrement (Michel, Marie-Noëlle, Gloria, Damien), merci à vous pour votre accueil dans la famille, pour votre intérêt sur mon travail ainsi que pour les repas de famille mémorables. J'espère que l'on va devoir continuer à ramener du champagne régulièrement.

Je n'en serais pas là sans ma famille. Maman, papa et toute ma famille proche, je vous remercie pour votre soutien et votre amour inconditionnel, vous avez tout fait pour que je réussisse dans la vie, vous avez toujours cru en moi et vous avez toujours fait tout ce que vous pouviez pour que nous ne manquions de rien et que l'on réalise nos rêves. Pour tout cela merci.

Enfin, je ne peux pas terminer sans remercier celle qui partage ma vie depuis toutes ces années. Merci à toi pour m'avoir soutenu toutes ces années, pour avoir tout quitté pour que je fasse cette thèse. Je ne serai pas ce que je suis aujourd'hui sans toi, sans ta confiance en moi et tes encouragements. Tu es ma raison de vivre, toi qui m'a offert le plus beau cadeau du monde.

*A toi qui arriveras bientôt...*





**Table of contents**

<b>Introduction .....</b>	<b>5</b>
<b>Chapter I. State of the art .....</b>	<b>5</b>
<b>I.1 “More electrical aircraft” .....</b>	<b>4</b>
<b>I.2 Overview of partial discharges.....</b>	<b>5</b>
I.2.1 Phenomenology and Paschen’s law.....	6
<b>I.3 Insulation systems for rotating machines.....</b>	<b>8</b>
I.3.1 Low-voltage machine insulation .....	9
I.3.2 Localization of Partial Discharges (PD) in low voltage motors.....	11
<b>I.4 PWM fundamentals.....</b>	<b>13</b>
I.4.1 General interest.....	13
I.4.2 Control strategy .....	14
<b>I.5 Partial discharges in machines fed by PWM inverters .....</b>	<b>16</b>
I.5.1 Voltage distribution under PWM .....	16
I.5.1.1 Influence of $dV/dt$ on voltage distribution .....	16
I.5.2 Overvoltages induced by PWM.....	19
I.5.2.1 The wave reflection phenomenon .....	19
I.5.2.2 Cable length influence.....	19
I.5.2.3 Conclusion .....	20
I.5.3 Partial discharge detection under PWM .....	21
I.5.3.1 Traditional detection methods.....	21
I.5.3.2 Partial discharge detection set-up.....	21
I.5.4 Investigation of sensor signals.....	25
<b>I.6 Conclusion.....</b>	<b>27</b>
<b>Chapter II. Experimental set-up .....</b>	<b>30</b>
<b>II.1 Sensor study .....</b>	<b>29</b>
II.1.1 Sensor geometry .....	29
II.1.2 Correlation research between calibrator voltage and the sensor response.....	30
II.1.2.1 Experimental set-up.....	31
II.1.2.2 Results .....	31
II.1.3 Delay induced by cable length.....	33
II.1.3.1 Experimental set-up.....	34
II.1.3.2 Results .....	34
<b>II.2 Sensor optimization.....</b>	<b>35</b>
<b>II.3 Role of the pressure : Experimental set-up.....</b>	<b>36</b>
<b>II.4 Reproducibility of the measurements.....</b>	<b>40</b>



<b>II.5</b>	<b>Influence of pressure under AC .....</b>	<b>41</b>
II.5.1	Influence of the sensor on detection .....	41
II.5.2	Influence of the cut-off frequency of the filter on detection .....	42
II.5.3	Spectral analysis .....	43
<b>II.6</b>	<b>Influence of pressure under PWM.....</b>	<b>46</b>
II.6.1	Influence of the sensor on detection .....	46
II.6.2	Influence of the cut-off frequency of the filter on detection .....	48
II.6.3	Spectral analysis .....	49
<b>II.7</b>	<b>Limits of the detection method .....</b>	<b>52</b>
<b>II.8</b>	<b>Conclusion.....</b>	<b>54</b>
<b>Chapter III.</b>	<b>Development of a digital processing method to remove noise .....</b>	<b>56</b>
<b>III.1</b>	<b>Context .....</b>	<b>55</b>
<b>III.2</b>	<b>Noise source.....</b>	<b>55</b>
III.2.1	Noise suppression techniques.....	56
<b>III.3</b>	<b>General understanding of the wavelet transform.....</b>	<b>58</b>
III.3.1	Wavelet definition.....	59
<b>III.4</b>	<b>Wavelet analysis.....</b>	<b>60</b>
<b>III.5</b>	<b>Continuous wavelet transform .....</b>	<b>61</b>
<b>III.6</b>	<b>Discrete wavelet transform .....</b>	<b>63</b>
III.6.1	First step.....	63
III.6.2	Second step.....	64
III.6.3	Third step .....	64
III.6.4	Results .....	65
III.6.5	Reconstitution .....	66
<b>III.7</b>	<b>Denoising by wavelet transform.....</b>	<b>68</b>
III.7.1	Settings parameters .....	68
<b>III.8</b>	<b>Applying the method .....</b>	<b>70</b>
III.8.1	Choosing between the CWT and DWT method.....	70
III.8.1.1	CWT test .....	72
III.8.1.2	DWT test .....	73
III.8.1.3	Final Choice .....	74
<b>III.9</b>	<b>Denoising .....</b>	<b>75</b>
<b>III.10</b>	<b>Automated choice of “mother” wavelet.....</b>	<b>78</b>
<b>III.11</b>	<b>Method validation.....</b>	<b>80</b>
<b>III.12</b>	<b>Conclusion.....</b>	<b>82</b>
<b>Chapter IV.</b>	<b>Investigations on electric motor test benches.....</b>	<b>85</b>

<b>IV.1</b>	<b>Filtering .....</b>	<b>84</b>
<b>IV.2</b>	<b>Partial discharge investigations on motor test benches.....</b>	<b>85</b>
IV.2.1	Experimental set-up .....	87
IV.2.2	Case 1: Filtering difficulties.....	89
IV.2.2.1	Comparison of the signal vs the sensor position .....	90
IV.2.2.2	Influence of the Current .....	91
IV.2.3	Case 2: Abnormal presence of surges .....	93
IV.2.3.1	The influence of rotation speed .....	93
IV.2.3.2	The influence of voltage magnitude .....	95
IV.2.3.3	Partial discharge detection.....	95
IV.2.3.4	Studying $dV/dt$ .....	96
IV.2.3.5	Signal analysis.....	99
IV.2.4	Case 3: Necessity of a deep analysis.....	102
IV.2.5	Case 4: “Simple” PD detection .....	107
IV.2.5.1	Study on the winding.....	108
IV.2.5.2	Denoising by CWT method.....	113
IV.2.6	Case 5: PD detection in machines fed by SiC inverter .....	114
IV.2.6.1	PD detection .....	114
IV.2.6.2	Temporal position of PDs.....	116
	<b>Conclusion.....</b>	<b>119</b>
	<b>Appendix .....</b>	<b>122</b>
	<b>References .....</b>	<b>127</b>



## **Introduction**



In aeronautics, the concept of the “more electrical aircraft” was able to grow thanks to the evolution of power electronics in recent years, the increase of power density, accompanied by a decrease in cost, which had considerably spread the use of power converters for Adjustable Speed Drive (ASD) applications. Until recently, one could find various energy sources used in aircraft. The different types of on-board energies were pneumatic, hydraulic, and electric energy. The concept of the “more electric aircraft” involves replacing pneumatic and/or hydraulic energy by the electric one. These two axes of evolution are respectively called “Bleedless” and “Hydraulicless” architectures. The problem of pneumatic and hydraulic systems is the difficulty in locating and correcting problems that may be present, and which can lead to stopping the aircraft on the ground and therefore inducing economic losses. The interest in removing one of these energy vectors is to increase the reliability and safety of onboard equipment while reducing weight and maintenance costs. However, due to the power demand, developing the electrical network resulted in an increase of the voltage magnitude. The use of electric motor is thus likely to increase in aircraft application.

There are two main families of motors: first, low-voltage motors with winding formed of cylindrical conductors wound randomly, and second, high-voltage motors with winding formed of rectangular conductors. These machines also have different built-in insulation systems to withstand the electrical stresses created by high voltage. These machines are also classified respectively as Type I and Type II.

Like any equipment, electric motors undergo more or less severe aging over time, influenced by various phenomena. These degradations can come from thermal, mechanical, or electrical phenomena. For electric motors, the weakest part is usually the electrical insulation system. The failure of this system generally results in complete motor failure. The use of long cables connecting the inverter to the motor may cause significant overvoltage at the motor terminals. In addition, the shape of applied voltage called “pulse width modulation” (PWM) is comprised of pulse trains. Because of these pulses, voltage is no longer distributed homogeneously along the coil. In that case, large differences in voltage between turns are present. Moreover, associated with the low pressure conditions present in depressurized areas of the aircraft, these important voltage differences may cause the appearance of partial discharge (PD). Partial discharges are electrical discharges that partially short-circuit a void inside the insulation. The discharges induce a phenomenon of erosion due to the bombardment of charged particles, chemical deterioration, and local thermal stresses on the insulation system. Partial discharges are the sign of the next insulation system failure.

Due to the criticality of PD consequences, it is necessary to detect the partial discharges ignition to assess the quality of electrical system insulation in the equipment and to qualify the system. There are many detection well known methods for AC and DC systems. However, detection is much more complex under PWM in low-voltage motors and more particularly in Type 1 motors that are used in more electric aircraft. The main problem with PWM power supply is that partial discharge signals are

embedded in the electro-magnetic noise generated by the switching due to their lowest amplitude than in Type II motor.

In order to determine the PD appearance in a motor, it is important to carry out these tests under real operating constraints (electrical, environmental, mechanical ...): on-line measurement is mandatory. However, despite the representativeness of the test, if the detection system modifies the constraints present on the system under test, the results will be biased. It is therefore necessary to use a system which does not affect the reliability and the test configuration of the system under test. A non-intrusive measurement makes it possible to satisfy these conditions.

The purpose of this thesis is to develop a detection and filtering method enabling non-intrusive on-line partial discharge detection in the aeronautical field to assess electrical insulation systems used in aircrafts.

This thesis is the result of three years of work within the “Reliability” team at the Saint Exupery Institute of Research and Technology in Toulouse, and in the “Dielectrics Material in Energy Conversion” team at the Laplace Laboratory in Toulouse. This work was also carried out in close collaboration with Airbus Group Innovations, Airbus, Liebherr, Zodiac, Safran and Actia.

This PhD dissertation is divided into four chapters. A brief description of the content of those chapters is given below.

#### **Chapter I: State of the art**

This chapter describes the “more electric aircraft” concept and the insulation systems used in low voltage motors. We provide a general description of the mechanisms of occurrence for partial discharges, along with a detailed presentation of the concept of PWM and its influence on electrical stress. Finally, an analysis of sensor output signals is proposed.

#### **Chapter II: Experimental set-up**

The purpose of this chapter is first to improve the understanding of the sensor used in order to optimize it and to observe the influence of pressure on partial discharge. The modification of the frequency spectrum relative to pressure for AC and PWM voltage is presented and discussed.

#### **Chapter III: Development of a digital processing method to remove noise**

Chapter III describes a noise reduction method based on wavelet decomposition. First, we present the state of the art concerning this method, followed by a comparison of the results of this method compared to analog filtering. We then propose an automated algorithm for choosing the input parameters for this method. Lastly, the method, its operation and the validity of the algorithm, are tested on simple samples.

#### **Chapter IV: Investigations on electric motor test benches**

The last chapter focuses on the partial discharge detection method applied to industrial test benches. Five specific cases and their associated analyses are developed to highlight the ability of the method to detect partial discharges. We also cover various issues that may occur during tests on industrial test benches.

Finally a conclusion of this work is presented and the possible future works are proposed.





## **Chapter I. State of the art**



## I.1 “More electrical aircraft”

Conventional architectures found in commercial aircraft consist of a multitude of energy types [1]:

- Pneumatic power
- Mechanical power
- Hydraulic power
- Electrical power

The disparity of these sources and their respective complexity lead to reduced efficiency of complete systems. For example, any pneumatic or hydraulic leak can cause a default for all equipment supplied by these energies. This induces a failure that forces the aircraft to remain on the ground, which incurs economic losses. In addition, this type of defect can be difficult to locate and correct.

This reasoning led to emergence of the “more electrical aircraft” concept. The main intention of this concept is to remove the pneumatic and/or hydraulic network to increase reliability and safety for onboard equipment while reducing overall weight and maintenance costs. Moreover the segregation of the defects appeared to be simpler for an electrical network

The “more electrical aircraft” concept is not new, as it was considered as early as World War II [2]. However, production capacity as well as existing power densities at that time, made this approach infeasible. It was not until the 1990s that it became more feasible to looking ahead towards new technologies to replace hydraulic systems with electrical systems. One of the major technological advances that helped to make the electric aircraft possible is the development of reliable power electronics that have high power density. New power converters based on these developments, and power switching devices based on semiconductors in particular, allow a new generation of aircrafts.

Today, new ways to generate, distribute, and use energy are studied in the field of aeronautics, especially for new aircrafts based on this concept.

The “more electrical aircraft” concept can be divided into two areas with respect to current aircrafts (Figure I.1):

- The plane referred to as “hydraulic-less” is achieved by removing hydraulic systems. The Airbus A380 is one example, different from “conventional” planes by the fact that one of three hydraulic systems was removed, and part of the flight control system is electrified (ailerons, spoilers...). This design can be found on other aircrafts such as the A350 and A400M.
- The plane referred to as “bleedless” is achieved by removing pneumatic systems. The Boeing 787 is a good example of this approach. The various pneumatic networks, such as defrost air conditioning systems, wing anti-icing, and engine starting systems, have been eliminated from this aircraft.

The all-electric aircraft is the implementation of these two axes.

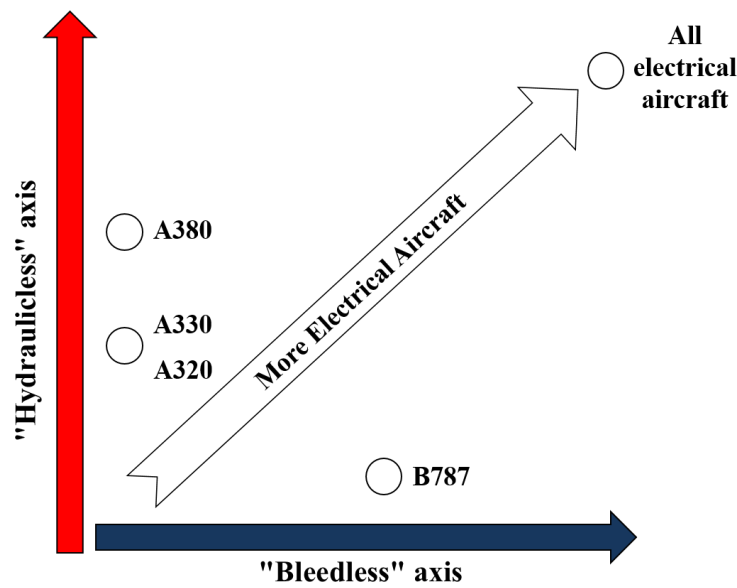


Figure I.1: More electrical aircraft axis

The electric network in a “conventional” aircraft consists of a three-phase alternating part at 115/200 V with a fixed frequency of 400 Hz, and a DC part at 28 V. Nevertheless, with the emergence of more electric aircraft, the energy requirement has increased and it was therefore necessary to raise voltage levels in order to limit cable diameter (gauge) while still meeting these energy needs. In that case, the electrical network is comprised of a three-phase AC part at 230 / 400 V with a variable frequency between 370 and 770 Hz, a DC part at  $\pm 270$  V (the 28 V and 115 V still remaining).

These new voltage levels and the use of power electronics induce phenomena that were unknown until now in aeronautics [3]. These phenomena affect machines reliability and cause premature aging of equipment insulation, or even their total failure. These phenomena are known under the name of partial discharge (PD).

## I.2 Overview of partial discharges

According to the standard definition [4], a partial discharge (PD) is an electric discharge that short-circuits a gap between two conductors. Generally, PD appears when there is a local concentration of electric stress in the insulation or on the surface of the insulation. These discharges appear in the form of current pulses with duration shorter than 1  $\mu$ s. The discharges induce a phenomenon of erosion due to the bombardment of charged particles, chemical deterioration, and a local thermal stresses of the insulation system [5].

Electrical insulation systems (EIS) are not perfect. These systems may age and defects can be found. We can first consider homogeneous insulation aging, which is due to different influencing factors:

- Environmental factors (temperature, humidity, gas types, corrosion ...)
- Electrical Factors (type of voltage, current, frequency...)
- Mechanical factors (torsion, bending, vibration...)

Premature insulation “aging” due to defects such as protrusions, contaminants (foreign particles), or vacuoles may be observed. These imperfections are defects that occur during manufacturing. Over time, and therefore during operation, these imperfections can propagate and ultimately cause the insulation to breakdown.

All these imperfections can be favorable sites for the occurrence of partial discharge. This is first explained by the fact that air has a lower dielectric strength than any other type of insulation (solid and liquid). Second, the electric field is enhanced in insulation because the relative permittivity of the insulation is always higher than the gas present in the cavities.

### I.2.1 Phenomenology and Paschen’s law

Upon a collision between a germ electron and a neutral gas molecule, if the energy transmitted by the impacting electron is sufficient, ionization of the species occurs. One will thus have a charged species (ions) and an electron extracted from that species. In turn, that electron and the first free electron will be accelerated and will ionize two other species, and so on. The attachment of electrons to gas molecules compensates the ionization until the electron energy is sufficient, and ionization becomes predominant compared to the attachment. This phenomenon is called an “electronic avalanche” [6].

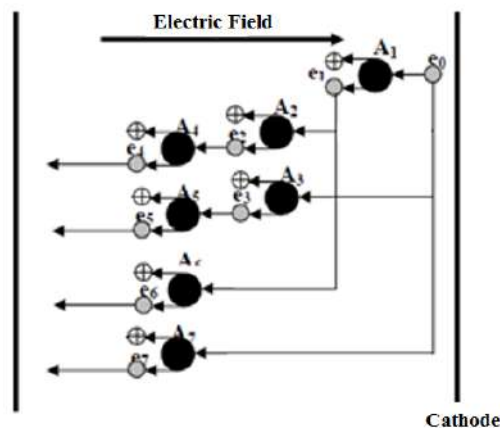


Figure I.2: Electronic avalanche phenomenon

To describe an avalanche, Townsend [7] provided a semi-empirical relationship for  $\alpha/p$ :

$$\frac{\alpha}{p} = A \times e^{\left(\frac{-B}{E/p}\right)} \quad (I.2.1)$$

With A and B, respectively in (torr<sup>-1</sup>.cm<sup>-1</sup>) and in (V.torr<sup>-1</sup>.cm<sup>-1</sup>), two constants dependant on the gas and on the reduced field E/p in (V.torr<sup>-1</sup>.cm<sup>-1</sup>), where p is the pressure in Torr and  $\alpha$  the mean number of ionizations carried out by an electron per unit of length (also called the first Townsend coefficient).

During the acceleration of ions in an electric field, the ions bombard the cathode and generate an electron emission. This emission is called secondary emission and is described by the second Townsend coefficient  $\gamma$ .

For a self-sustaining discharge, it is required for ionization and secondary emission to be sufficient to maintain the discharge. Townsend defined the criterion of self-sustaining discharges by the following relationship:

$$\gamma (e^{\alpha d} - 1) = 1 \quad (I.2.2)$$

Depending on the experimental conditions (pressure, gas, materials, geometry of the electrodes, etc.), different secondary processes may occur:

- Thermionic emission
- Field electron emission
- Work of metastable ( $\epsilon$  process) on the cathode
- Photoemission cathode ( $\delta$  process) by the action of photons created by the discharge
- Photo-ionization of the gas ( $\beta$  process) under the action of photons

Nevertheless, in the case of a Townsend discharge, the processes mentioned above are negligible against the bombardment of ions at the cathode. However, for example, the photo-ionization mechanism has an important place in the formation of a streamer type of discharge.

From the Townsend theory in gas, the Paschen law [8] describes how an electron avalanche is initiated by the electrons created by secondary emission.

This law is valid for homogeneous electric fields and metal electrodes. It predicts that the breakdown voltage of a gas is a function of the product of pressure p and interelectrode distance d.

$$V_c = \frac{Bpd}{C + \ln(pd)} \quad (I.2.3)$$

with

$$C = \ln\left(\frac{A}{\ln(1 + 1/\gamma)}\right) \quad (I.2.4)$$

Experimental results of breakdown voltages in different gases depending on the product PD are shown below.

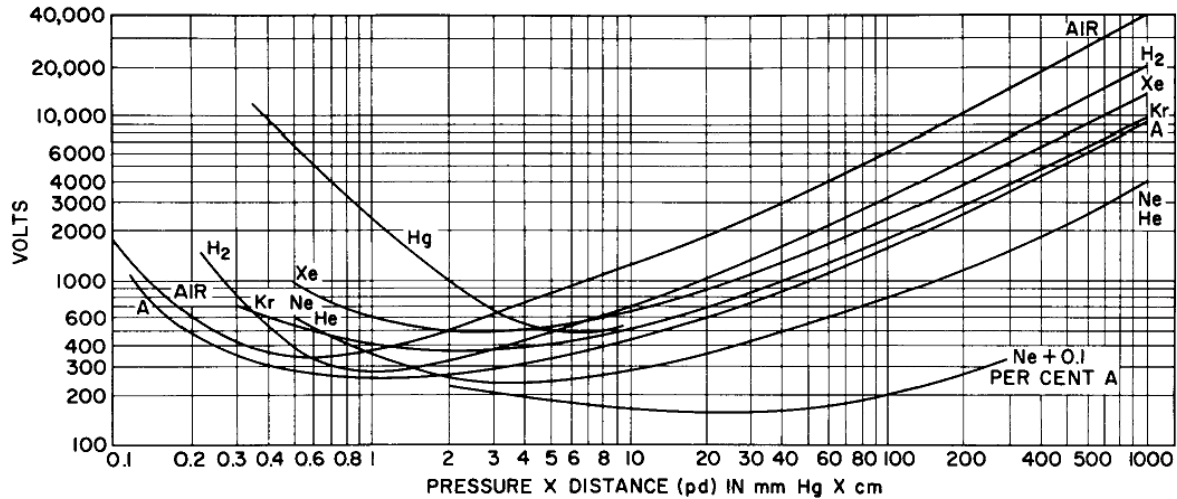


Figure I.3: Paschen's curve for various gases [9]

It can be seen that the Paschen curve has a minimum. For air, this minimum is about 320V which corresponds to the voltage levels of the more electrical aircraft (230 Vrms). This minimum corresponds to an inter-electrode distance of 8 microns at atmospheric pressure. A voltage lower than this value does not allow the electric discharge to start, whatever the conditions of pressure and distance.

One can thus observe that, in view of this minimum and new onboard aircraft voltages, there is a risk of occurrence of PDs in motors ([10], [11]). It therefore seems important to analyze the motors used in aircrafts in detail, and their insulation in particular.

### I.3 Insulation systems for rotating machines

Generally, AC rotating machines are classified in two main groups [12]:

1. Type 1: By definition, the insulation of a Type I winding “is not expected to experience partial discharge activity within specified conditions in their service lives”. Type I motors correspond to low-voltage rotating machines, which generally have a randomly arranged winding composed of cylindrical wires, and whose insulation does not contain mica.
- Type 2: By definition, the insulation of a Type II winding “is expected to withstand partial discharge activity in any part of the insulation system throughout their service lives”.



Type II motors correspond to high-voltage rotating machines, which use pre-compound coils formed of rectangular wires with mica insulation systems.

The motors used in the aeronautical context are Type 1 motors. Given the voltage encountered in “conventional” aircraft, insulation systems such as the ones use in Type 2 motors do not appear as necessary. In addition, the cost of the low voltage motors is much lower (and is therefore preferred to high-voltage motors). However, with changing voltage magnitudes associated with more electric aircraft, insulation systems are not designed to avoid the occurrence of partial discharges or to withstand the degradation phenomena associated with them.

### I.3.1 Low-voltage machine insulation

There is a large number of components that may be used in the insulation systems of low-voltage rotating machines. These various materials are shown in Figure I.4

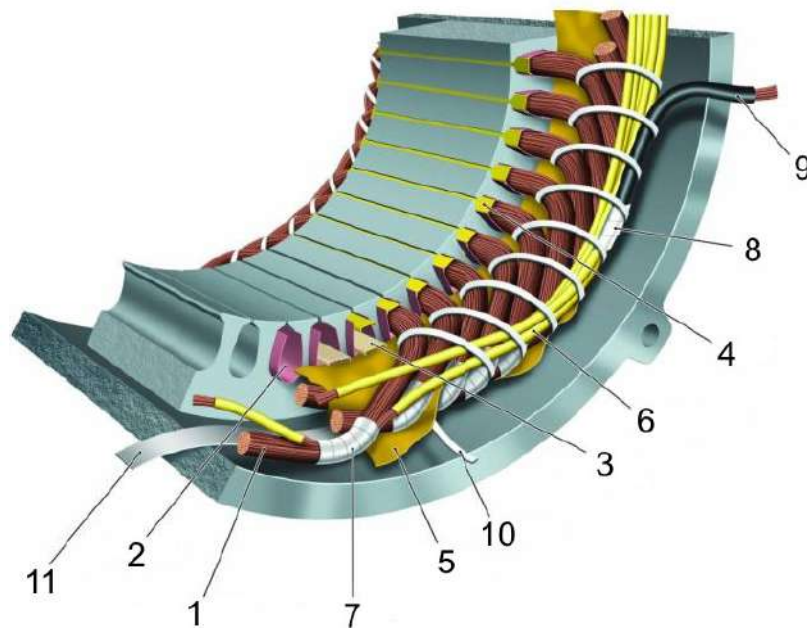


**Figure I.4: Overview of materials in a low-voltage insulation system: (1) turn insulation, (2) slot liner, (3) slot separator, (4) wedge, (5) phase separator, (6) lead sleeving, (7) coil-nose tape, (8) connection tape, (9) cable, (10) tie cord, and (11) bracing [13]**

The various insulating materials can be brought together into three major families:

1. Magnet wire insulation
2. Ground and slot insulation
3. Phase and endwinding insulation

#### 1) Magnet wire insulation

One of the most important insulation system is the wire insulation. In general, low-voltage motors are wound using round enameled wire. The magnet wire choice is a compromise between the filling ratio of the slots, mechanical and thermal properties, and the quality of electrical insulation. The thickness of the enamel does not exceed a few dozens of microns and it is not designed to overvoltages having a magnitude higher than 1 kV. As the arrangement of the turns is random, the first turn may be located near the last turn of the same coil. When the voltage variation is slow, the winding behaves as an inductive voltage divider and the voltage is distributed homogeneously along the coil. In the case of fast voltage changes like PWM pulses, the behavior is not the same and large voltage differences between these turns can be observed. This effect is detailed in Chapter I.5.1.1.

## 2) Ground and slot insulation

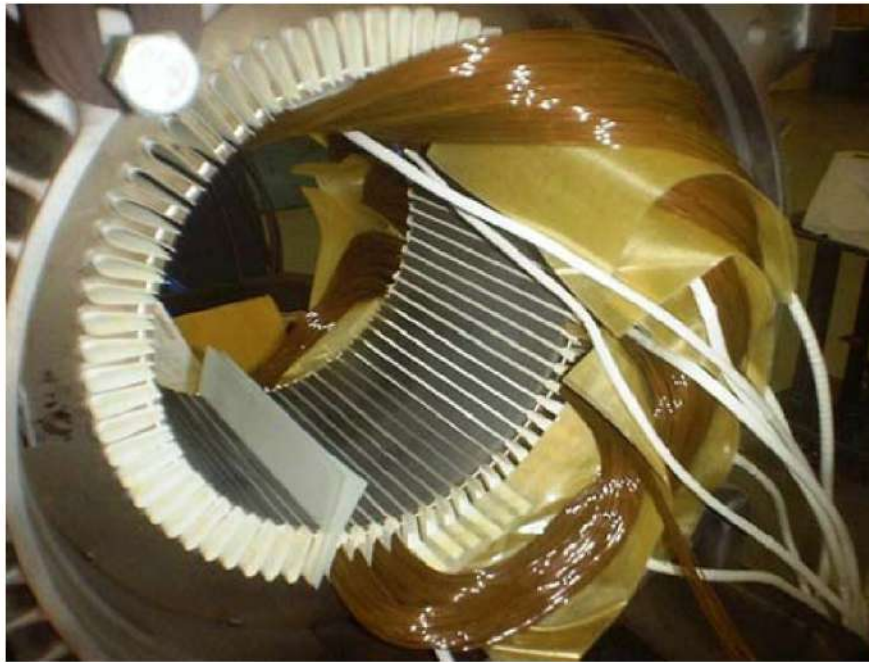
The insulation of a motor also includes all materials used to insulate the windings from the stator frame, the rotor, and any component connected to the ground. These materials provide electrical insulation and mechanical protection from the sharp angles of the slots. This mainly includes the slot liner, slot separator, and wedges shown in Figure I.5



Figure I.5: Slot liner, slot separator, and wedges seen during assembly [13]

## 3) Phase and endwinding insulation

Another important point is the insulation between phases. These components can isolate strands of a phase with respect to another. These insulation systems are localized in the slots or in the motor endwinding (Figure I.6).



**Figure I.6: Phase insulation in a partially-wound low-voltage stator [14]**

#### **4) Impregnation**

Impregnation is an insulation that can be applied to the previous three families. The purpose of impregnation is to replace any air gap in insulation systems with an impregnating liquid (resin or varnish). This impregnation improves heat transfer and mechanical strength but also acts as an insulation system.

### **I.3.2 Localization of Partial Discharges (PD) in low voltage motors**

Theoretically, given the nominal operating voltages of current machines, the insulation systems are supposed to be sufficient to protect equipment.

However, reality may be different, as insulation systems are not perfect and may have various types of defects. For example, a recurring defect is induced by improper impregnation. In that case, only the enamel of the wires withstands the voltage, which can lead to the appearance of PDs. Incorrect positioning or failure of insulation between phases or in slots may cause PDs. In addition, some locations can cause strong field amplification (sharp angle of the core facing the coil) and therefore increase the risk of PD occurrence.

To highlight these PDs, tests were carried out on a stator prototype with voltages exceeding the rated voltages and PWM like voltage. These tests were only intended to obtain visual confirmation of PD appearance areas with respect to the defects discussed above.

Three different occurrence areas can be seen in the figures below [15]:

- Between phases
- In the slot

- In the endwinding

Those photographs were taken using a long-exposure shutter in order to capture the light from the discharge at 100 mbar and at atmospheric pressure.



**Figure I.7: Partial discharges between phases (100 mbar)**



**Figure I.8: Partial discharges in the slot (100 mbar)**

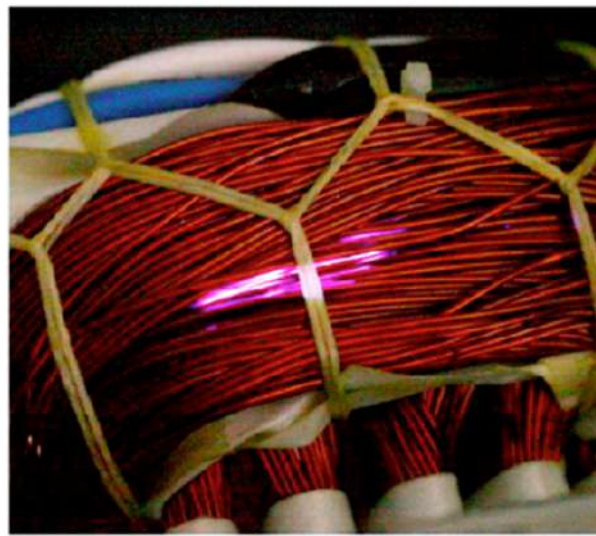


**Figure I.9: Partial discharges in endwinding (1013 mbar)**

These photos show that there is a risk for partial discharges to occur in low voltage motors under such voltage waveform.

The concept of more electrical aircraft not only causes a change in the voltage levels, but also a change in voltage sources. With the evolution of power electronics, motors are increasingly supplied by power electronics systems (inverters) using PWM voltage. It is very important to understand the characteristics of this voltage, as it is very different from AC and DC voltage.

## I.4 PWM fundamentals

### I.4.1 General interest

In the past, DC motors were widely used for applications that required controlling rotation speed. Speed control is very simple because varying the voltage amplitude causes a change in the rotational speed of the rotor. For applications requiring fixed speeds, the use of AC motors was preferred.

AC motors are currently used the most in low-voltage motors because their price, efficiency, and reliability are more appropriate than for DC motors. However, in some configurations, speed variation is one of the means for minimizing power losses. To change the speed of AC motors, it is necessary to use DC/AC or AC/AC inverters which make it possible to vary the amplitude of the applied voltage and the current frequency.

Due to their high price, these inverters were used in relatively few applications. As prices have decreased recent years, increasing numbers of inverters are used for functions called “Adjustable Speed Drives” (ASD). At the same time, the problems caused by these inverters are well-known. Notably, they are responsible for current and voltage distortions of the networks, and they are also a source of harmonic pollution of the networks.

In order to vary motor speed, the voltage inverter based on the pulse width modulation (PWM) switches the DC voltage source voltage into pulses of variable width at high frequencies on each phase. These pulse trains are used to reconstruct a fundamental variable frequency at the motor terminals, while rejecting harmonics. From an electromechanical point of view, only the fundamental is important. Nevertheless, for the insulation system, the presence of steep edges modifies the constraints with respect to the 50 Hz case.

Figure I.10 shows an example of an electromechanical chain.

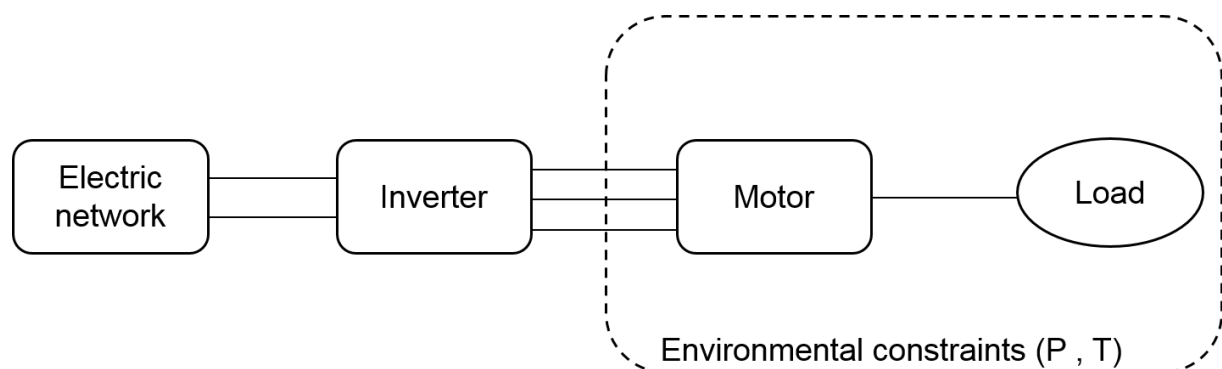
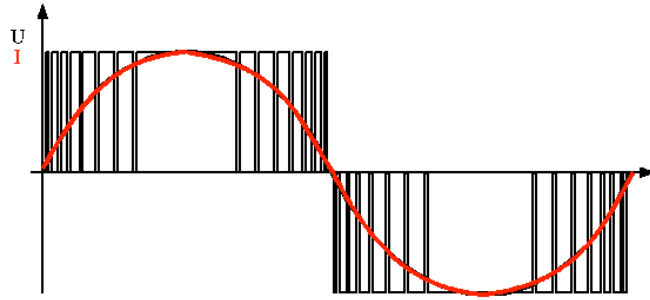


Figure I.10: Diagram of an electromechanical chain



**Figure I.11: PWM voltage between phases (black), current at the motor terminals (red)**

IGBTs (Insulated Gate Bipolar Transistors) used to create PWM voltage enable the generation of rising edges of tens of  $\text{kV}/\mu\text{s}$ , and can reach switching frequencies around 20 kHz. These improvements have helped reduce losses due to switching and motor torque. On the other hand, the reliability of these machines has declined dramatically. The first work on the subject was carried out by E. Persson [16].

The causes of motor failures may be due to different phenomena:

- High switching frequency increases electromechanical effort.
- The increase in dielectric and ohmic losses causes an increase in localized temperature.
- The waveform can create surges depending on the type and length of connections to the motor.
- The distribution of voltage is not uniform and is therefore concentrated on the first turns of the coils.

## I.4.2 Control strategy

Different control strategies exist to create PWM voltage. These strategies differ mainly on the control of harmonics created by the voltage.

There are two main families of PWM techniques [17]:

- Instantaneous PWM
- Calculated PWM

Instantaneous PWM may be local (controlling one commutation cell) or global (vector management controlling several commutation cells [18]). Generally, these strategies correspond to cases where the switching frequency  $F_d$  is large compared with the fundamental frequency  $F_s$ :

$$n = F_d/F_s \geq 20 \quad (\text{I.4.1})$$

For calculated PWM, forms of the square wave on a period of the fundamental are calculated to minimize parasitic harmonics. The results of these calculations are stored and used according to operating requirements.



The most conventional method is instantaneous PWM, and more precisely the “intersective” method. This method involves comparing the modulant (the signal to be synthesized) to a carrier wave, which has a generally triangular shape.

The output signal is equal to 1 if the modulant has a larger amplitude than that of the carrier, and 0 otherwise. Theoretically, the output signal varies at each intersection of the modulant and carrier.

The diagram below shows an example of three-phase sinusoidal PWM with  $f_{m1}$  and  $f_{m2}$  for the two commutation cell modulation functions:

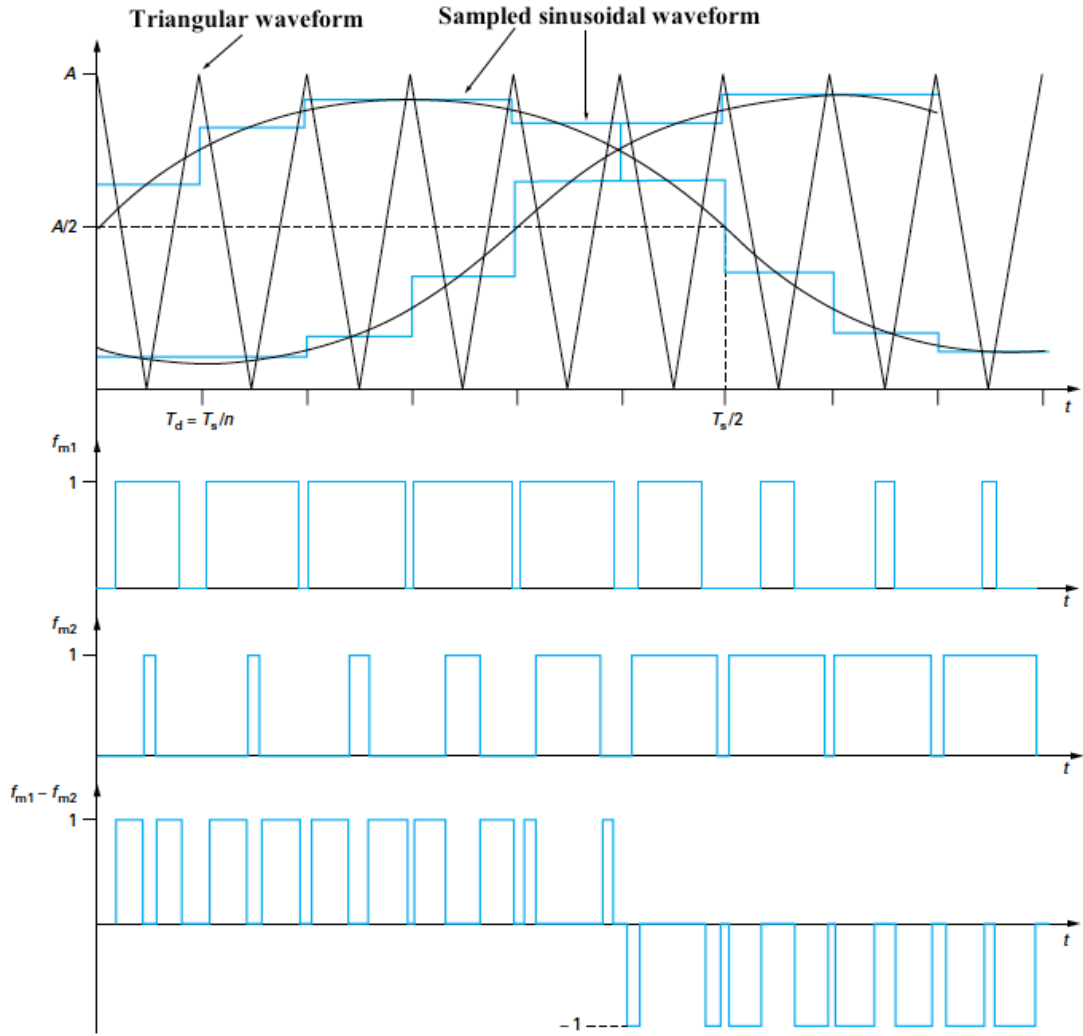


Figure I.12: Example of a three-phase sinusoidal PWM [19]

The output voltage  $v_{sT}$  is therefore the difference between the elementary voltages  $v_{s1}$  and  $v_{s2}$  of each cell and is expressed by:

$$v_{sT} = v_{s1} - v_{s2} = (f_{m1} - f_{m2})E \quad (\text{I.4.2})$$

In this section, we showed that there are different types of PWM controls for managing the created harmonics. As the voltage shape is very different from traditional forms such as AC or DC, it is important to focus on the influence of PWM on the electrical stress induced on the different insulation systems. Another important point concerns PD detection. There are many robust and validated methods for PD detection under AC and DC voltage, but methods are considerably less documented under PWM detection.

## **I.5 Partial discharges in machines fed by PWM inverters**

### **I.5.1 Voltage distribution under PWM**

Generally, under an applied voltage of 50 Hz, each stator phase can be considered as a simple “inductive voltage divider”. In this case, voltage distribution is linear at all times. In the case of sudden variations in voltages such that generated by an inverter, the voltage edge does not propagate instantly from one end to the other end of the coil. Losses in the magnetic core spread the front by damping it and capacitance between turns divert high frequencies [20]. Voltage distribution is thus not linear and each phase is no longer an “inductive bridge” but rather an equivalent propagation line [21].

#### **I.5.1.1 Influence of $dV/dt$ on voltage distribution**

There are many studies on the impact of the steep edges in machine coils. Modeling the distribution of the voltage along the stator phases is difficult because of coil complexity, geometry of the magnetic circuit, and the interaction of various electromagnetic phenomena. It is nevertheless possible to take an online approach for the equivalent transmission line with a focus on voltage distribution within the winding.

Figure I.13 shows an example of a conventional structure of an infinitesimal element of a transmission line with constant parameters to represent a coil. All the distributed parameters are defined per unit length:  $L_b$  is the inductance per unit length;  $C$  and  $C_i$  are the equivalent capacities of the inter-turn and slot base. Different resistances are used to take the losses into account: a part of  $r$  represents the resistive losses and skin effect in conductors of the winding,  $R_i$  to the dielectric losses, and the other part of  $r$  and  $R$  for losses in the magnetic part (hysteresis losses and by Eddy current).



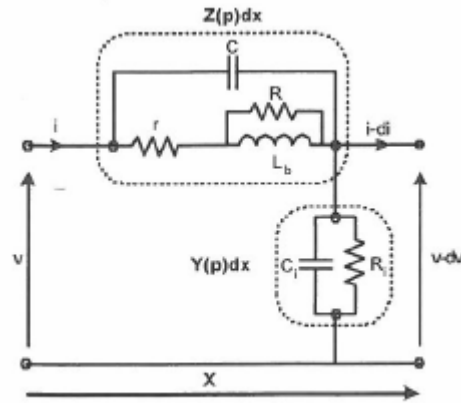


**Figure I.13: Infinitesimal element of equivalent transmission line**

As stated above, voltage is not distributed homogeneously along the winding during the application of steep edges. The non-instantaneous propagation of the edge and the distribution of the front due to losses (mainly in the magnetic core) contribute to increasing the maximum voltage between turns and, in particular, for phase input turns [21]. According to authors such as [22], 80% of the voltage for the fastest fronts is located at the terminals of the first coil (Figure I.14).

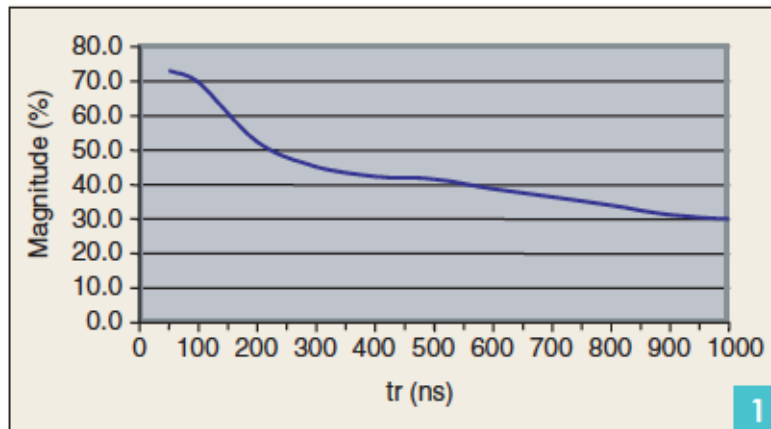


**Figure I.14: Percentage of the voltage across the first coil as a function of the rise time [22]**

Figure I.16 shows the non-linear nature of voltage distribution along a motor phase (Figure I.15). The insulation is highly stressed right after applying the front (Figure I.17). For longer times, voltage distribution looks like an “inductive voltage divider”.

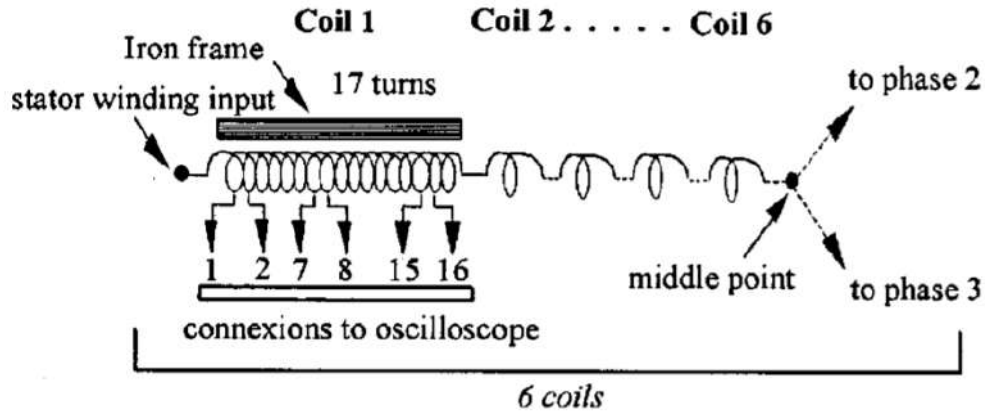


Figure I.15: Schematic representation of an equipped phase of the motor [23]

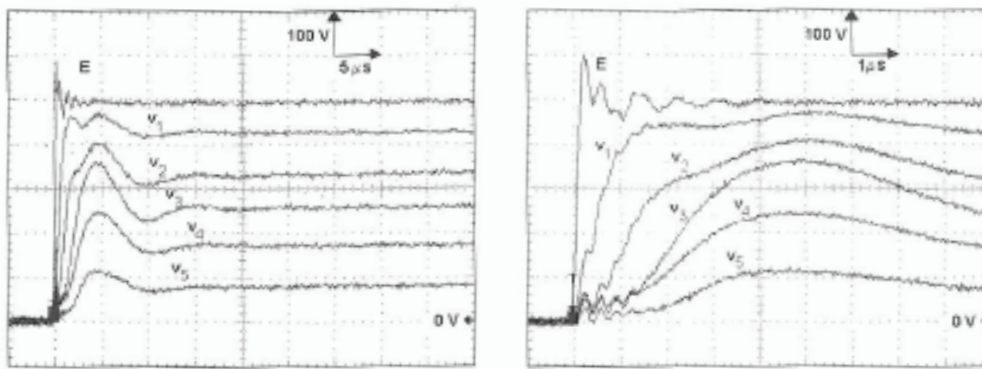


Figure I.16: Voltage phase/ground with the neutral point connected [24]

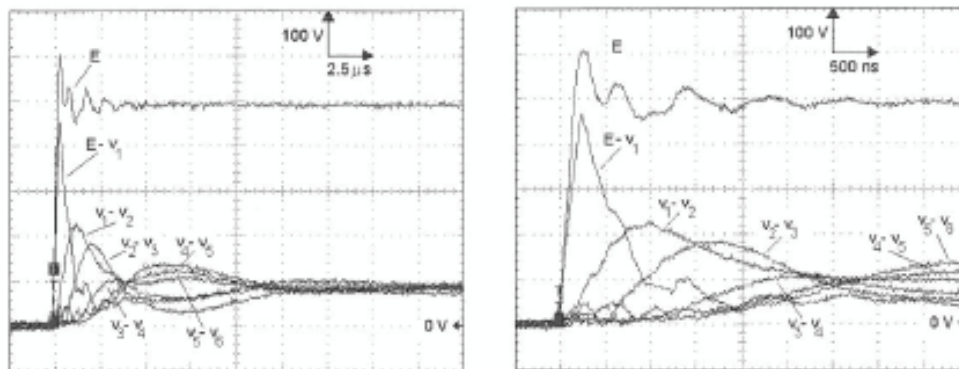


Figure I.17: voltage between coils [24]

In addition, another important parameter comes from the winding type used.

Since random winding is the most common technique for low voltage motors and therefore also in the MEA approach, the risks associated are that the first turn and one of the last turns of the first coil may be joined. In this case, 80% of the voltage is supported by a few tens of microns of enamel. Existing insulation systems are not dimensioned to withstand such severe stresses.

## I.5.2 Overvoltages induced by PWM

### I.5.2.1 The wave reflection phenomenon

The cable connecting the motor to the PWM inverter has a significant effect on the occurrence of overvoltages at the motor terminals. This phenomenon is explained by the fact that the cable behaves as a transmission line to which the coils of the motor are not suitable in terms of impedance mismatches. In this case, the voltage edges propagate along the cable and are partially reflected at the motor and inverter terminals (very low internal impedance). This phenomenon induces motor input overvoltages [25][26]. Theoretically, if the motor impedance ( $Z_m$ ) is very large with respect to the cable's characteristic impedance ( $Z_c$ ), the voltage at the terminal of the motor can reach twice the value of the DC bus of the inverter. In addition, with the voltage edge damping quickly in the winding, the first coil is subject to a significant voltage gradient, and the insulation between the turns is highly stressed. The amplitude of the reflected wave compared to the incident wave ( $V_i$ ) can be determined by the expression [27]:

$$V_r = V_i \frac{Z_m - Z_c}{Z_m + Z_c} \quad (I.5.1)$$

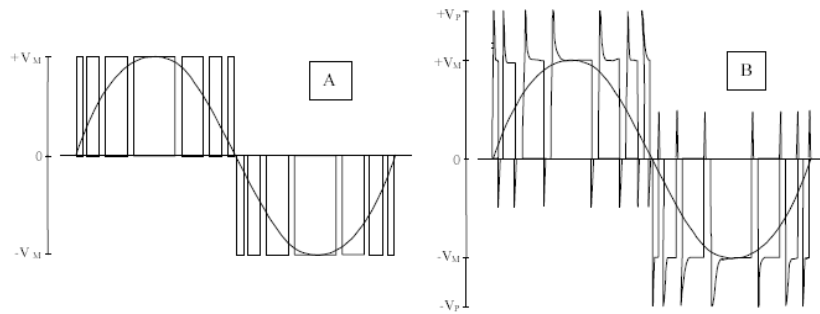


**Figure I.18: Voltage shape between phase output of the inverter (A) and the motor input (B) [28]**

### I.5.2.2 Cable length influence

The wave reflection phenomenon is not only related to the impedance difference, but also to the cable length [29]. It is considered that a complete reflection of the wave will appear if the round-trip propagation time of the wave through the cable is equivalent to the rise time of the voltage edge.

We can determine a “critical cable length”  $d$ , for which there will be total reflection of the voltage:

$$v = \frac{c}{\sqrt{\epsilon_r}} \quad (I.5.2)$$

$$2d = v \times t_r \quad (I.5.3)$$

with  $d$  the critical length of the cable,  $t_r$  the voltage rise time,  $c$  the speed of light ( $3 \cdot 10^8$  m/s), and  $\epsilon_r$  the relative permittivity of the cable insulation.

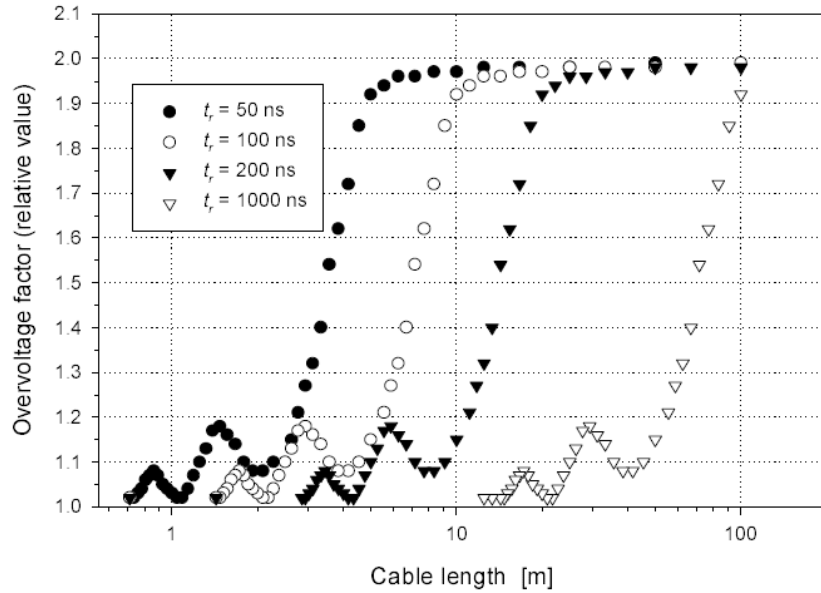


Figure I.19: Overvoltage at the motor terminals as a function of cable length and the edge rise time [28]

### I.5.2.3 Conclusion

The combination of steep edges, long cables, and impedance mismatch may induce overvoltages at the motor that can reach twice the voltage supplied by the inverter. These overvoltages, associated with the inhomogeneity of voltage distribution in the windings, create voltage differences between the turns that may exceed the Paschen threshold and thus cause partial discharge.

## I.5.3 Partial discharge detection under PWM

### I.5.3.1 Traditional detection methods

The presence of partial discharges can be determined by various physical phenomena associated with them. More particularly, this includes the electrical pulses, radio frequency pulses, acoustic pulses, light emission, and various chemical reactions such as ozone production [30].

- **Electrical pulse sensors:** Based on the fact that an electron current flow is created at each partial discharge event, a current could be measured, with the total current depending on the number of charges transported by the partial discharge. The current flow creates a voltage pulse across the impedance of the insulation system. The purpose of an electrical pulse sensor, called a conventional partial discharge sensor [31], [32], is to measure the resulting pulse.
- **Radio Frequency (RF) sensors:** partial discharges also create electromagnetic RF waves that propagate away from the discharge location site in the gaseous medium or within the windings. The discharge spectrum ranges from a few hundred kHz to several hundred MHz or more. A suitable bandwidth antenna could thus detect partial discharge activity [33].
- **Energy-based methods:** Since partial discharge creates light, RF, and pulse emission, energy is absorbed from the system and increases dielectric losses. Thus, a power factor tip-up method and another integration algorithm could be used.
- **Ozone detection:** One of the by-products of partial discharge activity in the air is the creation of ozone, which is a gas with a recognizable odor. The concentration increases as partial discharge activity at the surface of the insulation material increases. From inexpensive chemical measurement tools to electronic sensors, the ozone concentration can be measured, though it is affected by temperature, humidity, and airflow rates.
- **Acoustic and ultrasonic detection:** Partial discharges create a shockwave that can be detected by a microphone. A sound similar to frying could be heard if intense partial discharge activity is occurring.
- **Light:** Partial discharges emitting light that can be observed in a dark room with a photomultiplier, or even with the naked eye, when discharges occur at the insulating material surface.

### I.5.3.2 Partial discharge detection set-up

The description of the following system is from the thesis work of Thibaut Billard [34], [35]. The Laplace laboratory has developed a partial discharge detection system that can detect discharges in a

system supplied by PWM [36]. This system is based on an “on-line” and non-intrusive sensor. The detection system may be decomposed into four major parts: power supply, acquisition, sensor, and filters. Each of these parts is described in detail below.

### 1) Sensor

Using non-intrusive sensors is mandatory for equipment reliability. A simple sensor was developed for this purpose. Initially, the sensor was developed to offer a less expensive (regarding cost) alternative to inductive sensors. This sensor was made using a 1.5 m coaxial cable, then stripped on its cut extremity to expose the metallic inner core over a length of 1 cm. The coaxial cable is stripped further, but only to expose the inner insulator for 1 cm without any ground shield. This was done to prevent any undesired contact between the metallic inner core and the shortened ground shield. This sensor is not an antenna. It is sensitive to distance and must be placed as close to the discharge area as possible. In the case of stator tests, it is placed on the power cable close to the stator terminals.



**Figure I.20: Sensor based on coaxial cable**

### 2) PWM like power supply

The power supply is a PWM like inverter. This PWM inverter has been entirely conceived, designed, and built at the Laplace Laboratory. This PWM inverter can simultaneously supply two phases with bipolar controllable voltage waveforms. The high voltage source generates voltages up to 1.7 kV DC on the converter input and supports peak currents up to 50A. The IGBTs are designed to support up to 1.5 kV, which allows testing low voltage motors and searching for the PDIV.

The inverter provides modular bipolar voltage. The pulse duration, the time between pulses, and the switching frequency are adjustable, making it possible to create PWM voltage.

This system enables us to perform various tests, for example between one phase and neutral, or between two phases. This allows us to perform off-line testing relatively close to the actual stress that the test equipment can withstand. Voltage measurement is performed using a differential voltage probe.

As shown in Figure I.21, when the two command signals are similar, no voltage is applied across the two phases. When the two command signals are different, the output voltage is positive or negative, depending on which one is greater.

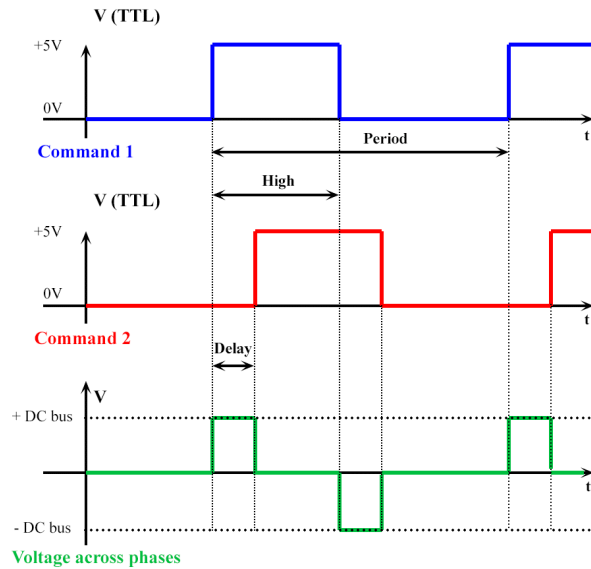


Figure I.21: PWM power supply and command

### 3) Filtering

The use of filters is essential in partial discharge detection, and more particularly in the case of PWM power supply [37]. The difficulty of detecting PD during steep voltage edges is to increase the signal-to-noise (SNR) to measure low amplitude signals with high-frequency components among large amplitude signals with low-frequency components. The bandwidth of the filter and its cutoff frequency are the most important parameters in this filter's design. The frequency spectrum of a discharge extends up to at least 1 GHz, as the noise generated by the PWM supply seems to not exceed a few hundred MHz (for the power supply used at the Laplace laboratory). The filter cutoff frequency should be greater than the frequency for noise suppression of commutations and must be adapted to the voltage rise time.

### 4) Acquisition

The acquisition tool used is an oscilloscope (Tektronix MSO 5204 Digital Oscilloscope) with a digital bandwidth of 2 GHz and a sampling frequency of 5GS/s. The frequency spectrum of a discharge extends up to at least 1 GHz, and with the cutoff frequency of the filters used being a few hundred MHz, it is possible to detect partial discharges.

### 5) Example of off-line measurement

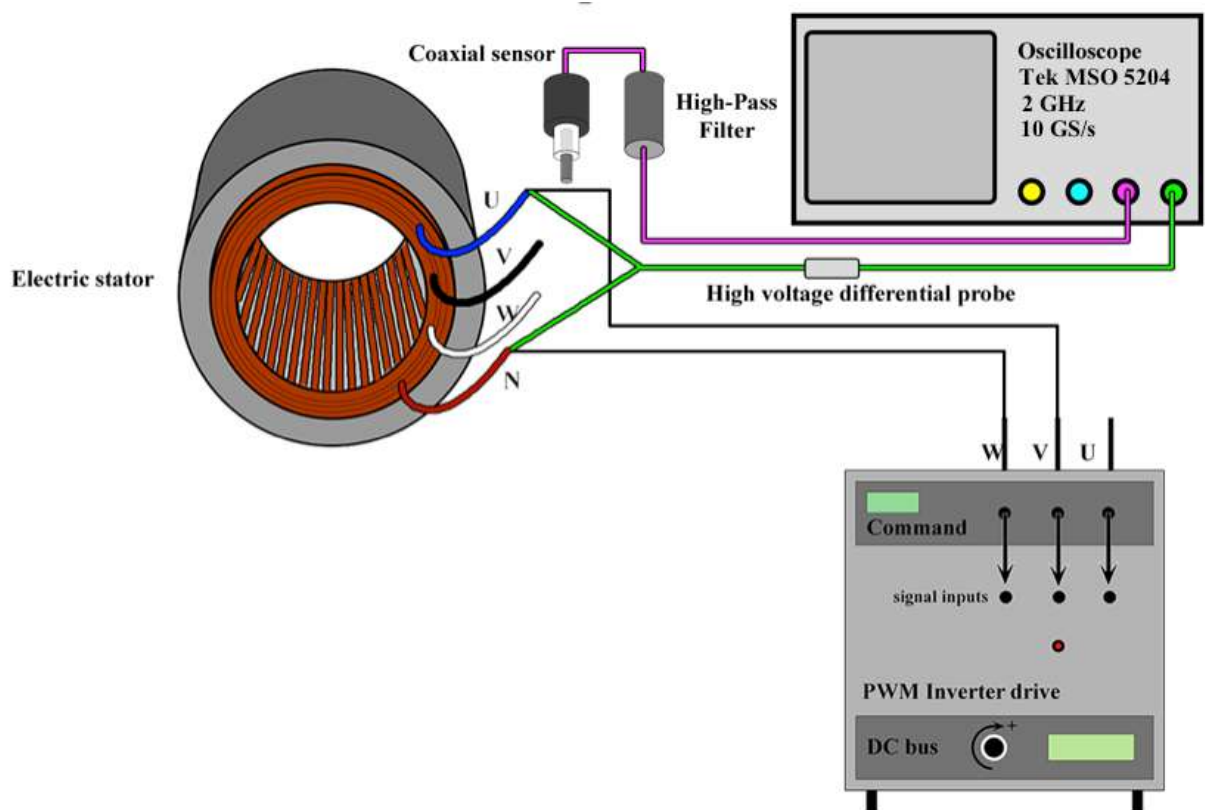


Figure I.22: Scheme of the complete off-line detection system

The influence of the filter is given in the following figures. Figure I.23 shows that it is not possible to observe anything with the noise induced by switching. In Figure I.24, one can see the effect of adding a high-pass filter. The filter eliminates the noise due to the switching and allows to observe the partial discharge signal. It is possible to say that the low amplitude signals are PD because they appear at a maximum voltage and at each change of polarity repeatedly.

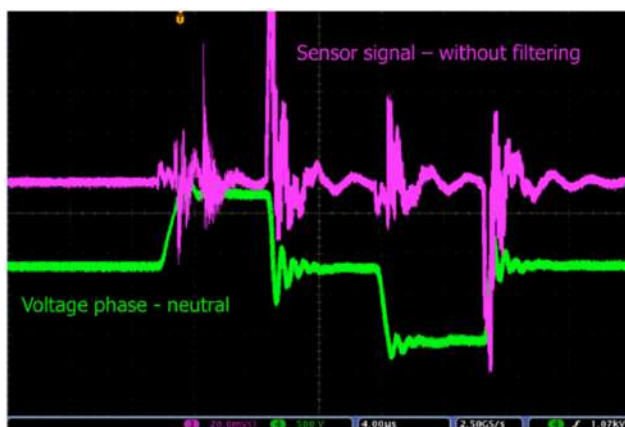


Figure I.23 PD detection without filtering

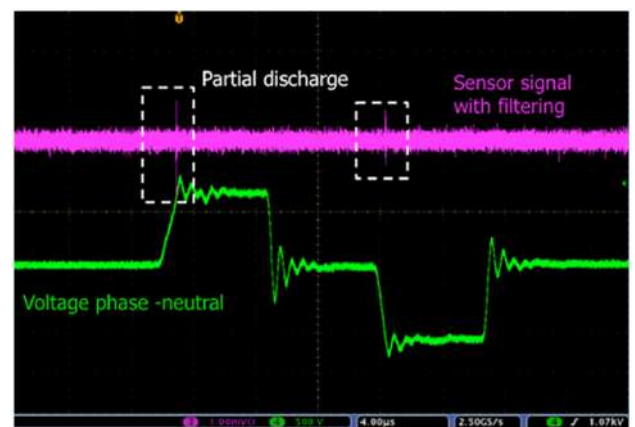
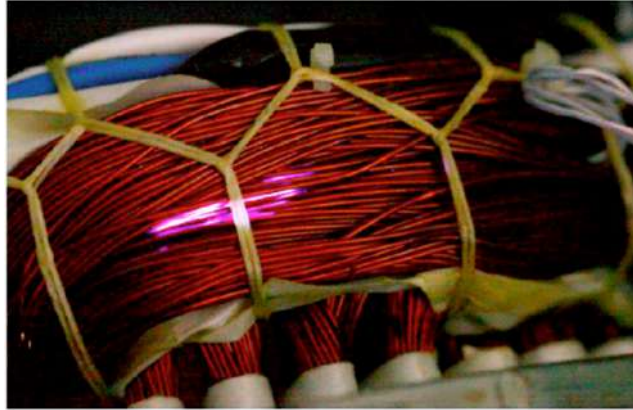


Figure I.24 PD detection with filtering



It can be seen below a photograph of the stator subjected to the voltage of the previous figures. “Glow” or “pseudo-glow” discharge is observed, which validates the fact that there are some partial discharges activity by correlation with the electrical detection [38].



**Figure I.25: Photo of the winding and presence of PD in the endwindings.**

### **I.5.4 Investigation of sensor signals**

As shown before, the method can detect partial discharges. However, not all sensor output signals are necessarily associated with PDs. Since the sensor is sensitive to quick changes in current, any phenomenon that induces this type of variation can cause a sensor response. The use of a high-pass filter eliminates much of the noise associated with switching, as well as external noise produced by the test bench or other equipment in the surrounding environment.

However, in some cases, the noise extending over a wide frequency range can cause a sensor response, which is similar to a discharge. It is therefore necessary to be able to discriminate the signals resembling PDs with respect to false positives. The easiest way to check that the observed signals correspond to partial discharges is to vary the voltage over a wide range to investigate the ignition and extinction of signals resembling PDs. If the signals are always present regardless of the voltage or for voltage values lower than  $320 V_{peak}$ , we can consider that the observed signals are false positives. In the case of tests on industrial test benches, voltage amplitude can either not be modified or only on a relatively small range, which prevents application of the method mentioned above. In this case, it is necessary to observe other signal characteristics to determine the presence or absence of PDs.

Different solutions are possible. One of them concerns observation of the voltage. In the case of low-voltage motors, partial discharges typically appear at the maximum voltage value, and therefore under PWM during quick voltage variations where surges or highest voltage values are commonly found. Another important point concerns the voltage value: we can be sure that the detected signals are false positives if there is a signal of interest at a maximum voltage value in the observed time interval, but there is no voltage differences higher than  $320 V_{peak}$  applied on the sample.

The figures below show a comparison between a PD signal and a false positive. In Figure I.26, the analysis is relatively simple because the maximum voltage does not exceed 150 V. In this case, we can be sure that the signal is a false positive because this level of voltage, and at atmospheric pressure, is below Paschen minimum.

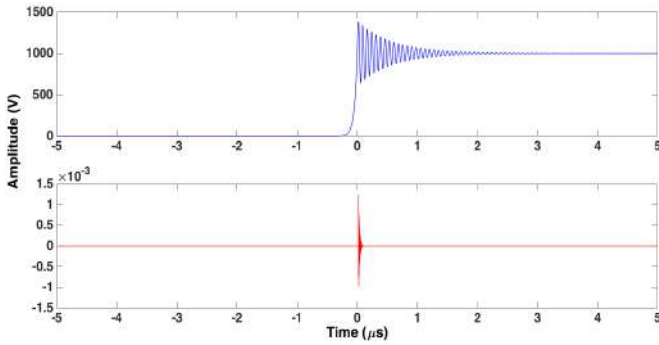


**Figure I.26: Example of partial discharge, voltage (blue) sensor signal (red)**

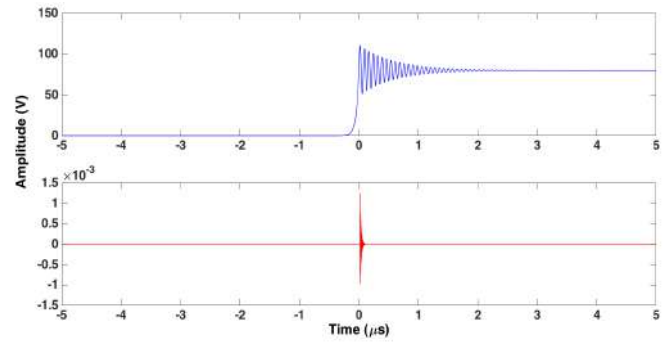


**Figure I.27: Example of false positive for a low voltage, voltage (blue) sensor signal (red)**

As mentioned previously, the temporal position is also important, and it may happen that signals seem to correspond temporally to the maximum voltage. However, thorough analysis is necessary to avoid errors while observing these signals.

An example of this type of case is provided below. By observing Figure I.28 and Figure I.29, it appears that the signals are identical and temporally correspond to the maximum voltage. However, as can be seen by zooming in these two signals (Figure I.30 and Figure I.31), we can see that they are not located in the same temporal position. The false positive signal is before maximum voltage. The signal appears for a voltage of 260 V. The occurrence of PD is unlikely to be seen at this voltage level. Such signals may be associated to the noise remaining after noise removal if the chosen cutoff frequency of the filter is not suitable. Another explanation is that the signal may correspond to a DP on another phase for a three-phase configuration.

It is, therefore, important to take into account the temporal position of the various signals observed while monitoring all voltage applied on the insulation system. Analysis of the different signal propagation times is also needed to ensure that delays or advances of observed signals are not induced by the set-up, but only by physical phenomena.

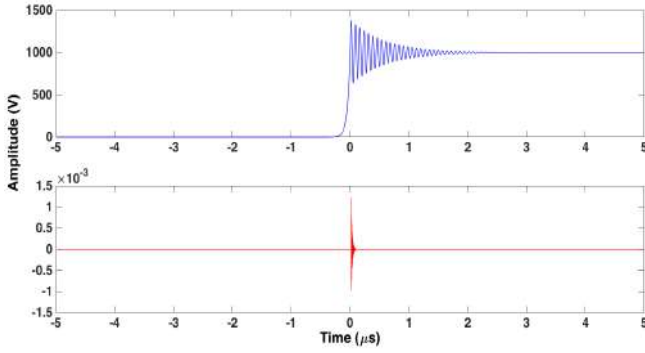


**Figure I.28: Example of partial discharge, voltage (blue) sensor signal (red)**

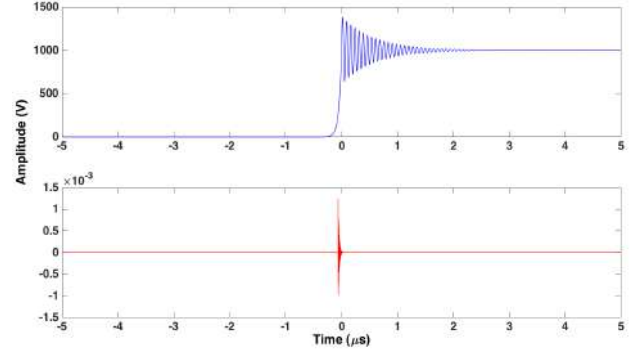


**Figure I.29: Example of false positive, voltage (blue) sensor signal (red)**

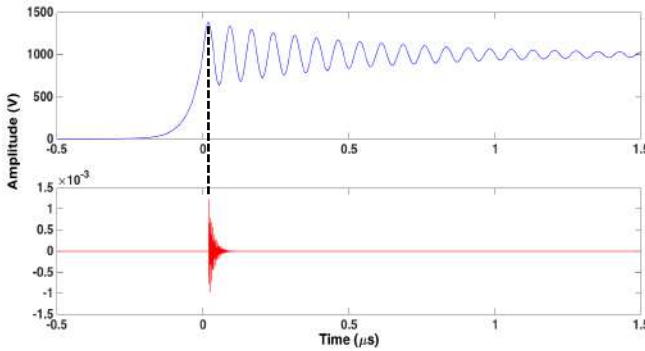


**Figure I.30: Zoom on the partial discharge, voltage (blue) sensor signal (red)**

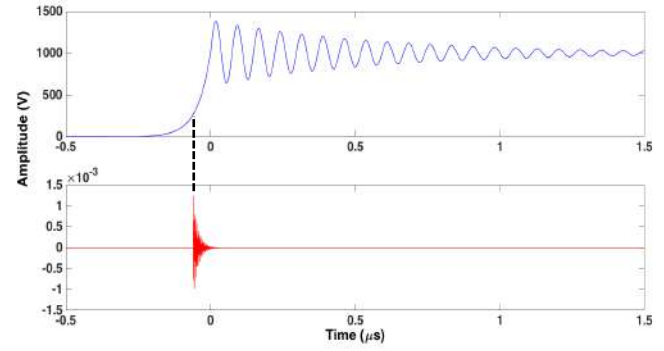


**Figure I.31: Zoom on the false positive, voltage (blue) sensor signal (red)**

Note that all the above signals come from simulation and are simply intended to highlight the analysis required to avoid confusing PD signals with false positives.

## I.6 Conclusion

Throughout this chapter, we have seen that the insulation systems of currently-used motors, associated with the evolution of on-board electrical networks, increase the risk likelihood of partial discharge occurrence. Increasing motor supply voltages by converters induces a change in stress applied to the various insulation systems found in motors. Moreover, the types of motors that match previously required aeronautical needs are no longer adapted to current electrical stresses. With the “more electric aircraft” approach, the insulation systems are not designed to prevent the occurrence of partial discharges or to resist the aging phenomena associated with them.

The implementation of a converter leads to another challenge related to the detection of partial discharge. Robust and reliable detection methods exist for equipment supplied by AC or DC voltage. On the other hand, detection is much more complex under PWM voltage, and specifically in the context of low voltage motors. For such motors, since the operating voltage is close to the PDIV, PDs appear mainly during the commutation and are embedded in the noise induced by switching. It was therefore

necessary to develop new detection methods and analysis procedures associated with these test conditions.

As the detection method development is relatively new, it is necessary to achieve a study on the sensor used to understand the observed phenomena. In addition, a study is required to ensure that the developed sensor is able to detect PDs regardless of environmental conditions.

These issues are discussed in the next chapter.



## **Chapter II. Experimental set-up**



One of the main points in detecting a phenomenon is to fully understand how the selected sensor works. In our work, it seemed mandatory to analyze sensor operation to accurately understand the physical phenomenon detected. In order to carry out this analysis, it was first necessary to propose a robust and standardized sensor in order to assess reproducibility of the results. Secondly, a study on the sensors used was necessary in order to know their influence. Finally, a correlation between a normalized signal (charge (pC) injected by a calibrator) and the output sensor signal was carried out in order to validate how the sensor works.

Some of the electrical equipment concerned by our work may be located in depressurized areas, and while operating, the temperature can vary widely. Pressure and temperature parameters have an influence on the discharge inception voltage and may also modify their nature [39]. Therefore, for such operating conditions, it is important to pay particular attention to the detection system characteristics in order to achieve the best SNR while filtering the noise induced by the voltage switching.

It was decided to study mainly the pressure in this chapter because it is the most impacting factor on the ignition of PDs. In addition, some equipments work in depressurized areas, while equipments operating in areas with high temperatures are less important in numbers

The aim of this chapter is to have a better understanding of the impact of these parameters on the PDIV.

## **II.1 Sensor study**

### **II.1.1 Sensor geometry**

One of the issues with home-made sensors (sensor presented in Chapter I.5.3) is the inherent lack of reproducibility in their elaboration and positioning. Clearly, slight variations can occur and may lead to changes in their response. Furthermore, sensor properties can evolve over time with handling. The solution we found was to use a Jack-SMA connector, connected to the end of a coaxial cable. This sensor is robust, inexpensive, and standardized. It also has about the same geometry and size as the home-made coaxial cable sensor. Another problem is the positioning of the sensor. Due to its geometry, achieving good contact and adequate holding on the power cable can be complex. For this reason, we developed special pliers to ensure good contact regardless of the cable gauge.





**Figure II.1: Jack-SMA type**

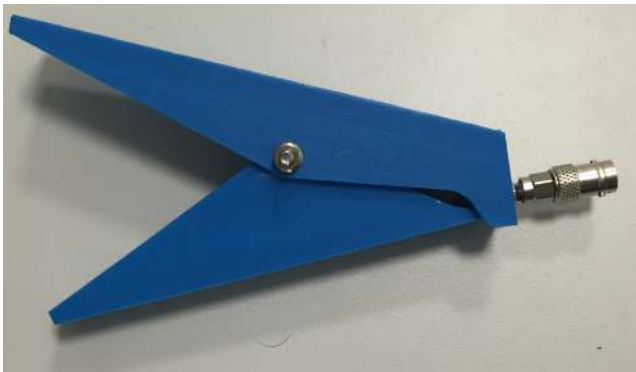


**Figure II.2: Jack-SMA with the holding system**



**Figure II.3: Zoom on the connection part**

## **II.1.2 Correlation research between calibrator voltage and the sensor response**

Generally, to calibrate a detection system based on electrical signals, a calibrator is used to create current pulses having a waveform similar to those of the PDs. To understand how the sensor works, it is necessary to compare the voltage associated with the current pulse and the sensor's output voltage.

### II.1.2.1 Experimental set-up

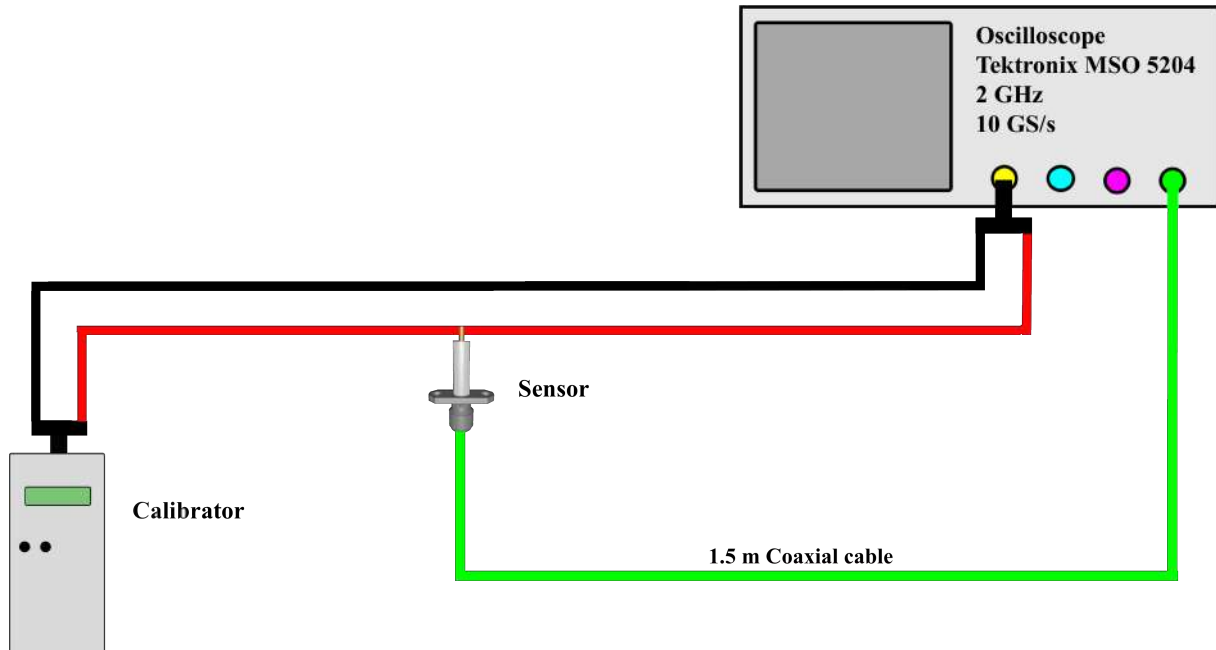


**Figure II.4: Diagram of the experimental set-up used to establish the correlation between calibrator voltage and sensor response**

### II.1.2.2 Results

In order to compare the different signals, it is important to remove the white noise induced by the measurement devices. This white noise is mainly due to the oscilloscope and can be separated into two components. The first component of noise is a fixed level of noise contributed primarily by the scope's front-end attenuator and amplifier. The second component of noise is a relative level of noise based on the scope's dynamic range, which is determined by the specific V/div setting.

To remove the white noise, the signals were filtered using an analogical low-pass filter with a cutoff frequency of 200 MHz.

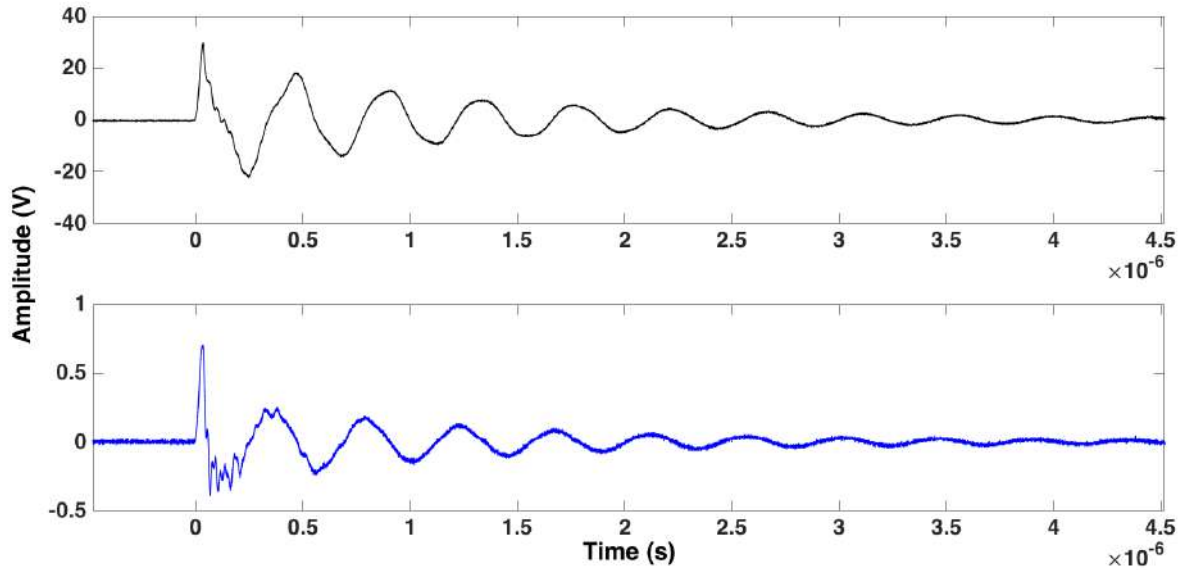


**Figure II.5: Calibrator voltage associated to a 10nC injected charge (black), Sensor signal filtered at 200 MHz (blue)**

Due to its working method, it is assumed that a capacitive coupling is induced between the core of the power cable and the metallic part of the Jack-SMA connector being used as a sensor. Moreover, it can be seen in the Figure II.15 that the signal of the sensor is in phase advance of  $90^\circ$  with respect to the signal of the calibrator. This phenomenon is characteristic of a capacitive phase shift. Since the current is in this case the derivative of the voltage with respect to time, the derivative of the calibrator signal must look like to the sensor signal.

However, since the amplitude difference between the derivative of the output voltage and the sensor signal is significant, the signal amplitude is normalized to allow comparison of the two signals. The derivative of the calibrator's output voltage was determined and compared to the sensor's output voltage. Good correlation of the voltage shape is found between the two signals (Figure II.6). The difference in amplitude and the waveforms can be explained by the transfer function, which should not be linear over the entire frequency spectrum. The sensor operation may therefore be considered as a capacitive coupling [40]–[43].

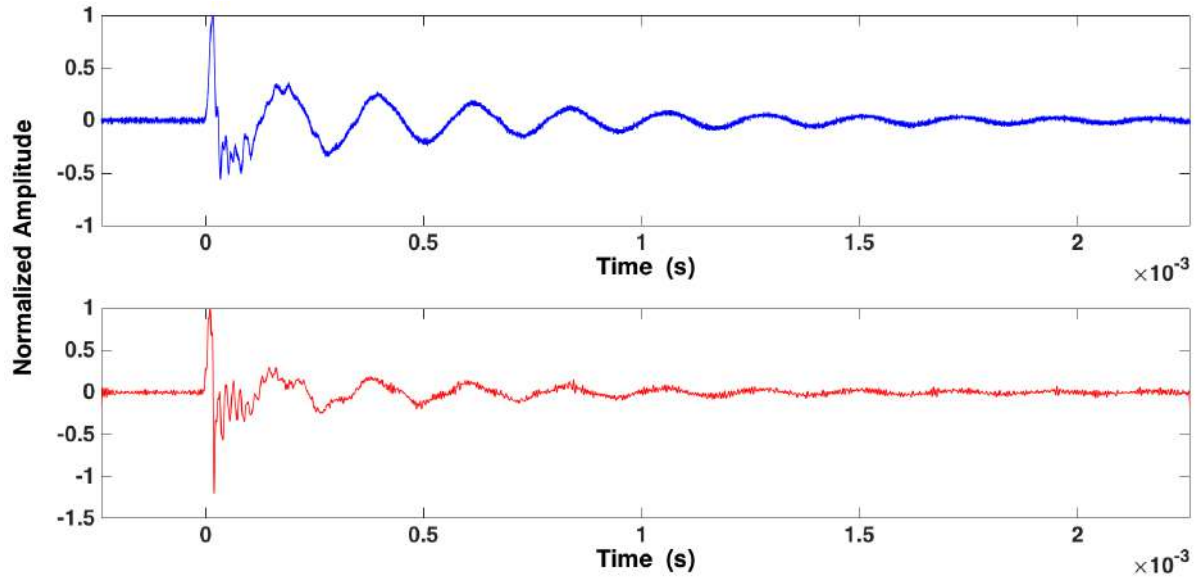


**Figure II.6: Sensor signal filtered at 200 MHz (blue), derivative calibrator voltage for 10nC injected charge (red)**

It is important to note that this sensor is sensitive to the dynamic of the partial discharge compared to the "standards" sensors, which are only sensitive to the amplitude of the discharge.

### II.1.3 Delay induced by cable length

A trivial, but important point to take into account when analyzing the sensor output signal is the propagation time between :

- the sensor and the oscilloscope
- the measurement voltage and the sensor
- the place where the measure is achieved and the system supposed to have PD

In Figure II.8 the observed signal is the voltage associated with the charge pulse injected by the calibrator.

### II.1.3.1 Experimental set-up

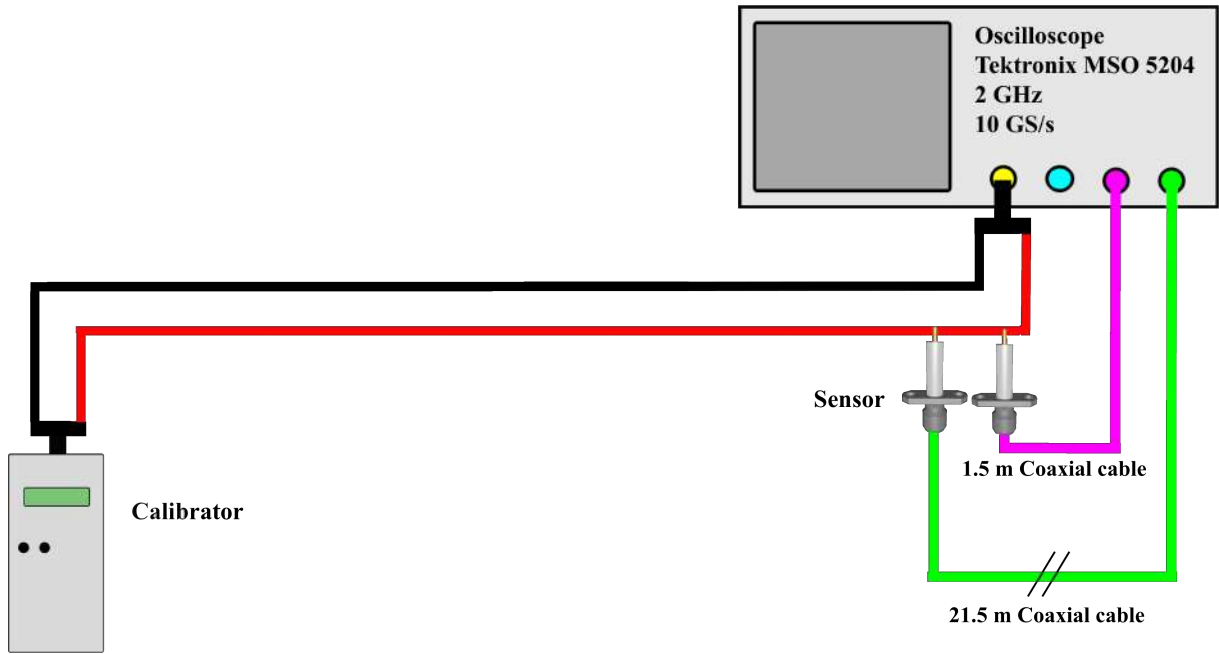


Figure II.7: Diagram of the experimental set-up used to establish the influence of cable length

### II.1.3.2 Results

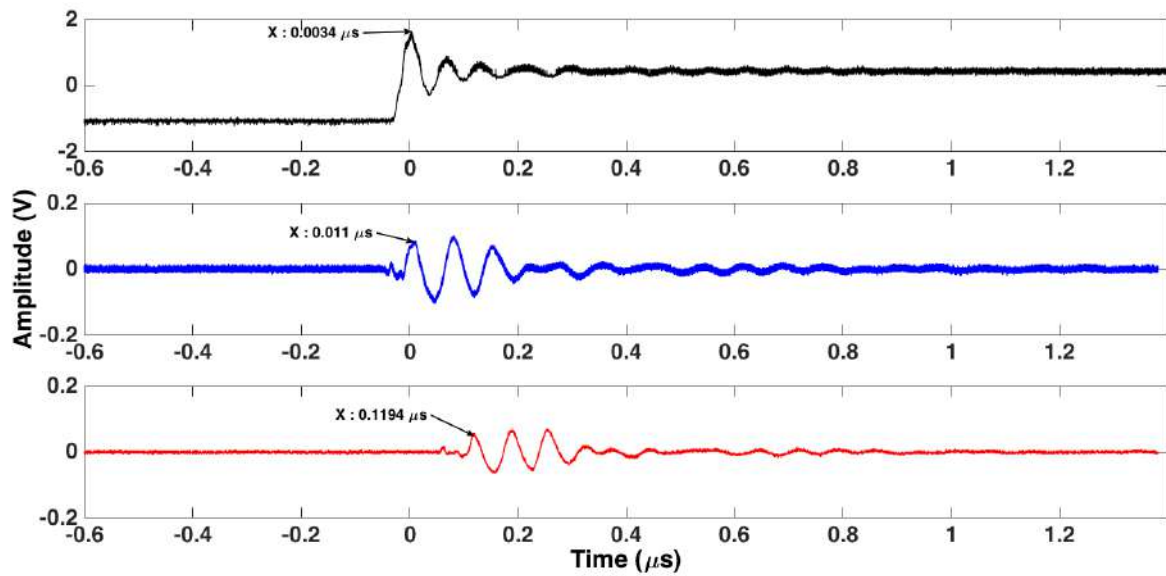


Figure II.8: Influence of cable length on signal position

As shown in Figure II.8, there is a delay of 7.6 ns between the calibrator signal (in black) and the sensor signal, connected to the oscilloscope via a 1.5 m coaxial cable. There is a delay of 108.4 ns between the two sensors. The first one (in blue) is connected to the oscilloscope with a 1.5 m coaxial cable, and the second one (in red) with a 21.5 m coaxial cable.

According to the data sheet for the coaxial cable we used (RG58 C/U), the nominal propagation velocity ( $v_p$ ) is 66% of the speed of light ( $c$ ). The cable length ( $L$ ) can be determined from the measured delay ( $\Delta t$ ) according to the following equation:

$$L = \Delta t \cdot v_p \quad (\text{II.1.1})$$

with  $v_p \approx 200\,000$  km/s

The calculation was performed to compare the result to the actual length.

**1) Delay induced by the first sensor**

$$L = 7.6 \times 10^{-9} \cdot v_p = 1.52 \text{ m} \quad (\text{II.1.2})$$

**2) Delay-induced by the second sensor**

$$L = 108.4 \times 10^{-9} \cdot v_p = 21.44 \text{ m} \quad (\text{II.1.3})$$

The actual lengths found by the calculation are within about 1% error. For our overall study of PDs, it will be important to take into account the delay induced by the connection in order to avoid making false assumptions [41].

## II.2 Sensor optimization

As previously stated and demonstrated, the sensor is based on a capacitive coupling. Sensor sensitivity and sensor signal amplitude can therefore be increased simply by improving the coupling capacitance value. This is achieved by increasing the contact surface by putting copper tape on the surface of the power cable to control the interacting area and thus the value of the induced capacity.

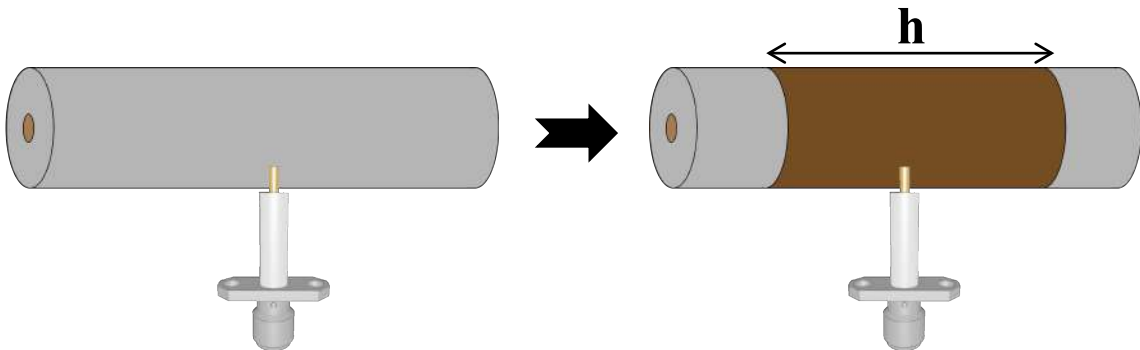


**Figure II.9: Simple optimization of the sensor sensitivity**

Induced capacity can be evaluated using the following equations:

$$R_0 \leq r \leq R_1$$

$$2\pi r h \epsilon_r \epsilon_0 E(r) = Q \Leftrightarrow E(r) = \frac{Q}{2\pi \epsilon_r \epsilon_0} \times \frac{1}{r h} \quad (\text{II.2.1})$$

$$\vec{E} = -\overrightarrow{\text{grad}}V \Leftrightarrow V_0 = \int_{R_0}^{R_1} E(r) dr = \frac{Q}{2\pi \epsilon_0 h} \left( \frac{1}{\epsilon_r} \log\left(\frac{R_1}{R_0}\right) \right) = \frac{Q}{C} \quad (\text{II.2.2})$$

The induced capacity is given by:

$$C = \frac{2\pi \epsilon_0 h}{\frac{1}{\epsilon_r} \log\left(\frac{R_1}{R_0}\right)} \quad (\text{II.2.3})$$

The influence of the increase of the coupling capacitance on the maximum amplitude of the observed signal is shown in Figure II.10.

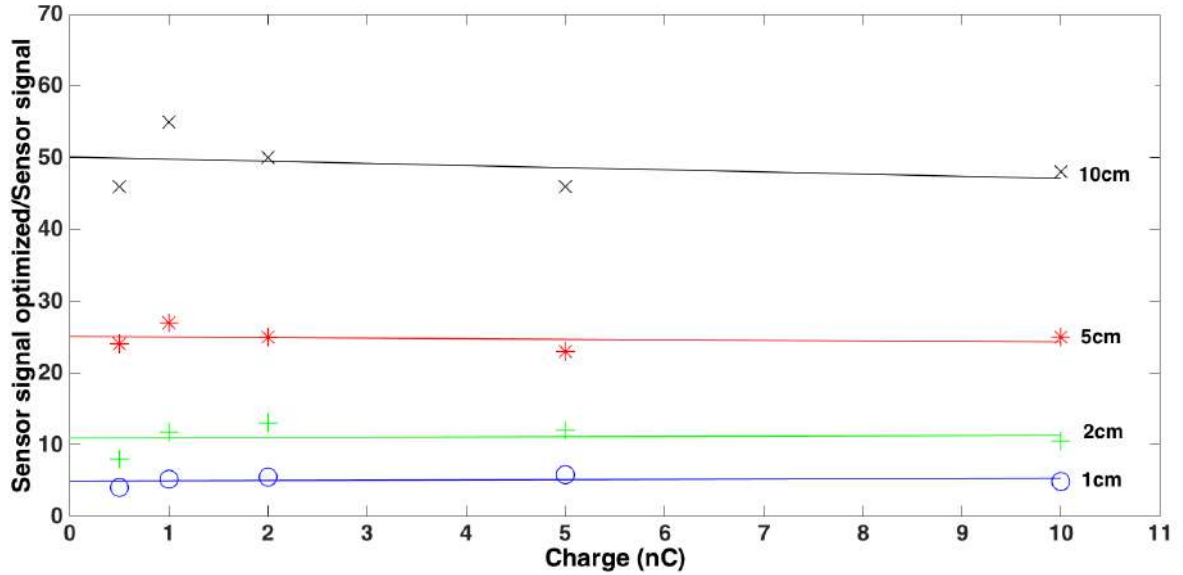


Figure II.10: Comparison between the amplitude of the sensor signal with and without optimization depending on the length of cylindrical capacity.

### II.3 Role of the pressure : Experimental set-up

For the experiments related to the impact of the pressure, two power supplies were used for these tests, first the PWM like power supply described previously (Chapter I.5.3.2) and the AC voltage was applied thanks to two autotransformers in series with a transformer to supply samples up to 3 kVrms (no.1 on the Figure II.14).

Moreover, non-intrusive current transformer sensor was also tested in such PWM environment (no.2 on the Figure II.14). This sensor essentially behaves like a transformer. The primary winding is actually the circuit in which partial discharge must be detected, with one cable going through a tore

ferrite loop representing the magnetic circuit. The output secondary winding thus provides an image of the current going through the primary winding. The bandwidth at -3dB is between 0.5 and 80MHz.



**Figure II.11: Rogowski coil**

Experiments were performed on twisted pair samples of enameled wires (nominal diameter  $\varnothing = 1.31$  mm) (no.3 on the Figure II.14). The twisted pair samples were made according to usual norms and recommendations [44]. This sample is representative of the winding that can be found in randomly wound motors.



**Figure II.12: Twisted pair of enameled wires**

To perform tests close to aeronautical conditions, a vacuum chamber was used with a sufficiently large volume to be able to perform tests on samples ranging from twisted pair to stator (no.4 on the Figure II.14). Pressure could vary from atmospheric pressure up to a few tens of millibars. Electrical connections were provided by high-voltage bushings.





**Figure II.13: Vacuum system**

The complete experimental set-up is described in Figure II.14 below.

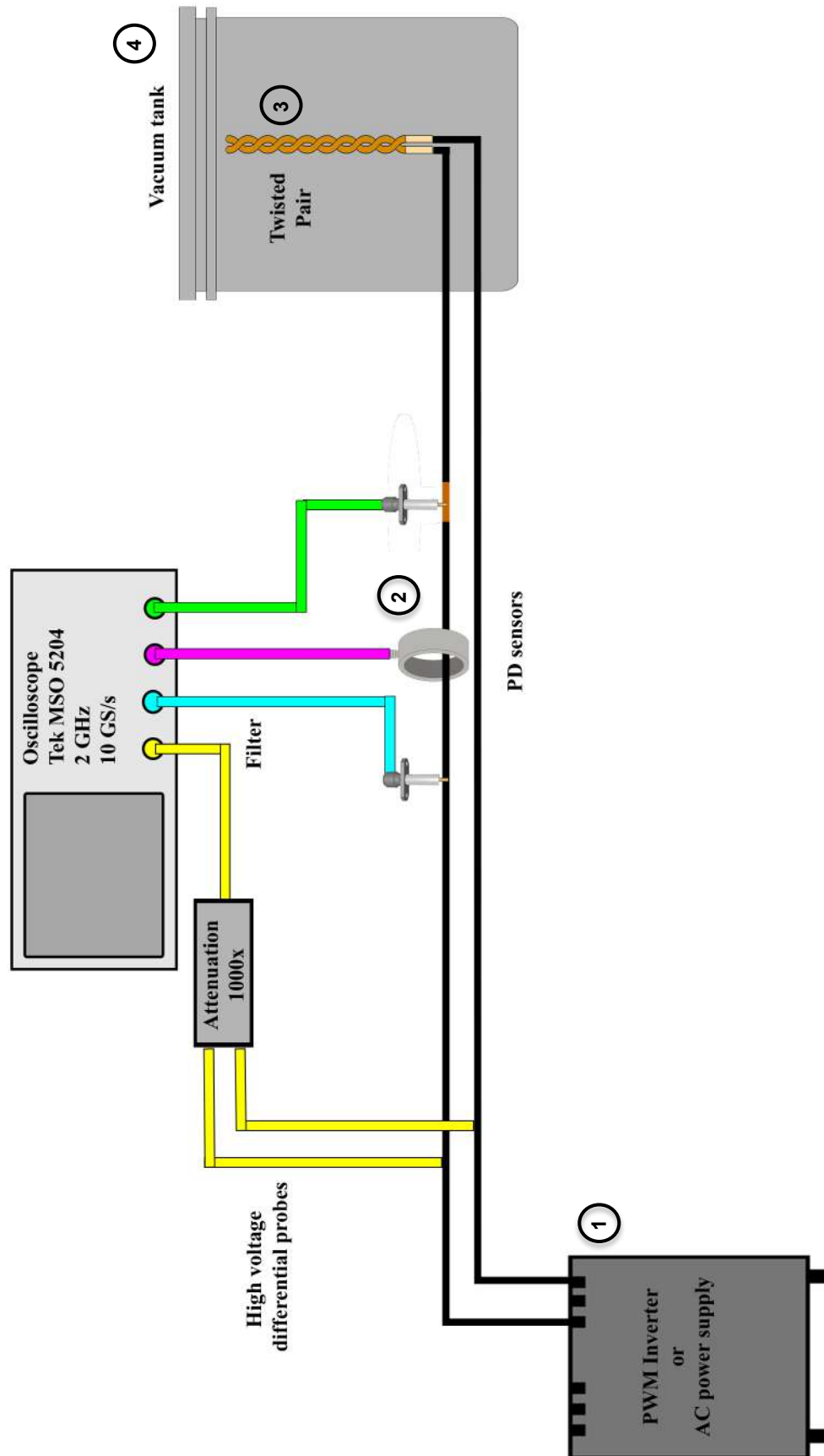


Figure II.14: Experimental set-up for tests at low pressure

## II.4 Reproducibility of the measurements

Twisted pairs were used and tested, and the results presented here correspond to a selection of three of them randomly chosen. These twisted pairs consisted of 10 twists, with diameter of the enameled wire about 1.31 mm. All voltages below are peak voltages.

**Table II.1: Comparison of PDIV and PDEV for different twisted pairs at atmospheric pressure under AC voltage**

	PT1		PT2		PT3	
Test number	PDIV (Vpeak)	PDEV (Vpeak)	PDIV (Vpeak)	PDEV (Vpeak)	PDIV (Vpeak)	PDEV (Vpeak)
1	954,6	933,4	940,5	926,3	954,6	926,3
2	954,6	940,5	947,5	919,2	957,4	933,4
3	954,6	926,3	947,5	919,2	954,6	930,6
4	954,6	933,4	947,5	905,1	947,5	933,4
5	954,6	933,4	947,5	916,4	947,5	936,2

Same study was performed under PWM-like voltage.

**Table II.2: Comparison of PDIV and PDEV for different twisted pairs at atmospheric pressure under PWM like voltage with a 200 MHz high pass filter**

	PT1		PT2		PT3	
Test number	PDIV (Vpeak)	PDEV (Vpeak)	PDIV (Vpeak)	PDEV (Vpeak)	PDIV (Vpeak)	PDEV (Vpeak)
1	1032	980	1032	1008	984	960
2	1032	1008	1056	1008	1032	1008
3	1056	1008	1056	1008	1056	1008
4	1056	1008	1056	1008	1056	1008
5	1056	1008	1056	1000	1056	1008

Given these results, we can consider that there is good reproducibility of results between the different twisted pairs allowing us to be confident on the results presented below. A slight difference can be observed on the PDIV between AC and PWM-like voltage, which is due to the filtering.

## II.5 Influence of pressure under AC

To study the influence of pressure on the ability of the method to detect PDs, tests were performed at different pressures under AC voltage and under PWM like voltage. The main idea is to compare the impact of this parameter on the discharge characteristics while enabling a comparison between the different sensors.

This involves two hypotheses:

- The partial discharge ignition voltage is the same, whatever the voltage waveform
- The nature of the discharge remains the same, whatever the voltage waveform

These assumptions will be discussed and confirmed in the following part.

### II.5.1 Influence of the sensor on detection

Three sensors were used for these tests: Jack-SMA sensor, Jack-SMA sensor with an additional capacitive effect (2 cm copper tape) and Rogowski coil. We first checked PDIV and PDEV at different pressures and AC voltage, since PDs are easy to detect under such conditions.

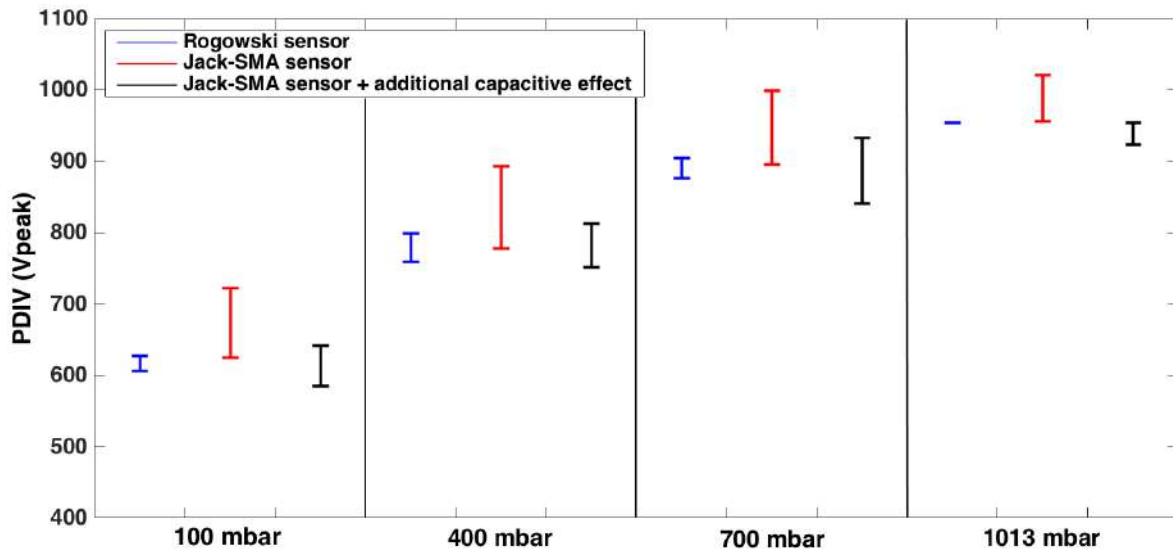


Figure II.15 : Influence of pressure on PDIV for three sensors under AC voltage

A decrease in PDIV is clearly observed with decreasing pressure. This phenomenon corresponds to expected behavior and is in good agreement with Paschen's law.

We compared the detected PDIV for each sensor. Jack-SMA sensor with an additional capacitive effect detects discharges first, it was then used under AC voltage to detect the PDIV. Subsequently, PDIV corresponds to the voltage at which the discharge is detected by the sensor used.

It can also be observed that the PDIV detected by the Rogowski sensor is close to the optimized Jack-SMA sensor. On the other hand, without increasing the capacitive effect, the Jack-SMA sensor detects the PDs for a higher voltage and the PDIV detected has a large error. This is explained by the fact that the SNR of this sensor is low without the increase of the capacitive effect, making it difficult to distinguish a signal associated with a PD and the noise.

## II.5.2 Influence of the cut-off frequency of the filter on detection

Detecting conditions used here were those described for the tests performed under PWM-like voltage, which requires the use of a high-pass filter, as explained previously. The main idea is to study the impact of pressure on detection, with respect to the change in the nature of the discharge. Since the frequency content may be modified in that case, adapting the cut-off frequency to detect PDs must be envisaged. As the filter is suspected of inducing errors on PDIV, we studied its impact under AC voltage at different pressure values.

These tests were performed at different pressure values with high-pass filters presenting cut-off frequencies of 50, 90, and 200 MHz and the Jack-SMA sensor with an additional capacitive effect.

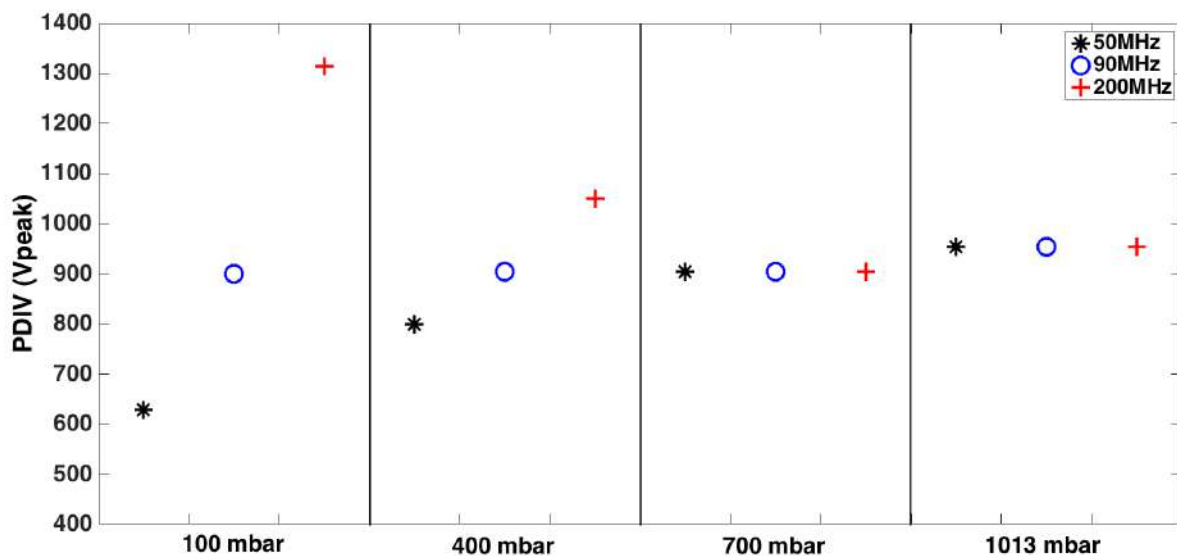


Figure II.16 : Influence of filter cut-off frequencies on the PDIV at different pressure values under AC voltage

The measured PDIV is artificially increased using high-pass filters (Figure II.16). It should be noted that the higher the cut-off frequency, the larger the PDIV at 100 and 400 mbar. One assumption is that the high-frequency components of the spectrum are too small under such conditions. It is therefore

necessary to increase the voltage to detect partial discharge (which already appeared at 444 V<sub>peak</sub>). Hence, with the 200 MHz filter, the PDIV is about three times larger than the one measured with the sensor without filtering.

This same phenomenon was not observed at atmospheric pressure and 700 mbar: the filter cut-off frequency had no impact on the PDIV (Figure II.16). This is a proof that modifying the pressure leads to a modification of the discharge spectrum.

### **II.5.3 Spectral analysis**

We then performed a study on the discharge frequency spectra for the different pressures under study. For each pressure level, 30 acquisitions of PD were recorded using the Jack-SMA sensor under AC voltage. We determined the spectrum of each and plotted their average value (Figure II.17).

Since the DPs do not appear at the same voltage as a function of the pressure, it can therefore be assumed that the amplitude of these discharges will vary as a function of the pressure. It was therefore decided to normalized the results in order to compare the shape of the PDs frequency spectra. For each pressure, the frequency spectrum has been normalized with respect to its maximum value. This normalization prevents the comparison of the amplitudes of these spectra as a function of the pressure. Nevertheless, it makes it possible to highlight the evolution of the most energetic frequency ranges as a function of the pressure.

It is obvious that the amplitude of the high-frequency components (40MHz – 100MHz) decreases with a decrease of the pressure while the amplitude of the low-frequency components (9MHz – 40MHz) increase. Moreover, at 100 mbar, for frequencies above 30 MHz, the signal amplitude is almost null despite some rays around 50 MHz that may contain a small portion of the discharge energy. A zoom on the y-axis confirms this assumption, with rays up to 70 MHz (Figure II.18). Some rays around 100 MHz can be observed at 100 mbar, though these rays do not match PD signals, but rather to noise induced by external systems during tests.

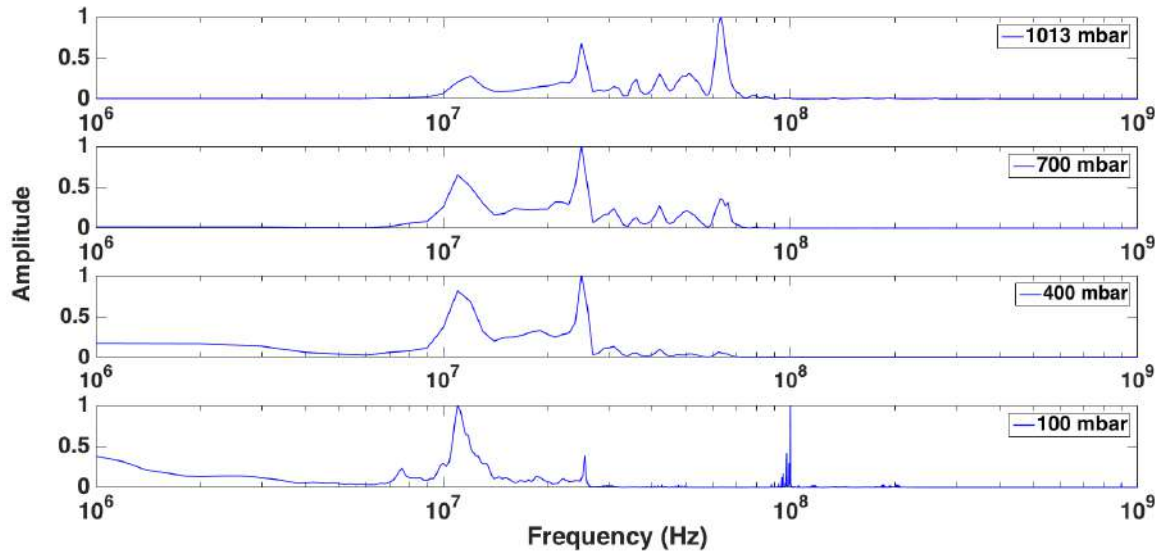


Figure II.17: Normalized changes of PD spectrum under AC voltage as a function of pressure

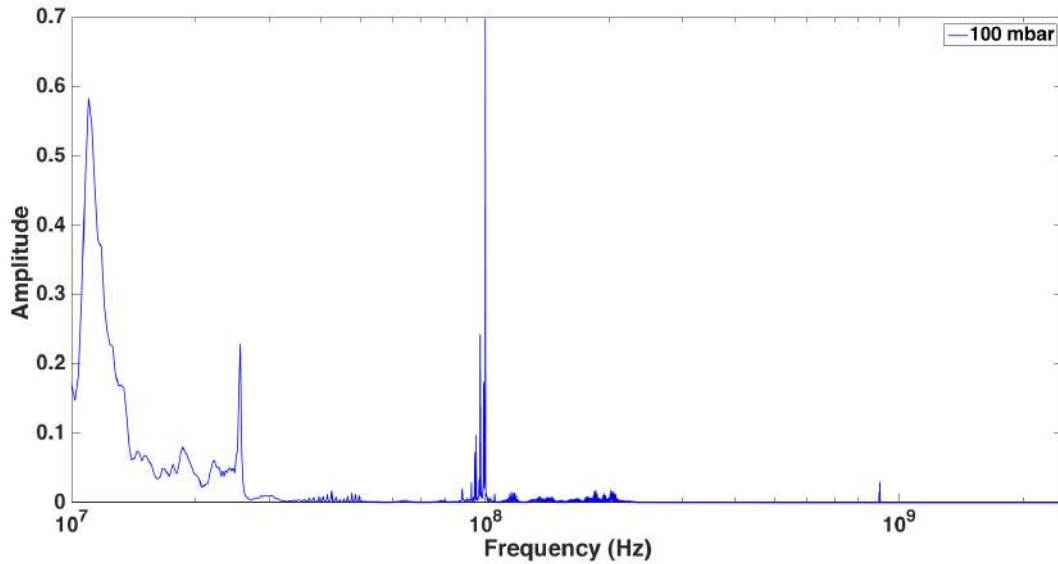
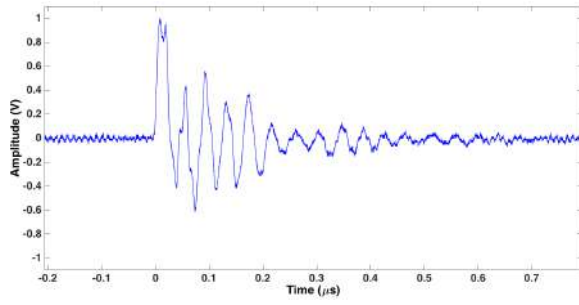
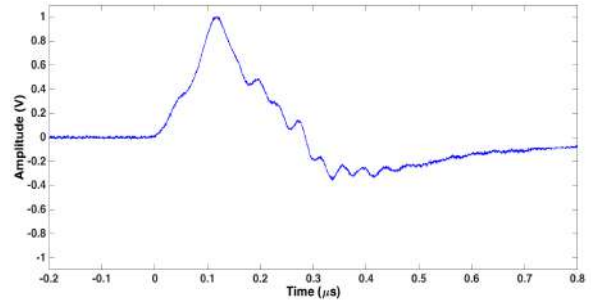


Figure II.18: Zoom on high-frequency components of partial discharges at 100 mbar

It is necessary to specify that certain characteristic frequencies can come from the detection circuit (resonances) and that is why the analysis is qualitative (normalized and observation of the relative variation).

It has been seen that the Jack-SMA sensor is sensitive to the dynamics of the discharge, so it can be assumed that the frequency shift as a function of the pressure comes from a variation in the rise time of the discharges and / or from a variation of the amplitude of the discharges.

We therefore compared two PD signals for two pressure values.

**Figure II.19: PD signal shape at 1013 mbar****Figure II.20: PD signal shape at 100 mbar**

At 100 mbar, the signal is completely different from the PD signal at 1013 mbar. The rise time of the front is about 121 ns and it is ten times longer than at atmospheric pressure (13 ns). This explains the observed frequency shift.



## II.6 Influence of pressure under PWM

### II.6.1 Influence of the sensor on detection

In the case of detection under PWM, it is not possible to detect the PDs without filtering the electromagnetic noise associated with the  $dV/dt$ . We therefore compare the response of the sensors without filtering and with high-pass filtering at 290 MHz.

It can be seen on the Figure II.21 that the noise coincide temporally with each of the  $dV/dt$ . The aim of the filtering will be to eliminate this noise in order to observe only the signals associated with the PDs.

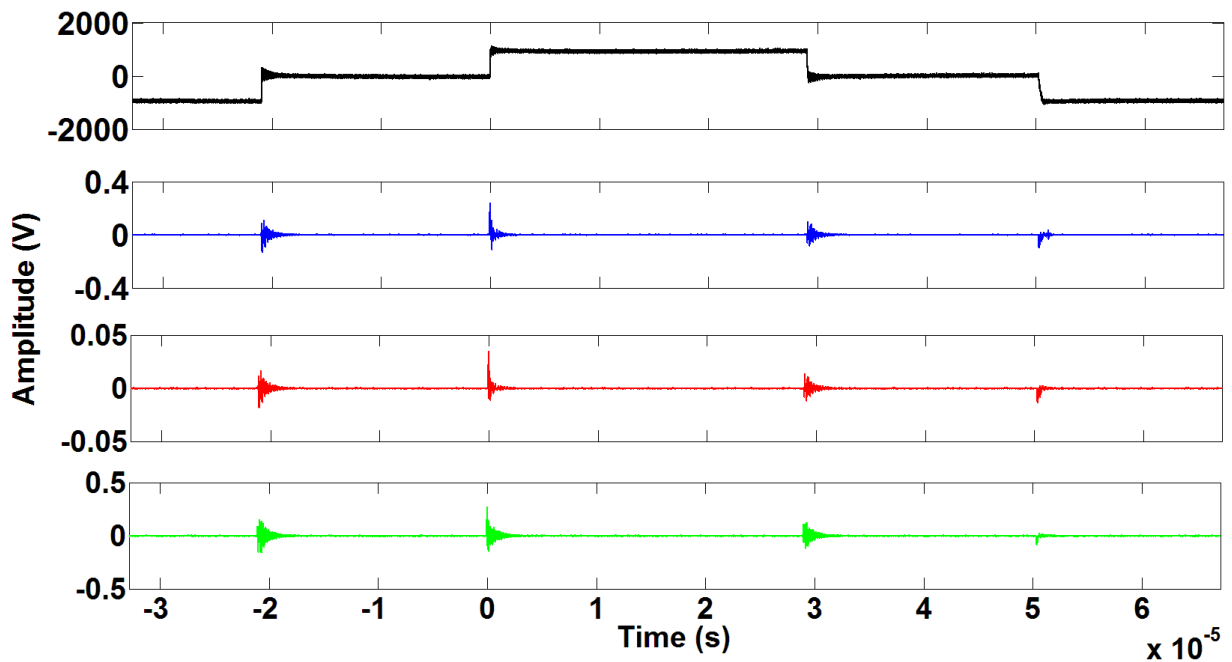


Figure II.21: PWM like voltage shape (black), Rogowski sensor signal without filtering (blue), Jack-SMA sensor signal without filtering (red), Jack-SMA sensor (with an additional capacitive effect) signal without filtering (green)

Subsequently all the sensor signals were filtered using high-pass filters having a cut-off frequency of 290 MHz.

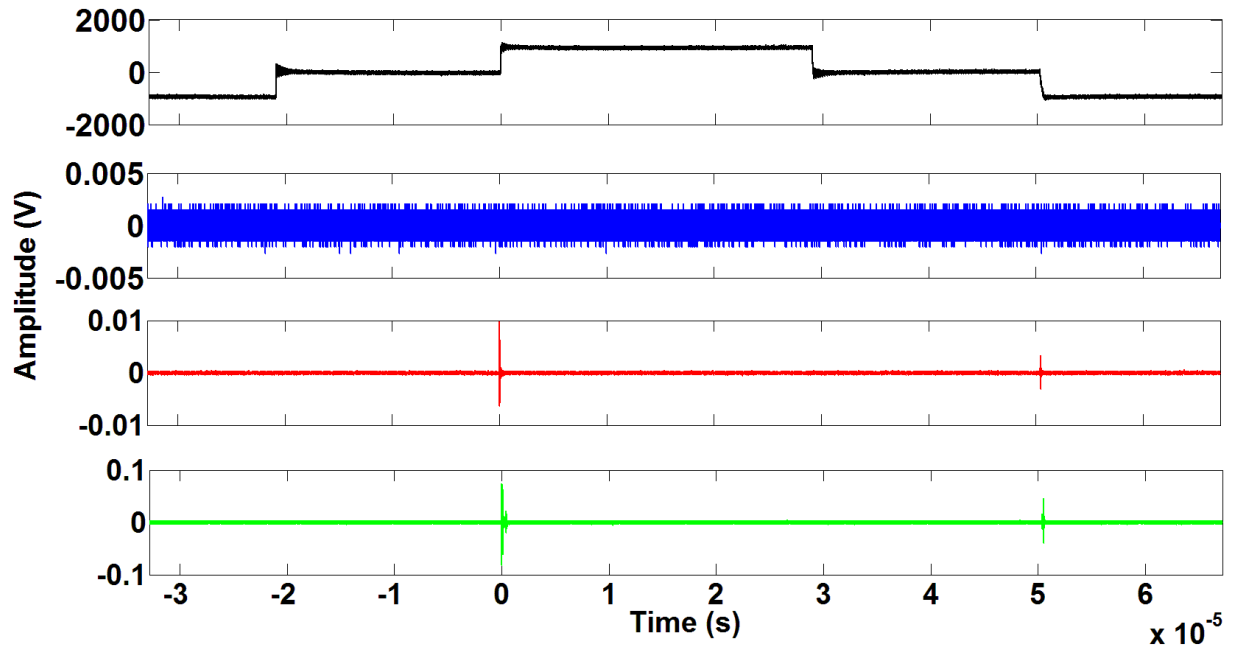


Figure II.22: PWM like voltage shape (black), Rogowski sensor signal filtered at 290 MHz (blue), Jack-SMA sensor signal filtered at 290 MHz (red), Jack-SMA sensor (with an additional capacitive effect) signal filtered at 290 MHz (green)

It can be seen that this cut-off frequency allows a complete denoising for the three sensors, nevertheless in the case of the Rogowski sensor the PDs signals also appear to be filtered. This is due to the fact that the bandwidth of this sensor is not sufficient when using high-pass filters. Indeed, the bandwidth (at -3dB) of the sensor does not exceed 80 MHz and since the filter cut-off frequency is higher, all the signals are filtered. Subsequently, only the optimized Jack-SMA and Jack-SMA sensors will be studied.

PDIV and PDEV were measured for different pressure values. Discharges were detected using a Jack-SMA sensor filtered analogically using different cut-off frequencies (185, 290 and 390 MHz). The PD signals were observed for the three different cut-off frequencies simultaneously. For the conditions under study, only the filter cut-off frequencies above 290 MHz provides full electromagnetic  $dV/dt$  noise removal.

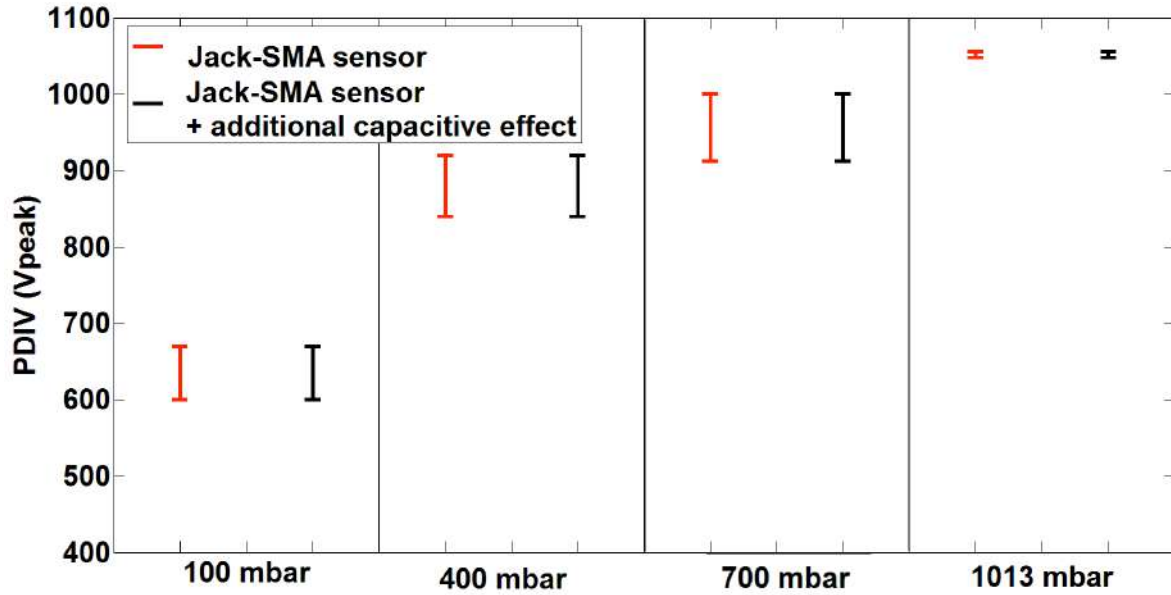


Figure II.23: Influence of pressure on PDIV for two sensors filtered at 290 MHz

Not surprisingly, the PDIV value decreases with pressure and whatever the filter for each pressure (from 100 mbar to 1013 mbar), PDIV remains the same. It can be seen in the figure that there is no difference on the PDIV between the Jack-SMA sensor and the optimized Jack-SMA sensor. This is due to the filtering, which eliminates a large part of the noise and therefore allows the detection of the PDs when their amplitude is sufficiently large. In some cases, since the amplitude of the PD is low, it is difficult to distinguish the signal associated with a discharge of the white noise induced by the acquisition system with the Jack-SMA sensor while the optimized Jack-SMA amplifies the signal associated with the PD and allows its detection.

## II.6.2 Influence of the cut-off frequency of the filter on detection

As we have seen previously, the cut-off frequencies do not influence the measured PDIV, but it is interesting to observe their influences on the amplitude of the PDs measured.

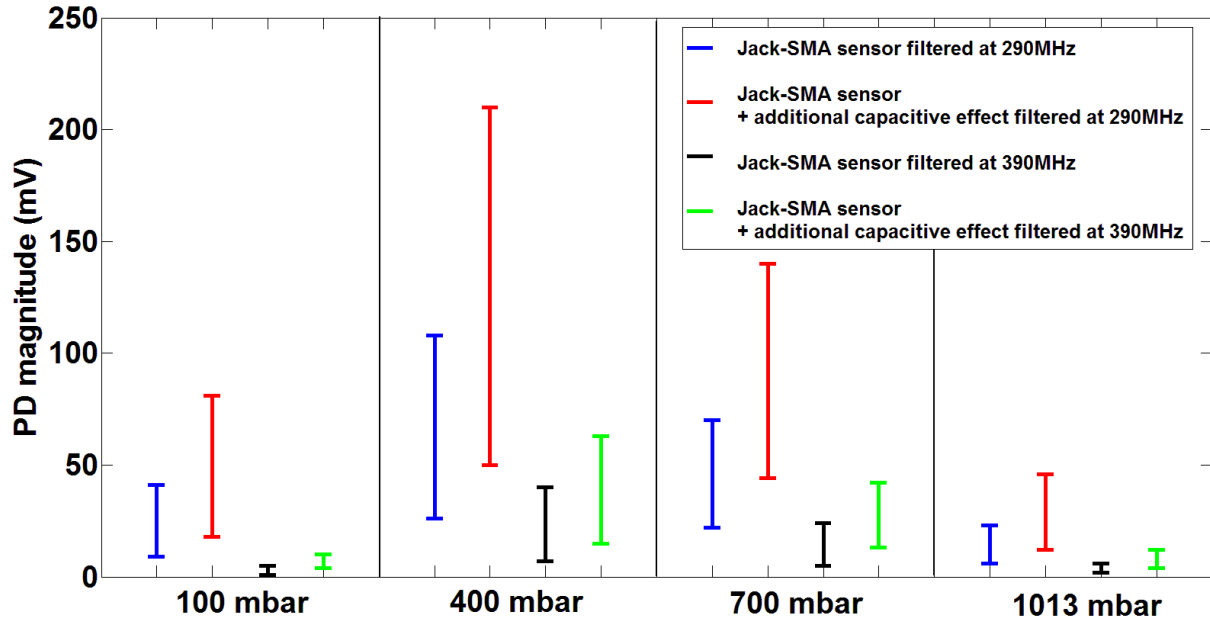


Figure II.24: Influence of filter cut-off frequencies on the PDIV at different pressure values for two sensors

It can be seen that an increase in the cut-off frequency of the filters induces a decrease in the amplitude of the measured PD signals. It can be observed that regardless of the cut-off frequency of the filters, the optimized Jack-SMA sensor makes it possible to recover a signal with a greater amplitude. The detection is thus improved because the SNR is higher.

However, under PWM, the cut-off frequency does not lead to errors on the PDIV. It is therefore important to study the spectrum of the PDs under PWM to understand this difference with the AC case.

### II.6.3 Spectral analysis

In order to confirm the influence of pressure on the amplitude of high-frequency components, the same study as the one performed under AC was undertaken for PWM-like voltage.

Nevertheless, it is more complex in this case to analyze the frequency content since it is necessary to remove all the noise induced during the switching while preserving the “entire” PD signal.

Hence, it was decided to follow the proposed procedure to carry out this study:

- Measure of PDIV (using the appropriate filter)
- Acquire the signal without any filtering, for a voltage value of 90% of PDIV (signal without PD)
- Acquire the signal without any filtering at PDIV (signal with PD)
- Calculate the difference between the signal with PD and the signal without PD
- Calculate the frequency spectrum of the difference

This procedure has some limits:

- If the filter is not adapted, there may be an error on the PDIV
- Generally for a voltage value of 90% of PDIV, the PDEV is reached but in some cases this may not be the case
- This procedure is only valid if the noise is repeatable, if the noise varies too much from one acquisition to another the analysis will be totally false

In this case, it can be seen that the amplitudes of the frequency components are in the same range for all the pressure values. It has therefore been decided to normalize all the frequency spectra with respect to the amplitude of an identical frequency component for the four pressure values. This makes it possible to observe the variation in the shape of the frequency spectrum as well as the modification of the amplitude of the frequency components as a function of the pressure.

The average of the signals with and without PD can be seen in Figure II.25.

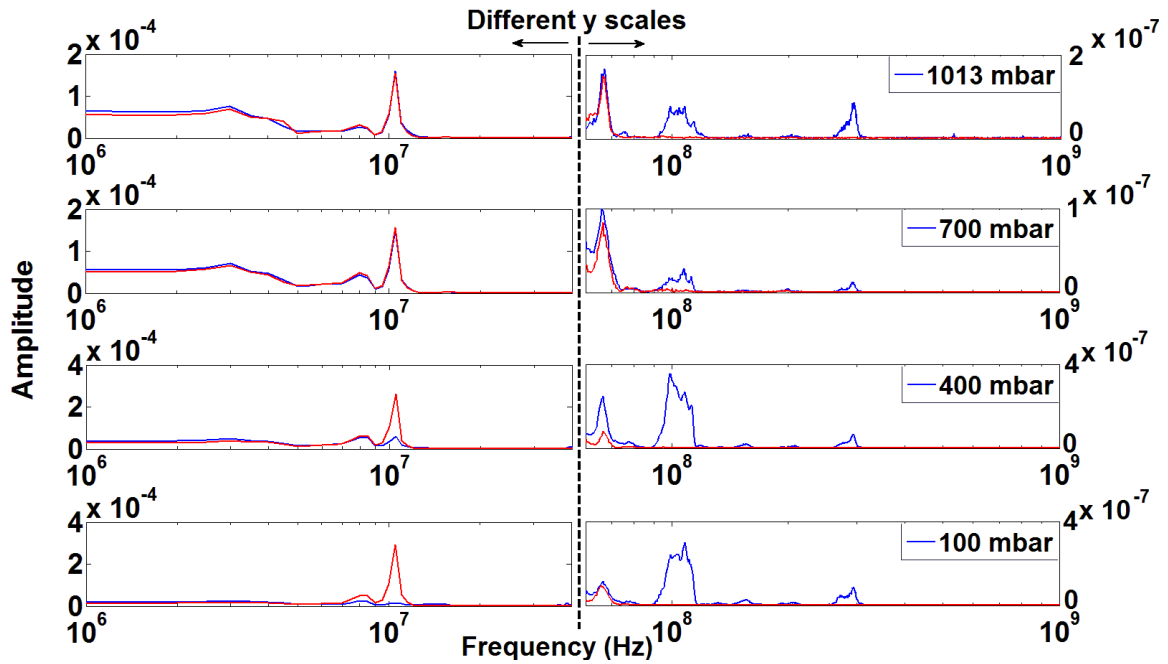


Figure II.25: Sensor signal spectrum without any filtering for a voltage value of 90% of PDIV (red) Sensor signal spectrum without any filtering at the PDIV (blue)

First of all, it is important to note that the spectrum of the PD signals under such conditions extends over a wider frequency range than that observed under AC voltage. The question is to know if this is due to a change in the discharges nature.

In the Figure II.26, the magnitude of high-frequency components (80 – 400MHz) decreases with pressure while the amplitude of the low-frequency components (8MHz – 80MHz) increase. Such

behavior may be detrimental to the accuracy of the PDIV measurements. For a pressure of 100 mbar, the magnitude of the components above 300 MHz for the PD spectrum is very small.

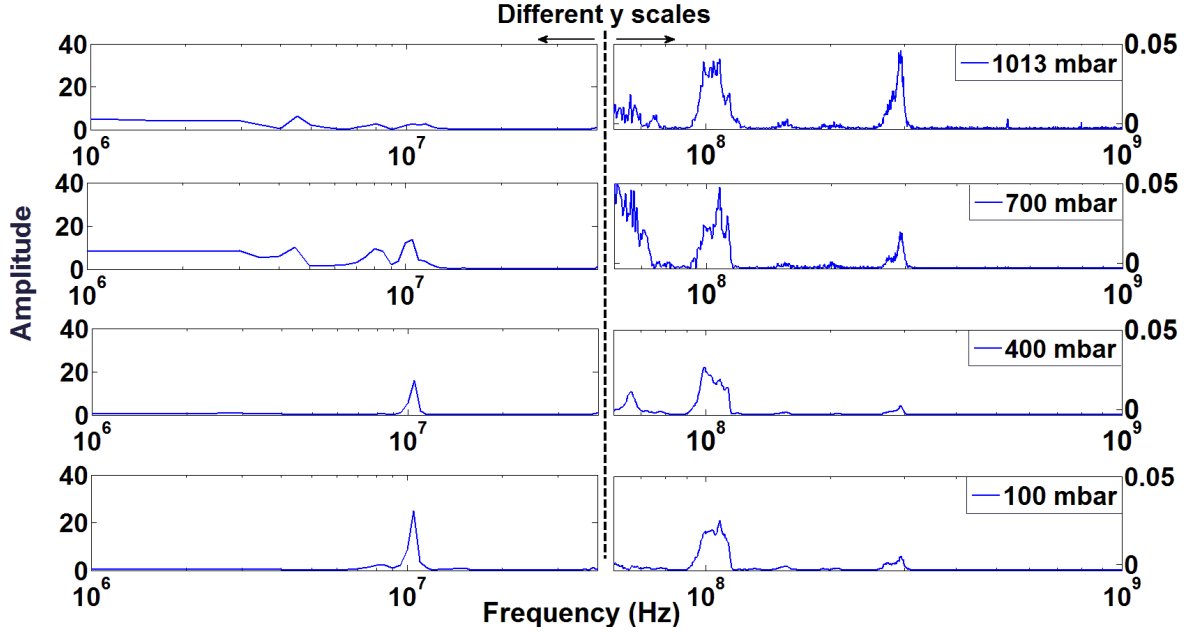


Figure II.26: Normalized changes of PD spectrum under PWM-like voltage as a function of pressure

It may be asked, how it is possible to detect PDs under PWM because it has been observed in the Figure II.26 that there are very few frequency components above 300 MHz and the cut-off frequency of the high-pass filters is about 290 MHz. This is due to the fact that our analogical filters are not perfect, according to the frequency response given by the manufacturer the different levels of attenuation are as follows:

- loss < 1.5 dB at 290 MHz
- loss of 3 dB at 245 MHz
- loss > 20 dB at 190 MHz

It is therefore possible to detect the PDs with this filter because, despite the cutoff frequency of 290 MHz, some of the lower frequency components are not attenuated.

## II.7 Limits of the detection method

It has been observed previously that the PD spectrum is modified when the pressure decreases. It therefore seemed interesting to determine the limits of the detection method. The PDIV research and the observation of the discharge amplitude have been carried out for a pressure range between 200 mbar and 40 mbar.

The study could not be carried out for lower pressure values due to the inaccuracy of the pressure measurement which was about 5 mbar and an error well above 10% below 40 mbar was observed.

The tests were performed under AC and PWM like voltage on twisted pair and the detection was achieved thanks to the Jack-SMA sensor.

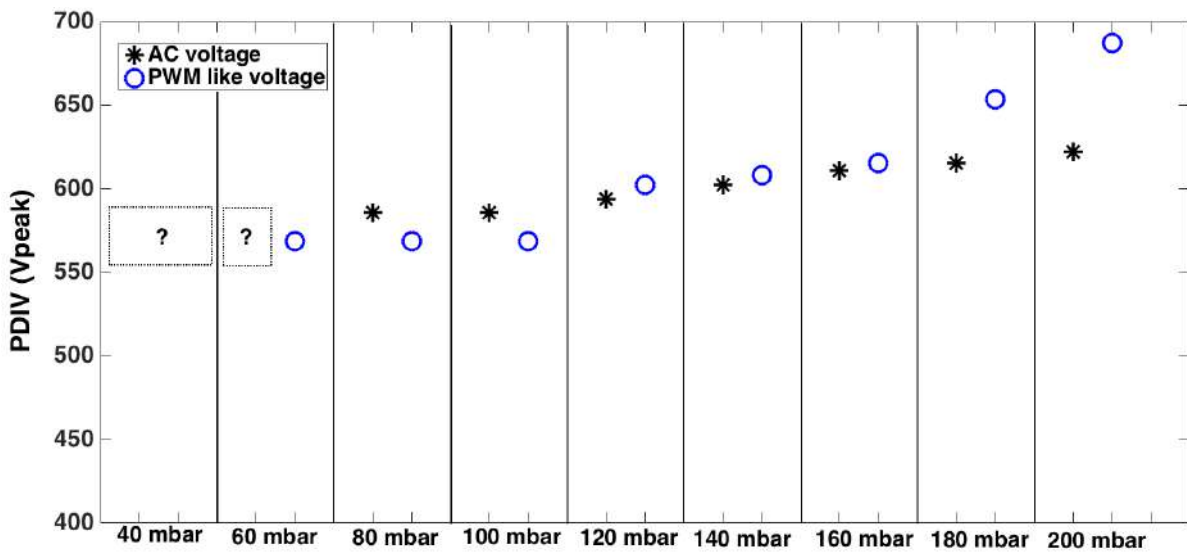


Figure II.27: Search for signal disappearance (PDIV)

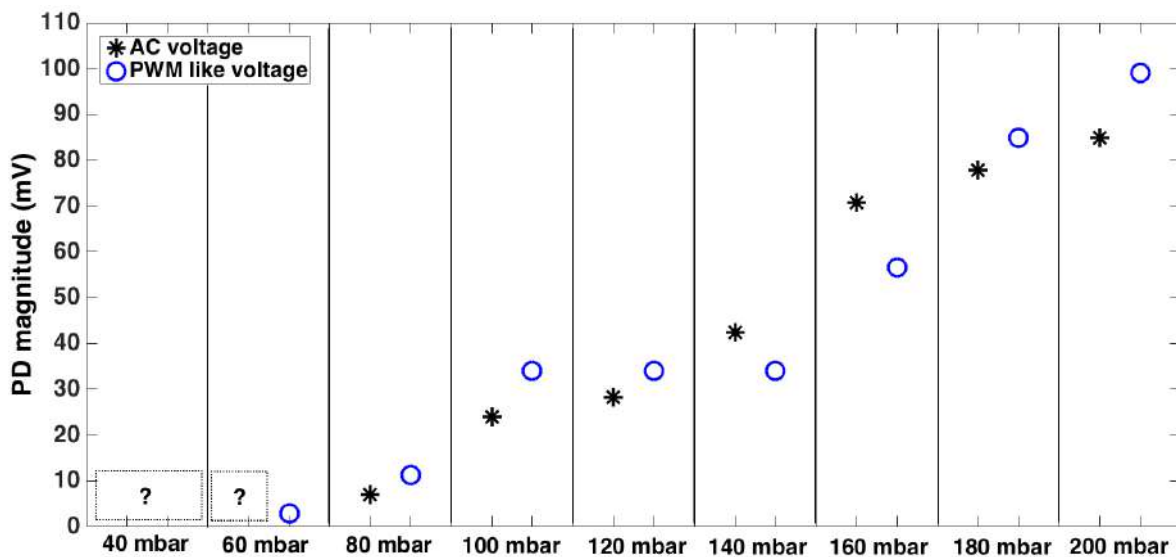


Figure II.28: Search for signal disappearance (PD magnitude)

First of all, it is important to specify that at 60 and 40 mbar a glow discharge was observed along the twisted pair for a voltage amplitude of 550 V under AC and PWM like voltage (Figure II.29).

Nevertheless, Figure II.27 and Figure II.28 show that at 40 mbar, no electrical signal is detected. At 60 mbar, PDs signal are only measured under PWM like voltage.

Compared to the AC case, it can be assumed that the signals disappear for lower values of pressure under PWM because the PDs spectrum spreads over a higher frequency range. A greater decrease in pressure is necessary to reduce the amplitude of the high-frequency components of the PDs signals.

Since below 40 mbar, whatever the voltage waveform, it seems that the frequency spectrum spreads over a frequency range too low to be detected using our systems. It will therefore be necessary to use another detection method, if applications in low pressure range are considered.

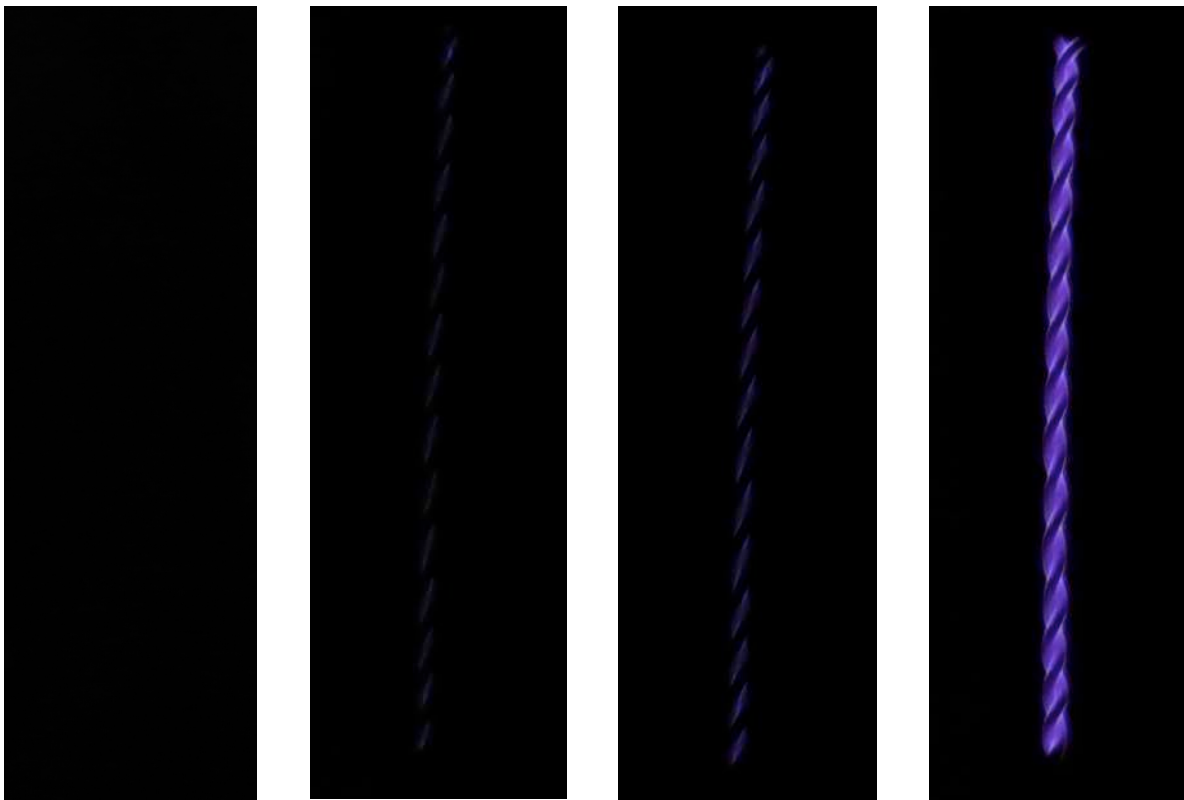


**Figure II.29: Influence of the pressure on the “light” emitted by PDs on twisted pair at PDIV for a frequency of 10 kHz**



## II.8 Conclusion

The results presented in this chapter showed that pressure has a significant influence on the detection of partial discharges, and specifically on their characteristics.

A decrease in pressure causes a change in the frequency spectrum of the partial discharge. High-frequency components of the discharge signals tend to decrease or even disappear under very low pressure.

In addition, the sensors used are sensitive to rapid current variations. If the frequency components are shifted to lower frequencies, the bandwidth of the sensors may not be sufficient to detect these signals. An error in determining the PDIV can be made in this case. Below 40 mbar (or 60 mbars) depending of the voltage waveform, the proposed method is no longer functional and the sensors no longer detected any signals, despite the presence of discharges [45].

As detection in PWM voltage requires the use of high-pass filters to remove the noise induced by switching, there may be a complete suppression of the frequency components associated with the PDs. However, we observed that the discharge frequency spectrum covers a much larger frequency range than with AC. Therefore, the method was functional regardless of the pressure and voltage form tested.

It would nevertheless be interesting to perform further analysis on the changing nature of the discharges according to pressure in order to optimize detection systems.

Such a study needs the development of a complete understanding of the discharge mechanisms versus the pressure and therefore of the nature of the discharge itself which is far from the objective of this work.

Noise filtering is an important issue. The choice of the cutoff frequency remains a difficult task because it is dependent on the analog filters available during testing, of the pressure as observed above as well as the expertise of the operator.

It thus seems important to optimize filter choice. To do this, it is possible to use digital filters that make it possible to have an infinite number of filters available. However, this solution still requires significant expertise regarding the selection of the filter cutoff frequency.

In the industry, it is often difficult to have an expert who can participate in all tests, especially if detection is included for health-monitoring applications. This is why it is necessary to develop a fully automated digital method to replace the expertise of an operator. The next chapter proposes such a solution.





## **Chapter III. Development of a digital processing method to remove noise**



### III.1 Context

When seeking to detect Partial Discharges in equipment supplied by inverter using PWM for e.g., a key challenge is to distinguish the raw signal with respect to electromagnetic noise induced by fast switching inverters. The magnitude of the signal associated with Partial Discharges generally has an amplitude of several tens of mV, while the magnitude of the noise signal is on the order of several hundred mV and depends on the voltage magnitude. From a frequency perspective, the spectrum of a discharge may extend up to the GHz range, while the noise spectrum does not extend beyond a few hundred of MHz [46].

In our work, a simple technique for observing the presence or the absence of a discharge was to filter the raw signal in order to retrieve only the high-frequency components of the signal using analog high-pass filters. While this technique works well, some external parameters can alter the discharge spectrum like the pressure for e.g..

Another important point is that in aeronautical environments, some equipment operates under pressure and temperature conditions that can vary greatly. These environmental condition variations can alter the signals associated with PD. The denoising technique must therefore work regardless of the operating conditions.

This chapter discusses the use of wavelets as digital processing for this purpose.

### III.2 Noise source

As PD measurement is performed in industrial environment, the presence of noise in the signal of interest is therefore inevitable. To be recognized as a PD, the detected signal should therefore appear with sufficient recurrence and be large enough to be detected as something other than just random noise.

We can divide the main sources of noise into four categories, classified by the type of interference they produce [47], [48]:

- **Periodic pulse interference** caused by power electronics or other periodic operations.
- **Discrete spectral interferences (DSI)** embody a continuous sinusoidal signal and can be caused, for example, by AM/FM radio emission or power line communication systems.
- **Stochastic pulse interference** amplitude and moments of random occurrence caused by operations of occasional workers, power electronics, lightning strikes...
- **Other noise** involving interference of the measurement circuit and ambient noise [49]

Of all the external interference types mentioned above, DSI can be identified and eliminated in the frequency domain, as that interference has a narrow band frequency spectrum centered around the dominant frequency, while PD pulses have a relatively wide frequency spectrum band. All PDs that occur at the same instant of periodic pulses are lost, which is undesirable. But it is very difficult to

identify and eliminate stochastic pulse interference because it has many features in common (both in time and frequency) with PD pulses. Methods to eliminate interference must thus be continuously explored to improve the sensitivity of PD measurements on-site and/or online.

In most cases, external interference can cause false indications, thereby reducing the credibility of PD measurement as a diagnostic tool. Since this is a recognized problem, significant research has been conducted in this area, and several techniques to remove this external interference have been proposed. Narrowband detectors achieve somewhat positive results, though best results were obtained by balanced bridge arrangements and by pulse-discriminating circuits [31]. But these analog noise suppression methods are laborious, requiring both additional equipment and critical adjustments that might not be very easy in on-line conditions.

Figure III.1 shows that it is impossible to distinguish the presence of the PD signal. The amplitude of the noise induced by switching under PWM voltage being too large compared to the PD amplitude.

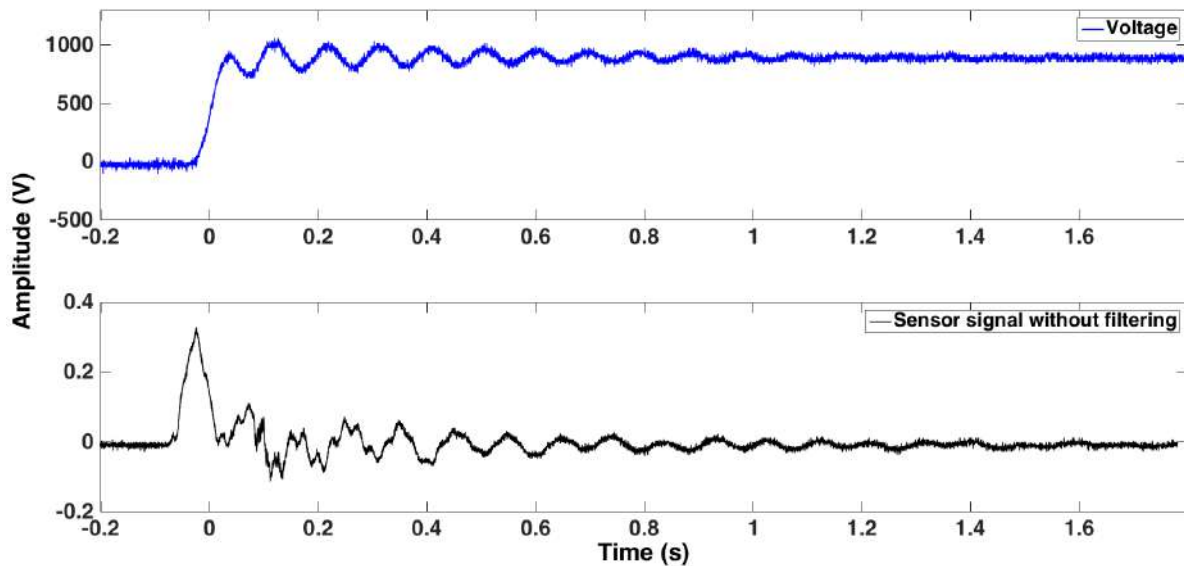


Figure III.1: Noisy signal induced by switching (black)

### III.2.1 Noise suppression techniques

The biggest problem with these measurements lies in their sensitivity and accuracy. Good sensitivity allows detection of low amplitude PD signals buried in noise. Good accuracy is related to the ability to distinguish signal PD from another similar shape of signals.

In literature, we can find different techniques for extracting PD signals from raw data. The article [50] performed a comparison of some of these noise suppression methods based on several parameters.

- Fast Fourier Transform-Based Denoising (Clustering techniques [51], [52])
- Low-Pass Filtering
- Wigner-Ville Distribution-Based Denoising
- Short-Time Fourier Transform-Based Denoising

- Least Mean Square Approach
- Frequency-Domain Adaptive Filtering
- Recursive Least Squares and Exponentially Weighted Recursive Least Squares Methods
- Matched Filtering
- Notch Filtering
- Wavelet Denoising

In this paper, all these methods are compared according to the Mean Squared Error (MSE) between the raw signal and the noise-suppressed signal as well as the execution time of filtering.

By definition, normalized MSE is:

$$MSE = \frac{\sum_{i=0}^n [Y(i) - X(i)]^2}{n\sigma_n^2} \quad (\text{III.2.1})$$

With X the noisy sequence, Y the filtered sequence, n the number of samples for which X is defined, and  $\sigma_n^2$  the total noise power.

Based on these criteria, Wavelet Denoising and Low-pass Filtering methods have proven to be the most effective. In our case, since the electromagnetic noise induced by switching has low-frequency components, the low-pass filtering is not possible. The best technique for extracting PD signals is therefore the Wavelet Denoising method.

Two types of measurements are made to analyze the discharge frequency spectrum for systems powered by the inverter: first the acquisition of existing noise for a voltage below the PDIV ( $\approx$  PDIV – 10% PDIV) and after, an acquisition for a voltage higher than the PDIV. Note that, in this case, the value of PDIV was determined by means of high-pass filtering.

The Short-time Fourier transform (STFT) results reported in Figure III.2 show that the spectral energy of only the disturbance propagates up to 150 MHz, but only during “on/off” switching. Thereafter, the remaining ringing is negligible (above 100 MHz). Figure III.3, shows that the spectral energy under PD spreads up to 350 MHz. It is therefore possible to filter noise and retrieve part of the PD signal [53]. However, finding this cut-off frequency can be complex and depends on the user’s experience. It is therefore necessary to use an automated method capable of matching all configurations.



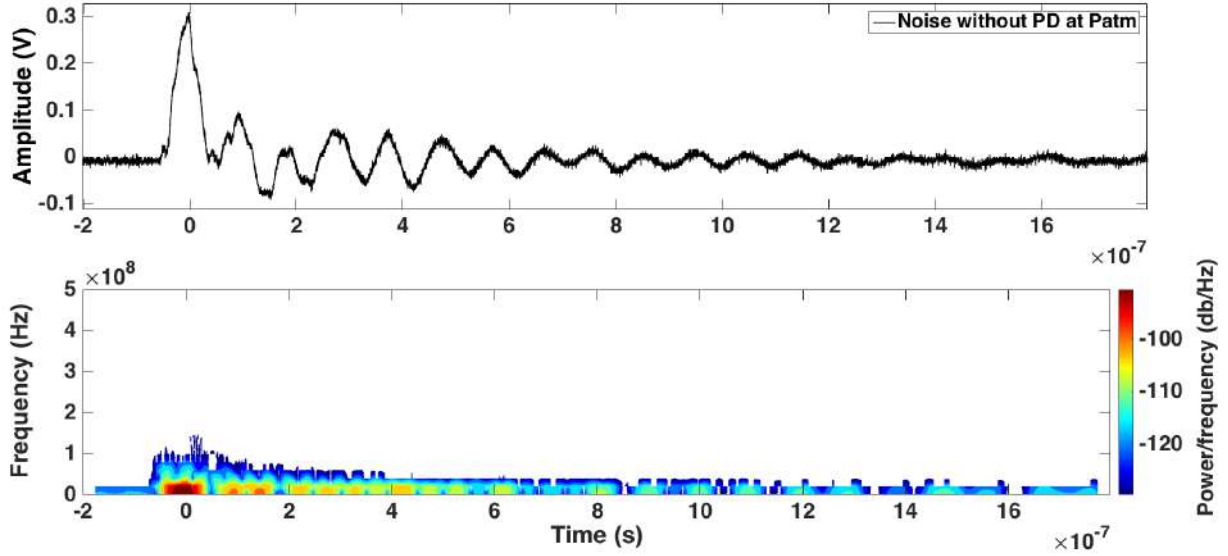


Figure III.2: Noisy signal induced by switching without PD (top curve), STFT of noise without PD (lower curve)

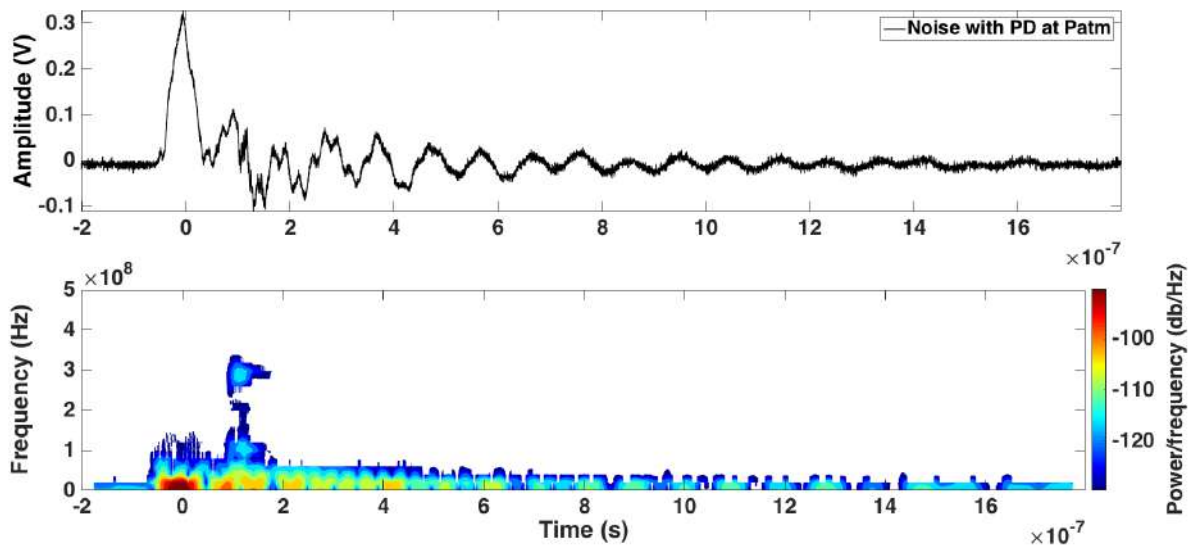


Figure III.3: Noisy signal induced by switching with PD (top curve), STFT of noise with PD (lower curve)

### III.3 General understanding of the wavelet transform

Invented by Jean Morlet, the wavelet transform (Wavelet Transform - WT), just as the Fourier transform (Fourier Transform - FT) is a mathematical signal processing tool that decomposes a signal into different basic functions. The basic functions of the FT being the sine and cosine, the result of applying this method provides information only on the frequency content of the signal of interest. The disadvantage lies in not knowing the moment at which each frequency component appears.

Besides that, the basic functions of the WTs called “wavelets” allow two-dimensional resolution in the frequency and time domains. The result of these two transforms represents the projection of a signal based on wavelets for the WT or complex exponential functions for the FT.

Moreover, in comparison, the FT shows extreme efficiency for analyzing periodic phenomena, time-invariant and stationary techniques, while WT screens all components produced by transients, of variable time and non-stationary [47], [54].

Therefore, with the PD signal being of a non-periodic nature and exhibiting very fast transient characteristics, the WT approach seems more suitable in this context. The method has proved its ability to denoise PD signals, but mainly under AC voltage and in the presence of white noise [49], [55]–[57]. It is therefore necessary to check whether this method is functional for denoising PDs occurring under PWM. We used this technique to remove noise superimposed on PDs.

### III.3.1 Wavelet definition

To understand the wavelet transform, it is first necessary to understand what a wavelet is. As its name indicates, a wavelet is a wave of limited duration. Generally speaking, a wave is an oscillating function, such as a sine wave extending over the entire time axis and therefore with an infinite energy. A wavelet is a wave of zero means and with finite energy concentrated over a time interval [54].

Mathematically, a function can be called wavelet if it fulfills admissibility and regularity conditions.

➤ Admissibility property

$$\int \frac{|\Psi(\omega)|^2}{|\omega|} d\omega < +\infty \quad (\text{III.3.1})$$

With  $\Psi(\omega)$  the Fourier transform of the wavelet function  $\psi(t)$ .

This property ensures the reconstruction of a signal without loss of information. It follows that a wavelet must have a type of spectrum band pass and a zero-time average. Given this latter feature,  $\psi(t)$  must have the shape of a wave.

➤ Regularity property

This property requires the wavelet function to be smooth and concentrated in time and frequency domains.

Figure III.4 provides a clear view of these two conditions with a wavelet called the “Daubechies” wavelet. While the sinusoid is periodic and therefore predictable, the wavelet has an irregular and asymmetrical feature. We can easily deduce that the signals with transients will be better interpreted from irregular wavelets than with sinusoids.

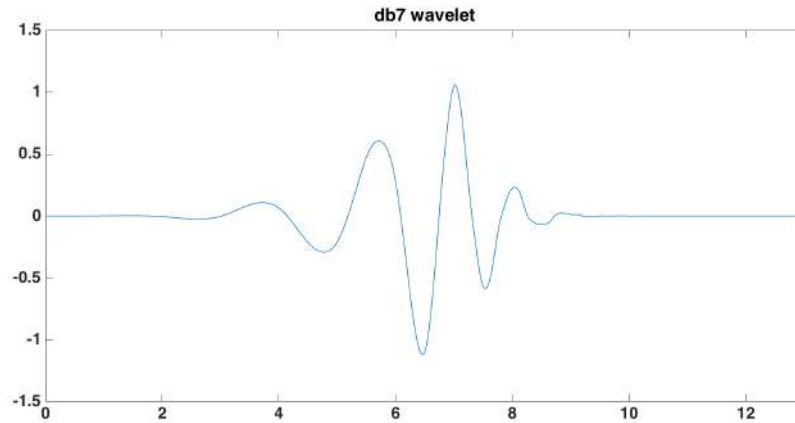


Figure III.4: Daubechies wavelet

### III.4 Wavelet analysis

The time-frequency performance given by the wavelet analysis makes it possible to divide the signal into several pieces and to analyze content separately. This method enables us to know all the frequency components of a signal present at a given time.

More specifically, wavelet analysis uses a “window” whose dimensions are adjustable to fractionate the signal and observe only a small portion (see Figure III.5). This window, contained in the wavelet function, is then moved along the signal. The spectrum is calculated for each position. This process is then repeated for other window sizes. Lastly, the result is a set of representations of time-frequency signals, where each has a different resolution. For that reason, wavelet transform is described as multi-resolution analysis, as it provides information from overview down to details.

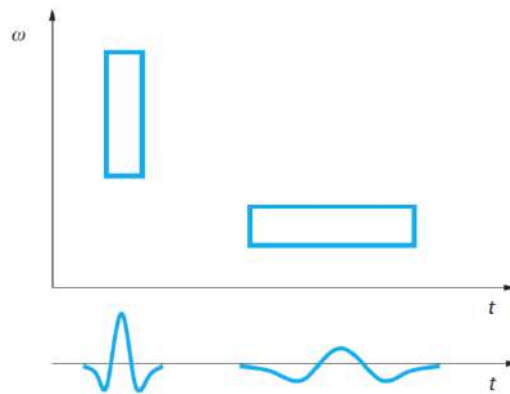


Figure III.5: Window and wavelet function

Upon application, terms of “scale” are used rather than frequencies. The scale is essentially the opposite of the frequency: large scales provide an overview, an approximation, while small scales insist on details. In fact, as the scale increases, the selection window is expanded to include an increasingly global view. The transition from large to small scales is used to gradually zoom in the signal of interest.

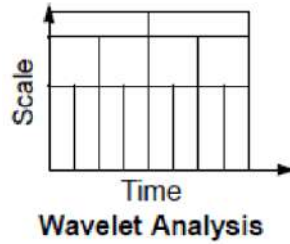


Figure III.6: Multiresolution decomposition

It is therefore reasonable to suggest that this signal-processing tool has many advantages, including:

- **Time-frequency analysis:** each frequency and time of occurrence are known.
- **Multi-resolution analysis:** low resolution for the overall view and high-resolution for details.
- **Local analysis:** surrounded by a portion of a long signal.

Two main areas exist in wavelet transformation: the continuous wavelet transform and the discrete wavelet transform from which many other variations are derived. The main theoretical concepts of these methods are described below.

### III.5 Continuous wavelet transform

The continuous wavelet transform (Continuous Wavelet Transform - CWT) of a finite energy signal, provides a series of two-dimensional coefficients  $\gamma(s, \tau)$  from this one-dimensional signal, locating the signal in the time and frequency domains, as defined by the following formula:

$$\gamma(s, \tau) = \int_{-\infty}^{+\infty} f(t) \psi_{s,\tau}^*(t) dt \quad (\text{III.5.1})$$

where

- $s$  (scale) is a scaling parameter,  $s > 0$
- $\tau$  (translation) is a second displacement parameter
- $\gamma$  are the wavelet coefficients, scale functions and position
- $\psi_{s,\tau}(t)$  are wavelets (basic)
- $*$  indicates complex conjugation

The WT calculates the correlation between the signal of interest and a modified wavelet  $\psi(t)$ . Thus, the more the analyzed signal portion and wavelet  $\psi_{s,\tau}(t)$  are similar, the higher the value of the  $\gamma$  coefficient. In fact, all  $\psi_{s,\tau}(t)$  wavelets are derived from a single function  $\psi(t)$ , called the “mother wavelet” scaled and translated as follows:

$$\psi_{s,\tau}(t) = \frac{1}{\sqrt{s}} \psi\left(\frac{t-\tau}{s}\right) \quad (\text{III.5.2})$$

With  $\sqrt{s}$  divider that is the energy normalization factor so that each “child” wavelet has a wavelet energy equivalent to that of the “mother” wavelet [58]. Obtaining a CWT consists applying five steps successively:

1. Choosing a “mother” wavelet.
2. Calculating the correlation index between the selected wavelet and the beginning of the signal to be analyzed, equal to the unit in case of perfect equality.
3. Continuous shift of the wavelet to the right on the time axis and repeating steps 1 and 2 until the end of the signal.
4. Scaling (expanding) the wavelet and repeating steps 1 to 3
5. Repeating steps 1 to 4 for all scales.

The theory presented above gives a good idea regarding the usefulness and operation of WT in the continuous area. However, in practice, the CWT form of equation (III.5.1) is not an option for three reasons:

1. **Redundancy:** CWT results from the continuous movement of a window, whose dimensions are also continuously changed along the signal of interest, and gives the level of correlation between the two. The basic functions in the continuous area do not respect the property of orthogonality, resulting in significant redundancy in the coefficients obtained.
2. **Infinity wavelet:** as every “child” wavelet results from a changed parameter of the “mother” wavelet, there is an uncountable number of basic functions, each leading to a different transform. Limits must be set to work with a reasonable number of functions.
3. **CWT of many functions have no analytical solution:** WT of some functions are only computable numerically, hence the need to use faster algorithms to benefit from the full power of the WT.

Because of these problems, the discrete wavelet transform (Discrete Wavelet Transform - DWT) was introduced. The DWT is described below, and it is worth specifying the major difference with the continuous version. First, both deal with discrete signals as measured with a certain sampling frequency. The continuous or discrete appearance, therefore, qualifies the analyzed signal. In fact, in the CWT case, it is the factor and translation scale which are continuously determined.

## III.6 Discrete wavelet transform

The successive steps from the continuous wavelet transform to the discrete model are detailed below.

### III.6.1 First step

A first step towards the discrete transform is to eliminate redundancy by discretizing the wavelet. Of course, the basic functions are continuous, but it is then the scale  $s$  and translation  $\tau$  parameters that vary stepwise and not continuously. The introduction of this property in equation (III.5.2) gives:

$$\psi_{j,k}(t) = \frac{1}{\sqrt{s_0^j}} \psi\left(\frac{t - k\tau_0 s_0^j}{s_0^j}\right) \quad j, k \in \mathbb{Z}; s_0 > 1 \quad (\text{III.6.1})$$

With  $j$  and  $k$ , respectively, parameters related to the wavelet scaling and translation.

In most cases, the parameters are fixed,  $s_0 = 2$  and  $\tau_0 = 1$ , in order to obtain a dyadic sampling frequency of the frequency axis and of the time axis, giving the following result:

$$\psi_{j,k}(t) = \frac{1}{\sqrt{2^j}} \psi\left(\frac{t - k2^j}{2^j}\right) \quad j, k \in \mathbb{Z} \quad (\text{III.6.2})$$

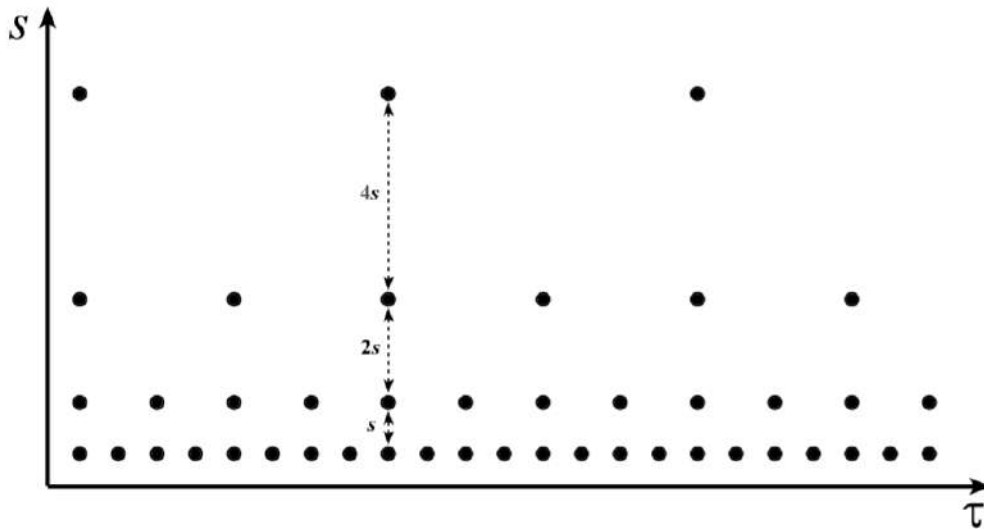


Figure III.7 : Localization of the discrete wavelets in the time-scale space on a dyadic grid [59]

The next step is to make the basic discrete wavelet orthonormal. The wavelets are then orthogonal to their own dilatations and translations, and this is made possible just by choosing a proper wavelet mother:

$$\int \psi_{j,k}(t) \psi_{m,n}^*(t) dt = \begin{cases} 1 & \text{if } j = m \text{ and } k = n \\ 0 & \text{otherwise} \end{cases} \quad (\text{III.6.3})$$

### III.6.2 Second step

The second disadvantage of CWT, that is, the infinite number of wavelets, is remedied by introducing the scaling function  $\varphi(t)$ . The concept is to set an upper bound to the index  $j$  in the discrete wavelet equation (III.6.2), in turn imposing a lower limit to reduce the wavelet spectrum. Figure III.8 provides a clear picture of the following explanation. When calculating WT, the wavelets are repeatedly expanded and translated in the time domain, this being carried out by increasing the indices  $j$  and  $k$  of equation (III.6.2). With index  $k$  varying the translation function, an upper terminal is automatically linked to the signal length to be analyzed. The extent of the wavelet spectrum is reduced by half each time that the index  $j$  is incremented by 1. As mentioned earlier, the spectrum of a wavelet can be seen as a band pass filter, and thus a series of dilated wavelets create a band pass filter bank as shown in Figure III.8.

If such a filter bank covered the entire signal spectrum, its reconstruction would be perfect, but the computing time would make the operation impractical. The function  $\varphi(t)$  is used for that reason: once the bandwidths of wavelet spectra reaches a defined minimum, such as from  $j = n + 2$  in Figure III.8, they are replaced by a low-pass filter formed by the spectrum of the scaling function  $\varphi(t)$ .

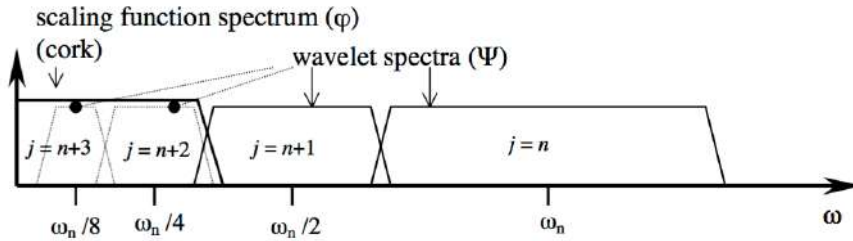


Figure III.8: Spectra of a scaling function  $\varphi(t)$  and a dilated wavelet  $\psi(t)$  [59]

The scaling function, with a spectrum similar to a low-pass filter coupled to dilated wavelets, and for which each spectrum is band pass type, forms a filter bank to cover the entire spectrum of the signal to be analyzed.

### III.6.3 Third step

Now, only the last CWT disadvantage remains to overcome, that is, the non-existence of analytical solutions before determining all the concepts necessary for defining the discrete wavelet transform. Implementing the WT as a filter bank can solve this.

The processed signals result in most instances of a time sampling. The last change to be made then is to make the discrete WT using an iterated version of a bank of digital filters.

It is possible to decompose the signal spectrum into various frequency bands thanks to wavelets and the scaling function. The successful design is to divide the signal spectrum by applying two filters: a high-pass and low-pass of the same bandwidth. However, the components selected by the low-pass filter still contain references to information that could be interesting. To retrieve these references, the application of two filters explained above is repeated with bandwidth reduced by half, giving two new sets of data. This can be repeated until satisfaction while the information is obtained. The WT is implemented as the repeated application of a bank of bandwidth filters, reduced at each iteration.

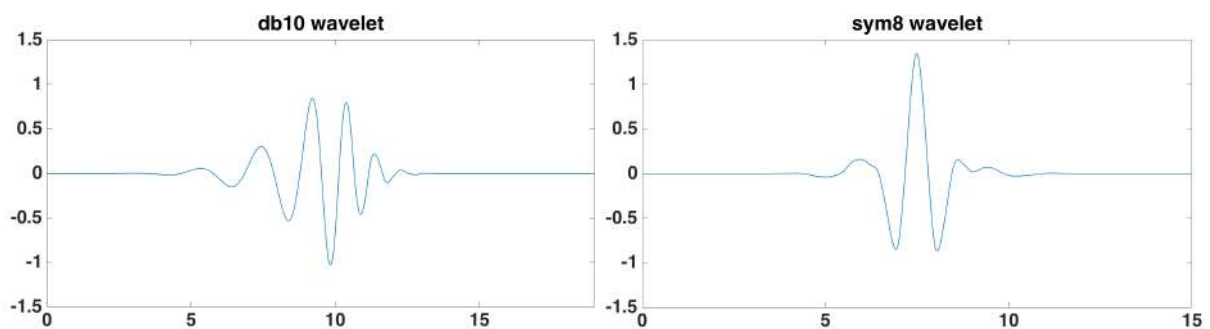
### III.6.4 Results

To summarize: the DWT performs a time-scale representation of a signal by digital filtering; filters of different cut-off frequencies are used to analyze the signal at different scales. Two filters, a high-pass (H) and a low-pass (L) therefore decompose the signal of interest into two parts, before being sub-sampled by two, to maintain the same amount of data to be processed at each iteration. Thus, low and high-frequency components are obtained, respectively called approximation coefficients (cA) and detail coefficients (cD) [48], [60]. The frequency content of these coefficients is limited by the Nyquist criterion.

Regarding the choice of the “mother” wavelet, it must be oriented to meet:

1. The existence of a scaling function  $\phi(t)$ .
2. The orthogonality of the results obtained by the WT.

Despite the variety of wavelet shapes, only some have those characteristics, the most common being Daubechies, Symlet, Coiflet [58]. Examples of these functions are shown below in Figure III.9. The integer K coupled to the diminutive of the name of the wavelet, for example, 10 in 'db10', is related to the number of zero moments.





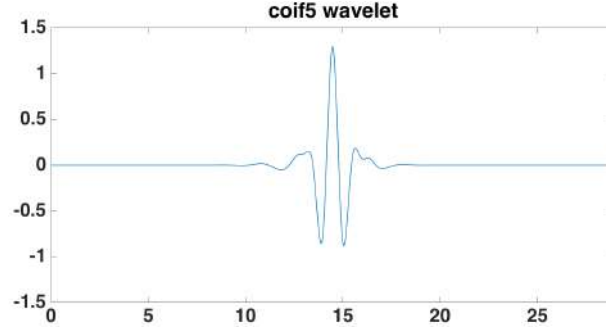


Figure III.9: Different wavelets shape: (from left to right: Daubechies, Symlet, Coiflet)

### III.6.5 Reconstitution

It is then possible to reconstruct the original time signal in reverse order. The approximation and detail coefficients are oversampled by two before passing through the synthesis filters, respectively low-pass filters (L') and high pass (H') synthesis. The filters used in the decomposition are called analysis filters, while those for reconstruction are called synthesis filters. Lastly, to retrieve the original signal, the high- and low-frequency components are added, a logical method called inverse discrete wavelet transform (*Inverse Discrete Wavelet Transform* - IDWT) expressed as:

$$f(t) = \sum_{k=-\infty}^{\infty} c(k)\varphi_k(t) + \sum_{j=0}^{\infty} \sum_{k=-\infty}^{\infty} d(j,k)\psi_{j,k}(t) \quad (\text{III.6.4})$$

with  $\varphi_k(t)$  and  $\psi_{j,k}(t)$  respectively obtained through the scaling function  $\varphi(t)$  and the mother wavelet  $\psi(t)$  as follows:

$$\varphi_k(t) = \varphi(t - k) \quad (\text{III.6.5})$$

$$\psi_{j,k}(t) = 2^{j/2}\psi(2^j t - k) \quad (\text{III.6.6})$$

with  $c(k)$  and  $d(j,k)$  representing respectively the coefficients of approximation and detail  $j^{\text{th}}$  level of the original signal.

Figure III.10 illustrates the principle where  $S$  is the starting signal and  $cAi$  and  $cDi$  are the approximation and detail coefficients at level  $i$ . The original signal, having been a  $J$ -level decomposition here, is retrieved by summing the coefficients of the approximation of the  $J^{\text{th}}$  level, every detail coefficient obtained from the  $1^{\text{st}}$  to the  $J^{\text{th}}$  level.

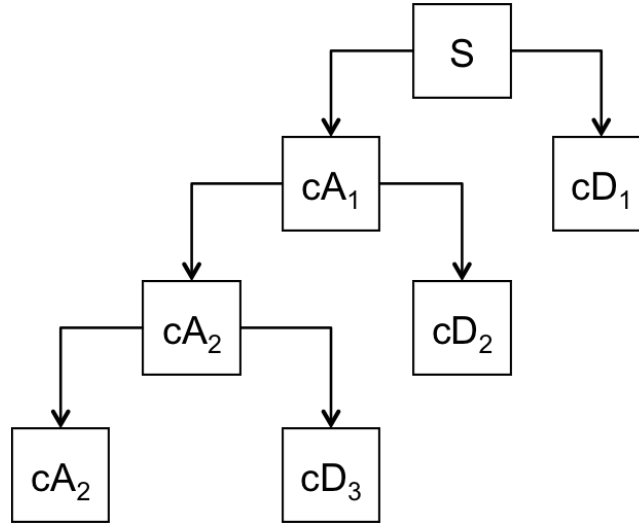


Figure III.10: Diagram of multilevel decomposition by DWT

It should be stated that the perfect reconstruction of the original signal could not be obtained in all cases. For this, the analysis and synthesis filters must be properly selected. Indeed, the step of subsampling the high- and low-frequency components induced distortion, or more exactly the spectra overlap phenomena, thus preventing reconstitution of the initial signal during the reconstruction step. To counter this problem, the choice of filters is not left to chance. During the multi-resolution analysis of a signal, orthogonal bases can be built from functions, such as scaling functions  $\varphi(t)$  and wavelet  $\psi(t)$ . These bases are then calculated by using a pair of filters  $h[n]$  and  $g[n]$  [61].

$$\frac{1}{\sqrt{2}}\psi\left(\frac{t}{2}\right) = \sum_{n=-\infty}^{+\infty} h[n]\psi(t-n) \quad (\text{III.6.7})$$

$$\frac{1}{\sqrt{2}}\varphi\left(\frac{t}{2}\right) = \sum_{n=-\infty}^{+\infty} g[n]\varphi(t-n) \quad (\text{III.6.8})$$

with

$$h[n] = \frac{1}{\sqrt{2}}\langle\psi\left(\frac{t}{2}\right), \psi(t-n)\rangle \quad (\text{III.6.9})$$

$$g[n] = \frac{1}{\sqrt{2}}\langle\varphi\left(\frac{t}{2}\right), \varphi(t-n)\rangle \quad (\text{III.6.10})$$

and

$$g[n] = (-1)^{1-n}h[1-n] \quad (\text{III.6.11})$$

### III.7 Denoising by wavelet transform

Noise removal of raw data using WT requires identifying noise components in order to ensure that signal reconstruction is free of unwanted components. The ability to differentiate noise compared to PDs signals can be improved by knowing various characteristics specific to each noise component: frequency bands occupied, shapes, attenuation . . .

It is essential to distinguish the noise components hidden in the signal in order to avoid removing high-frequency characteristics leading directly to the loss of valuable information, as would be the case when analyzing partial discharge signals.

The majority of existing techniques for noise suppression showed satisfactory performance for removing discrete spectral interferences (DSI). Indeed, DSIs are the easiest to detect as they do have some components to specify frequencies. On the downside, the largest difficulty in this area lies in the treatment of random types of impulsive interference whose time and frequency characteristics are very similar to those of PD signals [62].

The procedure for the standard denoising method proceeds in three steps:

1. Decomposition consists in selecting a mother wavelet and a level J to retrieve the coefficients resulting from application of the WT from the first to I levels.
2. Choice of the elimination coefficient threshold to suppress some components considered as unnecessary.
3. Reconstruct the original signal-free components suppressed by Step 2.

#### III.7.1 Settings parameters

To proceed with the optimal removal of interference, several parameters related to the nature of the signal of interest must be determined. Among them is the choice of the “mother” wavelet, determining the maximum level of decomposition, and lastly, the thresholding method.

##### 1) “Mother” wavelet

The selection of the “mother” wavelet used to analyze a signal is very important. Indeed, the application of DWT will provide even more maximum value coefficients if the shape of the wavelet is similar to that of the desired signal.

The theoretical shape of a PD signal follows that of a damped exponential pulse (DEP), or damped oscillatory pulse (DOP), depending on the detection circuit. Many studies have reached conclusions about the effectiveness of “Daubechies” wavelets designated by the abbreviation *dbK*, “Symlet” *symK*, and “Coiflet” *coifK*.

The WT can be defined as a similarity measurement. The more the wavelet and analyzed signal are similar, the higher the coefficients obtained after decomposition will be. A simple criterion for determining the optimal wavelet is to calculate the correlation coefficient first between a pulse PD and

the various existing wavelets. The higher the correlation, the better the similarity between the shape of the wavelet and that of the PD signal, which involves achieving higher coefficients.

The selection of the mother wavelet is generally based on the digital model of a PD pulse. However, in practice, the shape of a pulse PD varies depending on the detection method, test object, type of PD, location of PDs, and signal propagation and attenuation method. This significantly complicates the implementation of a filtering universal method.

## 2) Decomposition level

In general, the level of decomposition of a signal by DWT is limited to:

$$J = [\log_2 N] \quad (\text{III.7.1})$$

with  $N$ , the length of the analyzed signal. Nevertheless, as we use MATLAB® software [63], the length of the filter implemented by a wavelet then restricts the maximum possible number of levels.

$$J = \text{fix}(\log_2(N/N_w) - 1) \quad (\text{III.7.2})$$

with **fix** which rounded to the integer closest to zero and  $N_w$  corresponding to the length of the decomposition filter associated with the selected “mother” wavelet [60].

With respect to computation time, achieving the maximum level of decomposition is not recommended. The question of “when to stop” the analysis is then raised. A compromise must therefore be set between the speed of the algorithm and quality of results. This is done by evaluating multiple criteria. The most-used are the signal-to-noise ratio (SNR) and the correlation coefficient (CC). SNR expresses the signal power divided by the power of the ambient noise signal; CC measures the similarity between the original and filtered signal to eliminate interference and thus restore the PD signal with little distortion. Large SNR and CC values are sought.

The level of decomposition is therefore often selected by trial and error, or according to the frequency bands determined by the sampling frequency. Indeed, the greater the sampling frequency is, the greater the decomposition depth will be in order to recover the entire frequency spectrum.

## 3) Thresholding method

A very important concept is the thresholding method and the applied threshold value. With this, all component values above a determined limit are canceled.

The application of the thresholding can be either hard or soft:

### 1. Hard thresholding

$$f_h(x) = \begin{cases} x & |x| \geq t \\ 0 & \text{else} \end{cases} \quad (\text{III.7.3})$$

This function is known to keep the abrupt changes of the signal  $x$

2. Soft thresholding

$$f_s(x) = \begin{cases} \text{sign}(x)[|x| - t] & x \geq t \\ 0 & \text{else} \end{cases} \quad (\text{III.7.4})$$

This function is recognized for its effectiveness in relatively regular signal portions but unfortunately it sometimes overly smoothes some spikes.

Applying a hard threshold is generally preferred for PDs. Indeed, the coefficient values associated with PDs are higher and then give a better signal-to-noise ratio than soft thresholding.

## III.8 Applying the method

### III.8.1 Choosing between the CWT and DWT method

When the energy of the signal is finite, not all values of decomposition are needed to exactly reconstruct the original signal, when a wavelet that satisfies some admissibility condition is used. Usual wavelets satisfy this condition. In this case, a continuous-time signal is characterized by the knowledge of the discrete transform. In such cases, discrete analysis is sufficient and continuous analysis is redundant. But when a signal is recorded in continuous time, or on a very fine time grid, both analyses are possible. Due to the sample rate of the oscilloscope we used, both techniques are possible. To compare the two methods, our study focuses on the quality of denoising (signal-to-noise ratio) as well as its speed. Calculation times given below are not necessarily interesting as such, since they depend on the computer used to study both methods. However, the ratio of their respective duration is interesting because it enables highlighting the speed of one method with respect to the other.

To perform these tests, PD measurements were achieved on twisted pair of enameled wire fed by a PWM like power supply at atmospheric pressure (Figure III.11). The signals denoised by wavelet transform are compared to analogic filtered signals.

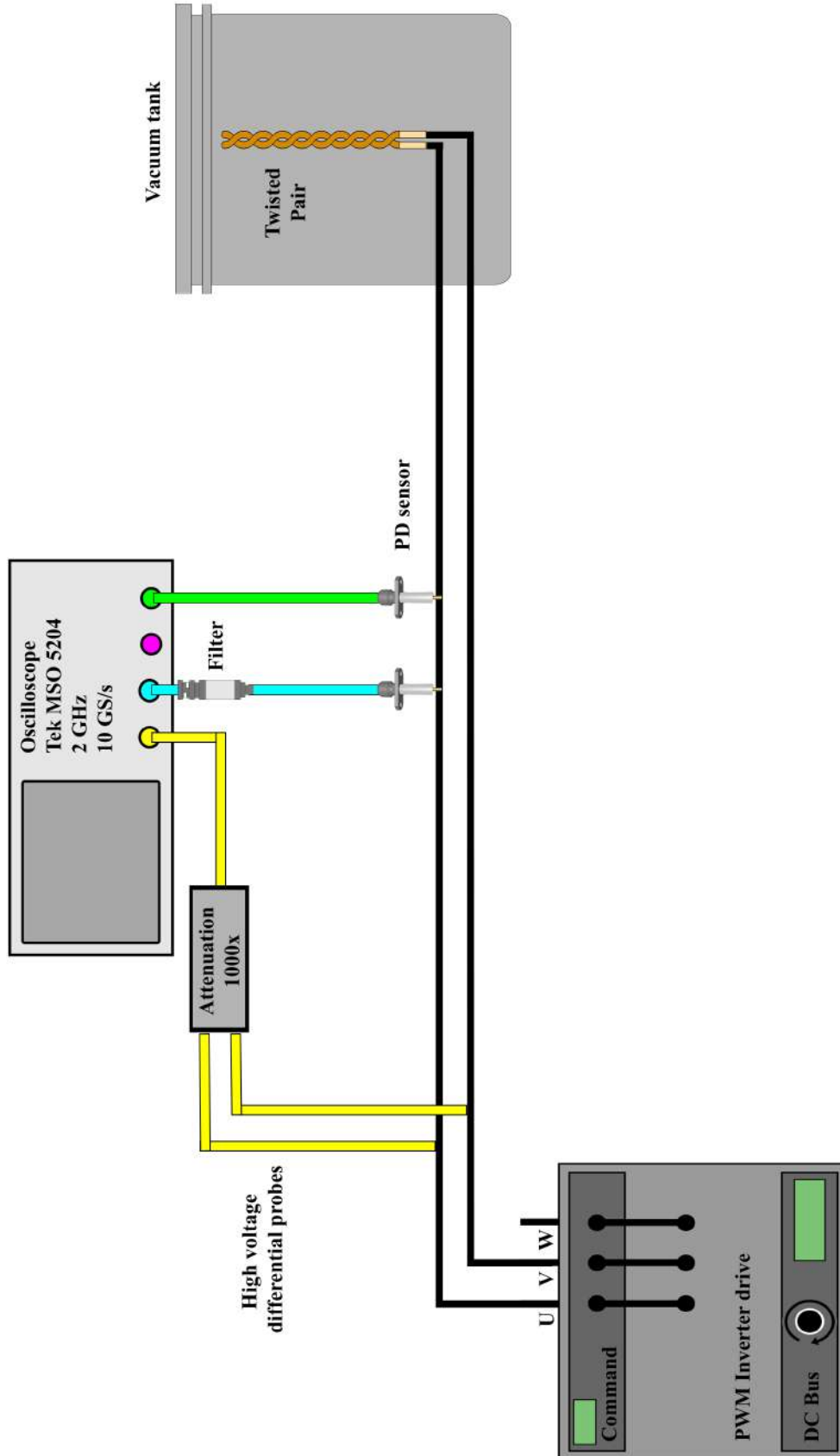


Figure III.11: Experimental set-up no. 2

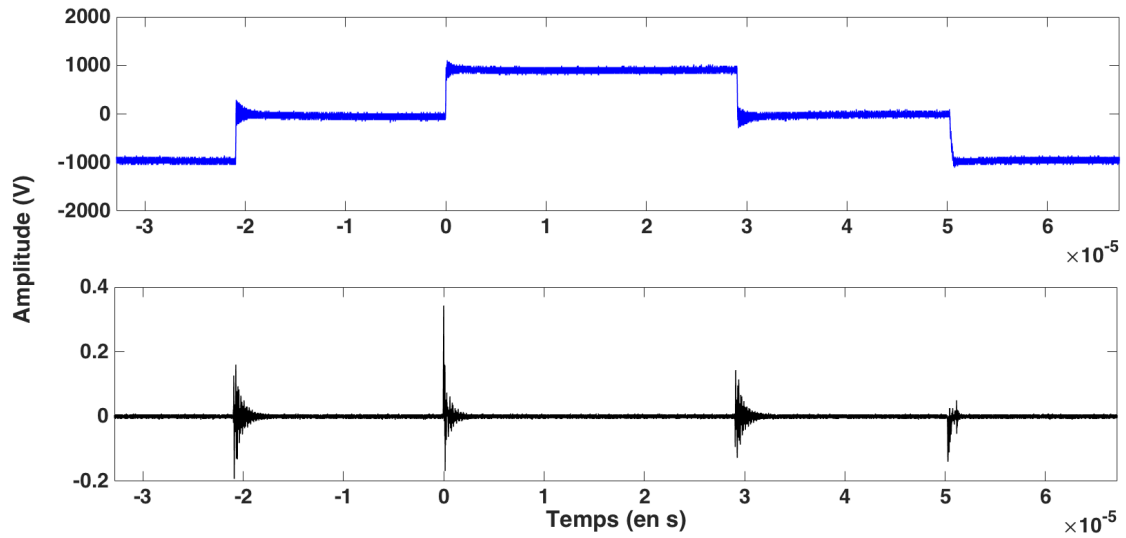


Figure III.12: PWM like voltage shape(blue), sensor signal without filtering (black)

To compare the two methods under optimal conditions, the “mother” wavelet “db8” was chosen, notably because it is a wavelet that seems to allow better extraction according to the bibliography [57], [58], [60]. Preliminary tests were carried out in order to reconstruct only the PD signal. For this purpose, with DWT, decomposition levels 1 through 4 are used to reconstruct the PD signal; for CWT, scales from 1 to 16 are used to reconstruct the signal.

Table III.1: Relationship between decomposition level (DWT) and scales (CWT)

Decomposition level (DWT)	1	2	3	4	5	6	7	8	9	10
Scales (CWT)	2	4	8	16	32	64	128	256	512	1024

### III.8.1.1 CWT test

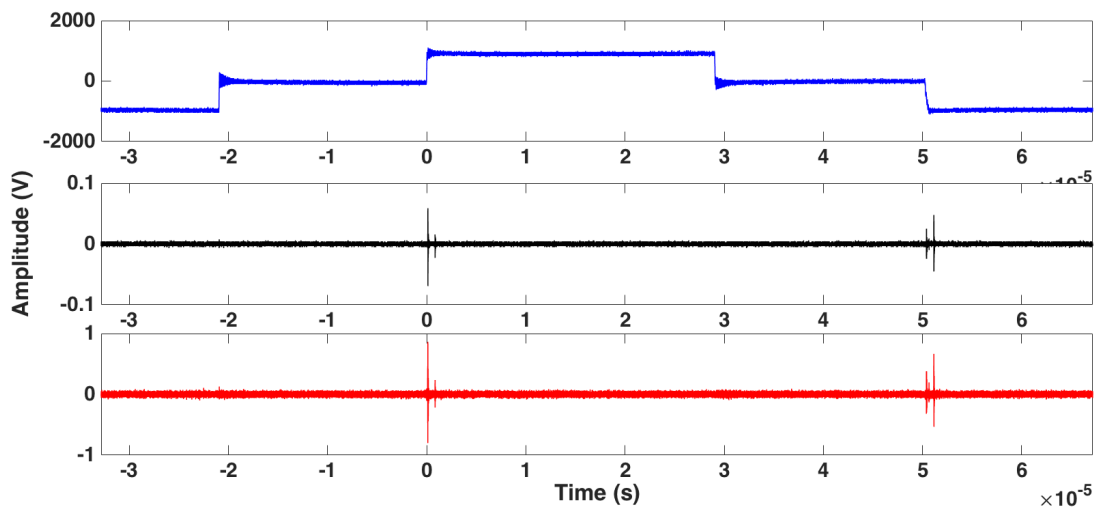


Figure III.13: PWM like voltage (blue), sensor signal filtered analogically at 200 MHz (black), sensor signal reconstructed by CWT (red)

Figure III.13 shows that the shape of the signal reconstructed by CWT is the same that to the filtered analogic signal. The amplitude of the signal during reconstruction by wavelet transform is much larger than the signal filtered analogically. This is explained by the significant redundancy of signals corresponding to different scales that can be seen in Figure III.14. This redundancy induced a significant error on the amplitude of signals after reconstruction. The aim of this work is only to detect, and not to find the precise value of the amplitude, which is why that redundancy is interesting. In the case of CWT, the SNR is 247 while that of the signal filtered analogically is about 21. The computation time for the CWT is about 1.8 s in this case with an “ordinary” personal computer.

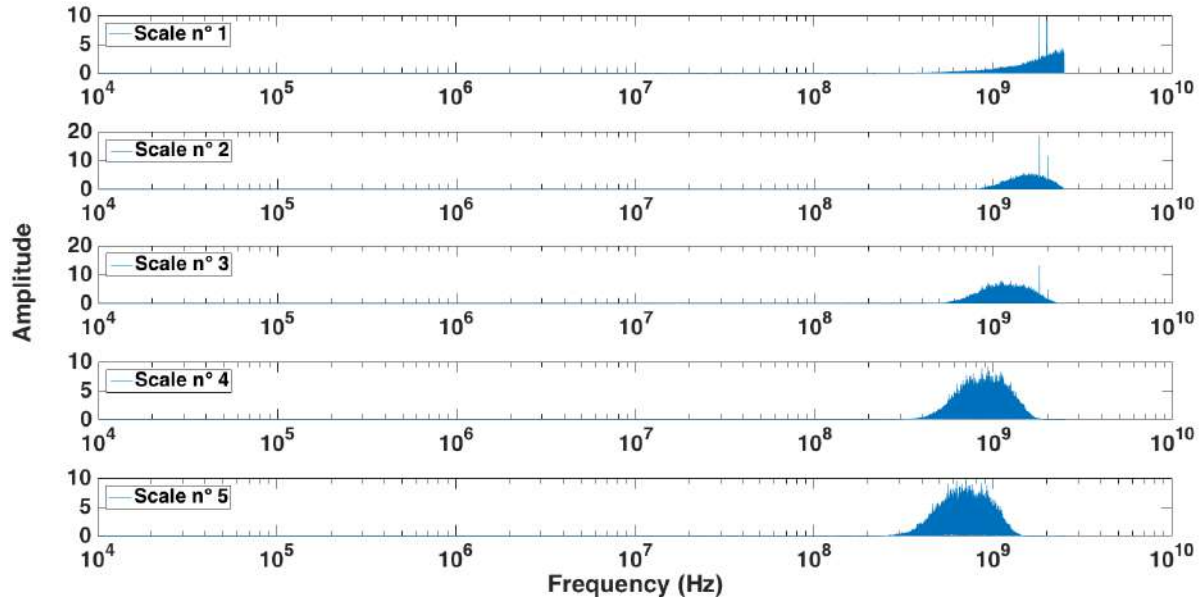


Figure III.14: Fast Fourier Transform (FFT) of CWT scales 1 to 5

### III.8.1.2 DWT test

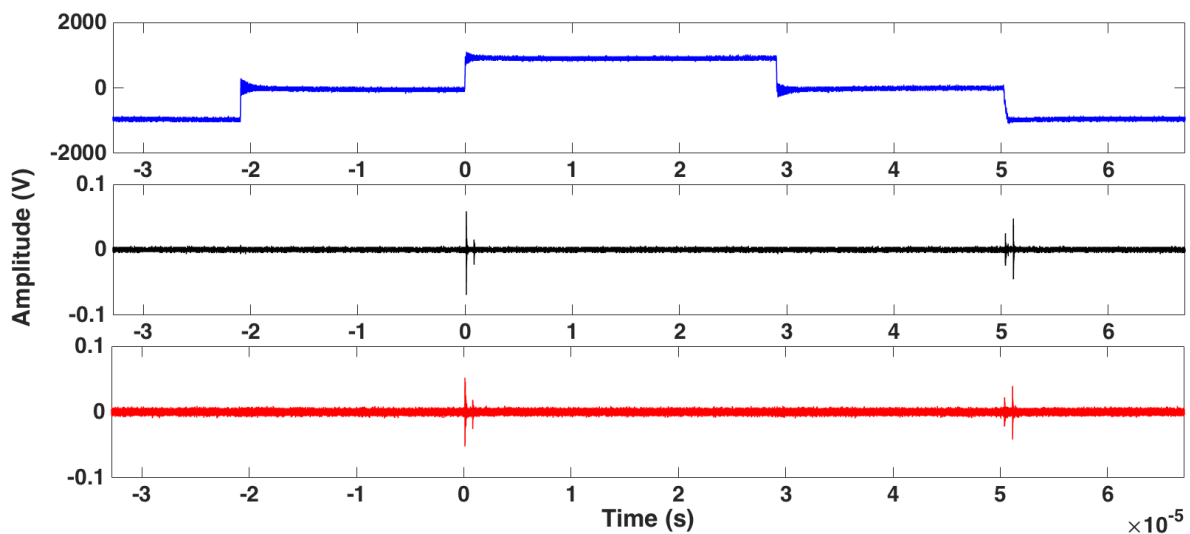


Figure III.15: PWM like voltage (blue), sensor signal filtered analogically at 200 MHz (black), sensor signal reconstruct by DWT (red)



In the case of the DWT, it can be seen in Figure III.15 that the shape of the signal reconstructed by CWT is also the same that to the filtered analogic signal. However, in this case, the amplitude of the signal reconstructed by wavelet is equivalent to the signal filtered analogically. This is explained by the fact that redundancy is much lower in the case of DWT. Figure III.16 shows that the levels of decomposition cover a broader spectrum and have lower redundancy than CWT. In the case of DWT, SNR is 43. The computation time for DWT application is about 0.9 s in this case.

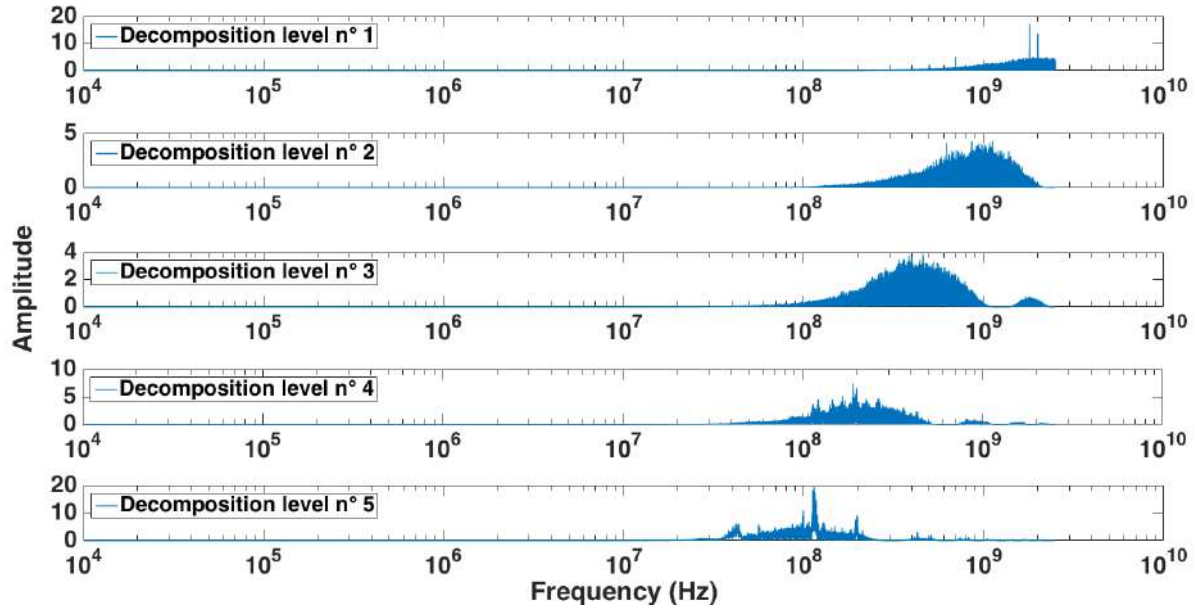


Figure III.16: FFT of DWT decomposition levels 1 to 5

### III.8.1.3 Final Choice

Given the previous results, it can be seen that the amplitude and SNR of CWT are much more higher than with DWT. Despite the significant error induced by the redundancy of the different scales, in order to observe partial discharges, this error improves the visibility of signals of interest because it increases the SNR indirectly.

DWT outperforms CWT in terms of computation time because, to reconstruct a signal in the same frequency range, CWT requires a larger number of scales than the amount of decomposition levels necessary for DWT. Furthermore, if reconstruction requires a large amount of decomposition levels or scales, this time is increased greatly. For example, to reconstruct a signal from 10 levels of decomposition for DWT or 1024 scales for CWT, the computation time with the same computer as that used previously is 187 s for CWT and 1.2 s for DWT. However, to extract PDs, only the first levels or scales are interesting, because a focus on high-frequency components is sufficient to remove all noise-induced switching. In this case the computation time is of the same order of magnitude between the two methods, but the CWT allows a better SNR.

CWT was therefore selected in order to extract the PD noise signals.

### III.9 Denoising

The wavelet transform is mainly used to reduce the noise cited in the section III.2. However, in the case of partial discharge detection, the problem must be considered from another point of view. With the conventional way of using wavelet transform, the signals associated with PDs would be removed and only the signals induced by switching would be preserved. The usual method for denoising signals reconstructed by CWT or DWT is a thresholding of the different decomposition levels. However, this method is no longer appropriate for detecting PDs because the PD signal amplitude is well below noise signals.

It was therefore necessary to find an alternative to this method to denoise the final signal. For this, we considered that the frequency spectrum of the discharges generally extends between a few hundred MHz and GHz. Regarding the spectrum of noise switching, it depends on the switching speed and more particularly on the associated  $dV/dt$  and  $di/dt$ . It has been observed that for  $dV/dt$  below  $10 \text{ kV}/\mu\text{s}$ , the frequency spectrum does not extend beyond a few hundred MHz.

It has been noted when using wavelet transform that each decomposition level corresponds to a specific frequency band:

- First decomposition levels  $\rightarrow$  frequency bands centered around high frequency
- Last decomposition levels  $\rightarrow$  frequency bands centered around low frequency

From this observation, it is possible to observe the signals associated with PDs in the first decomposition levels only. These decomposition levels are therefore used to reconstruct the signal of the PDs.

The signal used to study noise suppression is shown in Figure III.17.

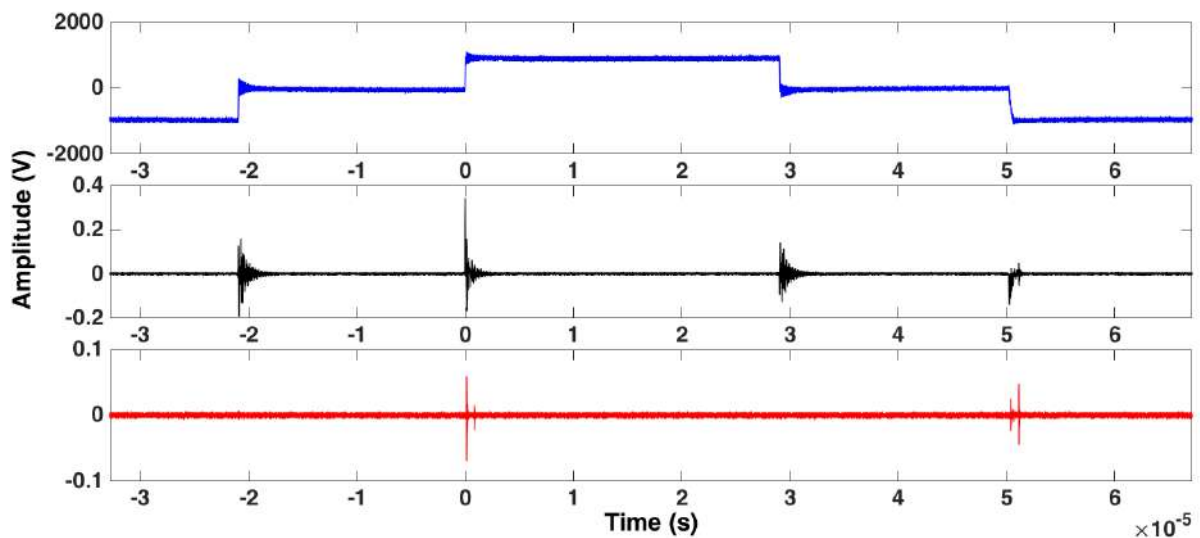


Figure III.17: PWM like voltage shape (blue), sensor signal without filtering (black), sensor signal filtered analogically at 200 MHz (black)

The CWT method was applied to the sensor signal without any filtering to obtain the different scales. Temporal reconstruction of each scale from levels 1 to 10 is shown below. We can see in Figure III.18 that, from levels 1 to 5, there are only two events that appear on the signals and correspond temporally to switching. From level 5, there are 4 events in each of the signals and each of them corresponds to a switching. In this case, it can be considered that there is noise because each signal corresponds temporally to each voltage edge.

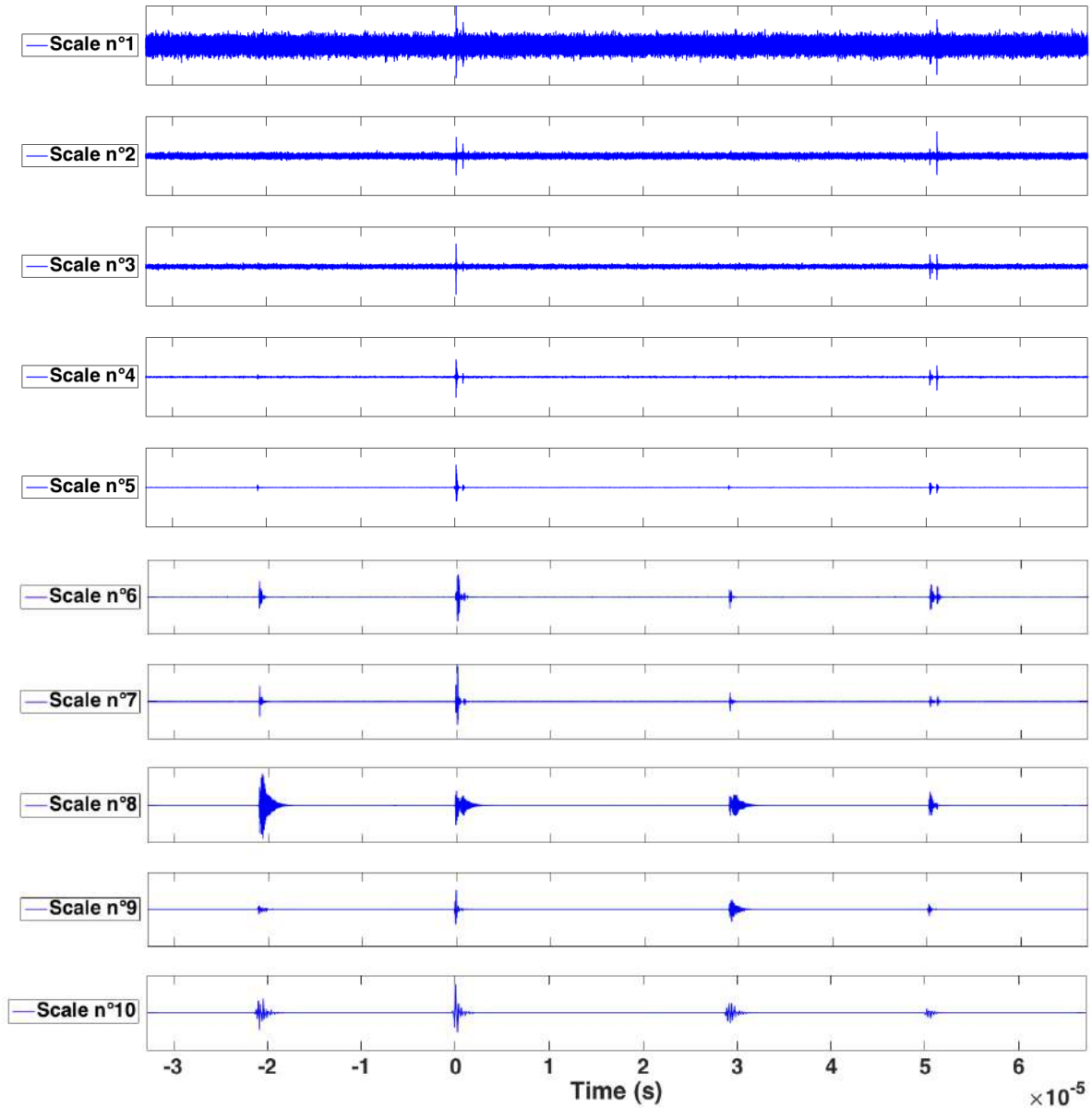


Figure III.18: Temporal representation of scales 1 to 10

To validate the proposed method, two reconstructions were compared. The signal in Figure III.19 was reconstructed using the scales 1 to 10, while the signal in Figure III.20 was reconstructed with the scales 1 to 5.

The first signal obtained is very different from the signal filtered analogically. Moreover, it can be seen that noise is not completely removed. For the second signal reconstructed from the first 5 levels, the shape of the reconstructed signal and the signal filtered analogically are identical. Not only that, but all noise seems to be removed.

We observed therefore that the proposed method is functional for extracting noisy PD signals.

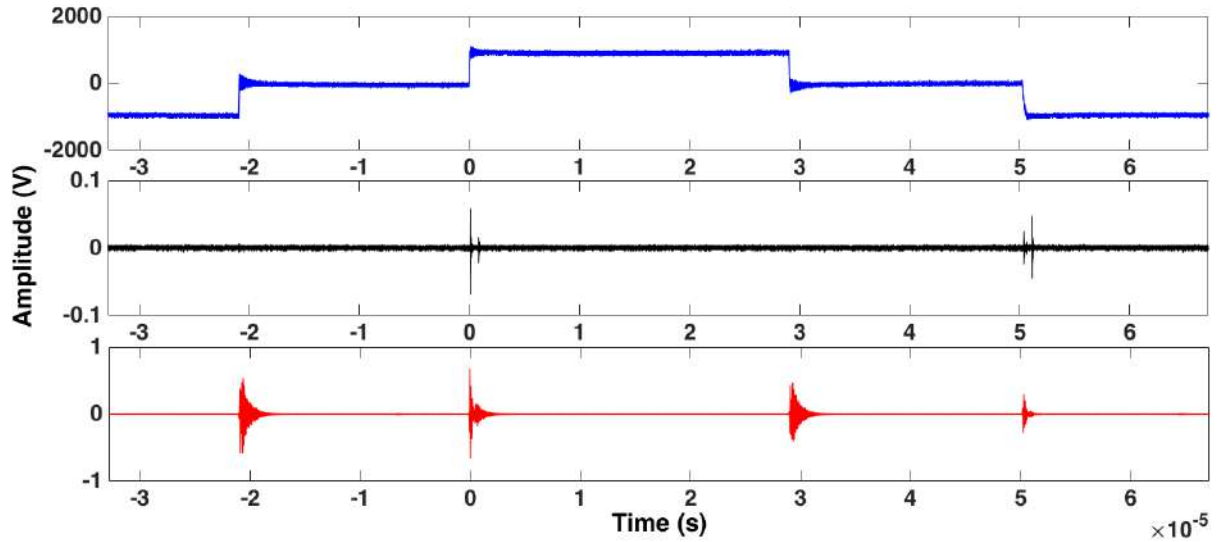


Figure III.19: PWM like voltage (blue), sensor signal filtered analogically at 200 MHz (black), sensor signal reconstructed by CWT from Scales 1 to 10 (red)

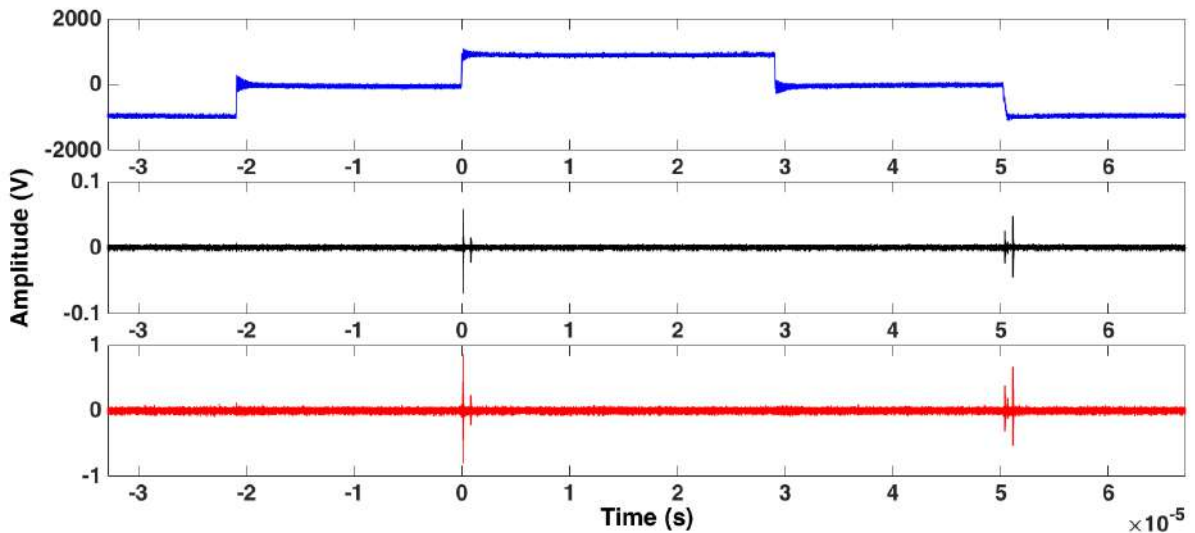


Figure III.20: PWM like voltage (blue), sensor signal filtered analogically at 200 MHz (black), sensor signal reconstructed by CWT from Scales 1 to 5 (red)

### III.10 Automated choice of “mother” wavelet

The choice of the “mother” wavelet is one of the most important parameters for a denoising method based on the wavelet technique. Indeed, this choice impacts the quality of noise suppression directly. This choice is often realized by the correlation between the wavelet shape and the PD signal. Since it is difficult to know the shape of the spectrum induced by switching ahead of time, it is necessary to use an automated method, independent of the waveform characteristics of the signal under test.

The method was proposed by [57]. The selection criterion of the “mother” wavelet is based on the energy and entropy of each of the decomposition levels.

The first step of the method consists in finding the decomposition level containing the information associated with the discharge signal. For this, the energy content is considered for each level of decomposition. Using the equation (III.10.3), the decomposition level at which the signal is the least noisy, as compared to other levels of decompositions, is determined. The highest “energy slop for detail sub-band” (ESDS) value shows the most informative decomposition level, where  $L$  indicates the level of decomposition and  $ED_x$  is the decomposition level energy at scale  $x$ .

$$x = [2, 3, \dots, L - 1] \quad (\text{III.10.1})$$

$$ESDS_x = ED_x - ED_{x-1} + ED_x - ED_{x+1} \quad (\text{III.10.2})$$

$$ESDS = \max(ESDS_x) \quad (\text{III.10.3})$$

Once the decomposition level presenting the most useful information has been determined, it is necessary to choose the mother wavelet that maximizes the energy contained in the previously-determined level of decomposition. Each decomposition level corresponds to a specific frequency range. If the signal has frequency components in this band, wavelet coefficients in the decomposition level are significant. The energy at each decomposition level is given by equation (III.10.4), where  $a$  corresponds to the decomposition level,  $N$  is the number of wavelet coefficients,  $W(a, i)$  indicates the wavelet coefficients at decomposition level  $a$ , and  $i$  is a variable changing from 1 to  $N$ .

$$E(a) = \sum_{i=1}^N |W(a, i)|^2 \quad (\text{III.10.4})$$

Another important point is the distribution of wavelet coefficients. As PDs are fast phenomena, energy is concentrated in a very short period of time. Entropy is defined as the probability distribution of a random variable. In our case, we looked for low entropy because it corresponds to a high concentration of energy. In equation (III.10.5),  $a$  corresponds to the decomposition level,  $p_i$ , which is given by equation (III.10.6), is the ratio of each decomposition level component energy to total decomposition level energy.

$$E_{entropy}(a) = - \sum_{i=1}^N p_i \cdot \log_2(p_i) \quad (III.10.5)$$

$$p_i = \frac{|W(a, i)|^2}{E(a)} \quad (III.10.6)$$

The optimal wavelet maximizes energy in the frequency range of interest of the signal while minimizing entropy. The sub-band energy to entropy (SBETE) is calculated for each wavelet and the SBETE presenting the largest value is considered as the optimal wavelet to denoise the signal.

$$SBETE = \frac{E(a)}{E_{entropy}(a)} = \frac{\sum_{i=1}^N |W(a, i)|^2}{-\sum_{i=1}^N p_i \cdot \log_2(p_i)} \quad (III.10.7)$$

The flowchart for this method is shown below in Figure III.21

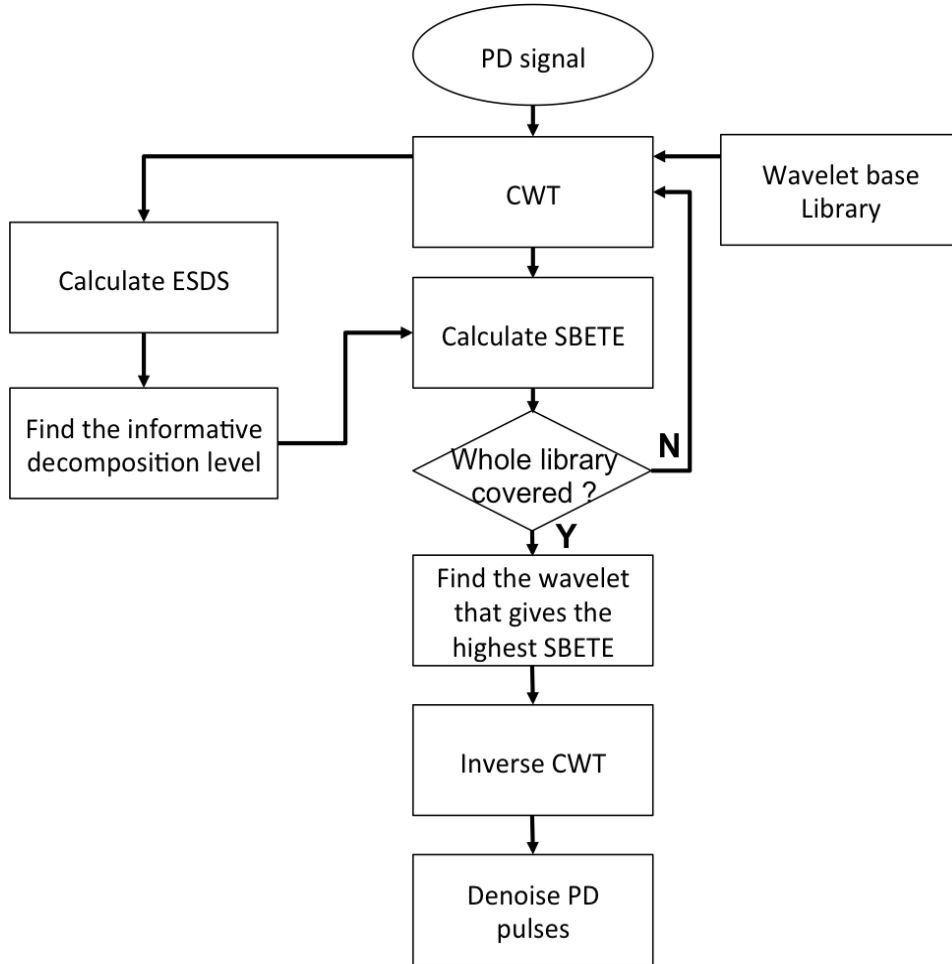


**Figure III.21 Method flowchart**

### III.11 Method validation

For validation, the method was applied by first fixing the mother wavelet as “db7” and after by using the automatic choice method of the mother wavelet.

The results can be seen below in Figure III.22 and Figure III.23, representing respectively the PD signal reconstruction with a mother wavelet “db7” and the wavelet defined automatically (in this case “coif1”).

First, we observed that the two reconstruction signals are similar both to each other and to the filtered analogical signal. The only difference between the two reconstructions is the signal amplitude. Reconstruction with the automated choice enables retrieving a PD signal having an amplitude twice as large as the one reconstructed with wavelet “db7”.

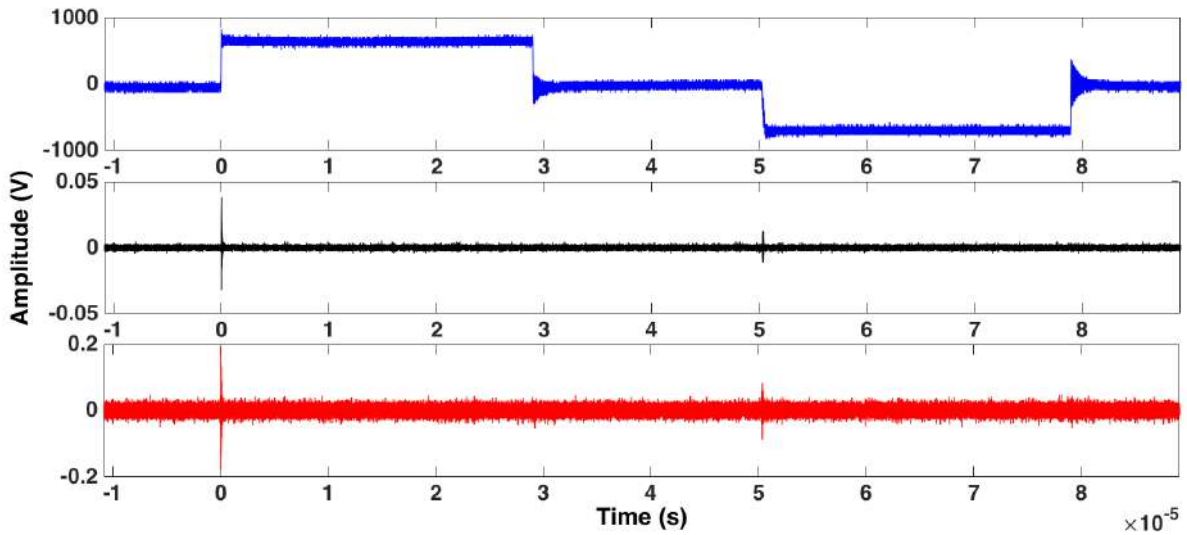


Figure III.22: PWM like voltage shape (blue), sensor signal filtered at 200 MHz (black), PD signal reconstructed by CWT with a mother wavelet “db7” (red)

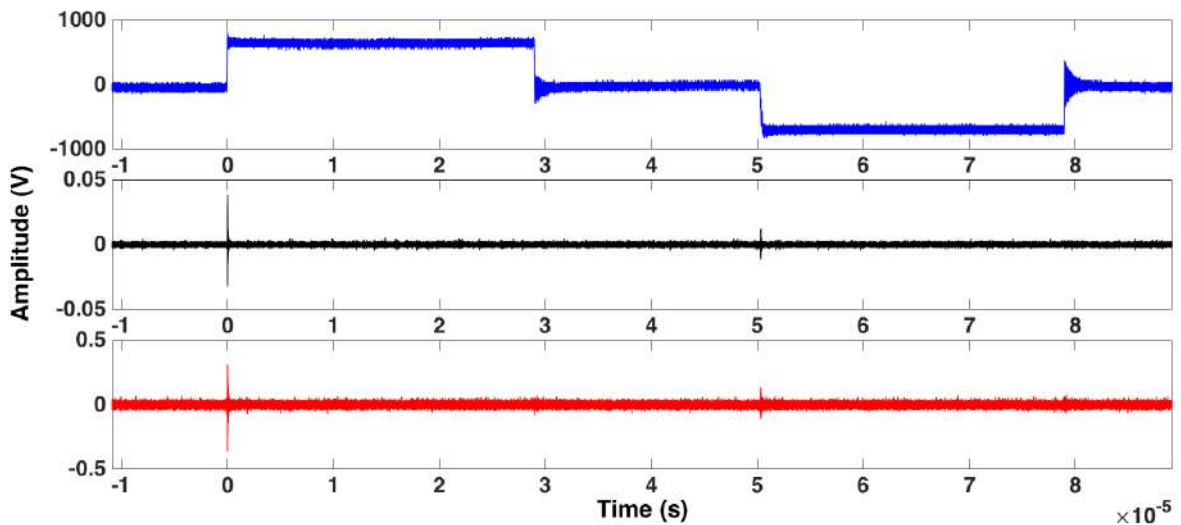
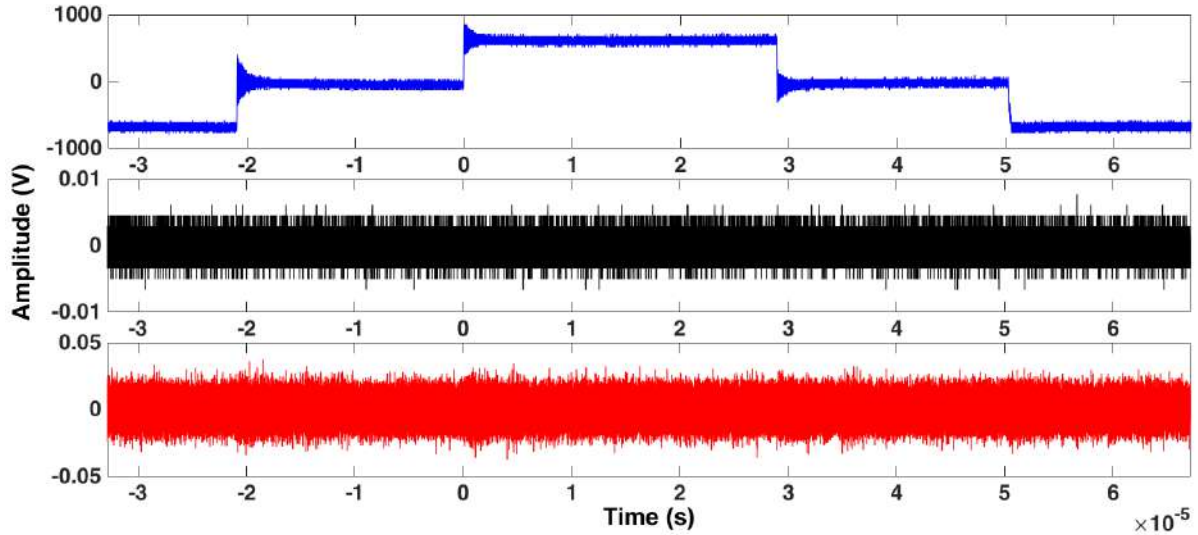


Figure III.23: PWM like voltage shape (blue), sensor signal filtered at 200 MHz (black), PD signal reconstructed by CWT with the automated choice of the mother wavelet (“coif1” in this case) (red)

Another important point to check to validate the complete denoising method is to ensure that the method detects no signals when there is no PD ignition and ensure that it is always effective to remove noise.

The test was performed at a voltage below the PDIV. In this case, the PDIV was about 1 kV, therefore, the applied voltage was 900V.



**Figure III.24: PWM like voltage shape below the PDIV (blue), sensor signal filtered at 200 MHz (black), PD signal reconstructed by CWT with the automated choice of the mother wavelet (“coif1” in this case) (red)**

Figure III.24 shows that all noise is suppressed and that the method does not detect any signals characteristic of PDs.

The last point to check is that the method is able to denoise the signals whatever the pressure. The Figure III.25 shows the ability of the method to denoise the signal at 100 mbar. In this case, the PDIV was about 580 V.



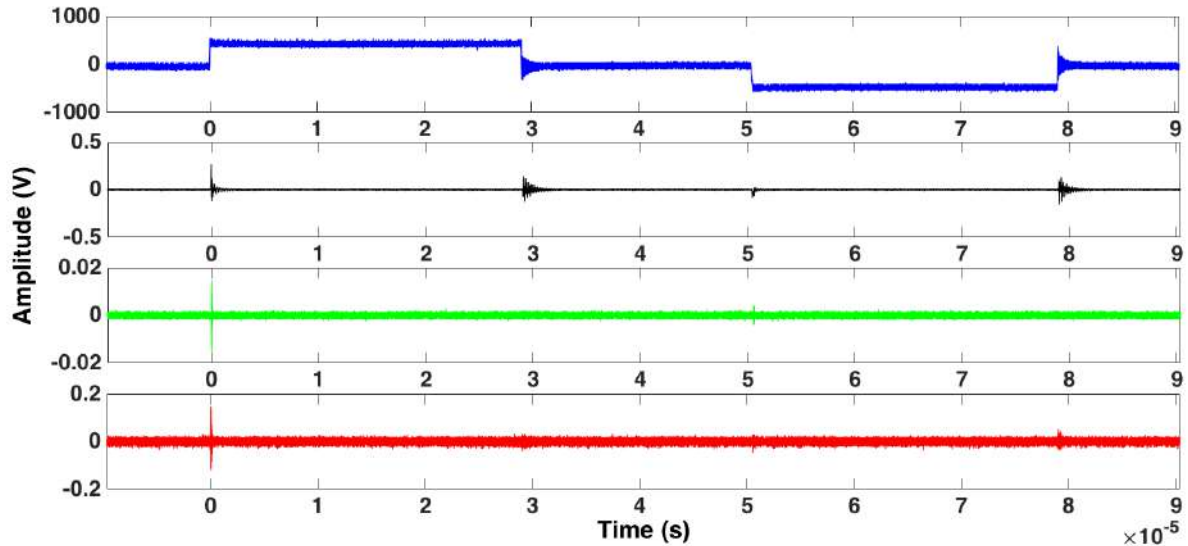


Figure III.25: PWM like voltage shape below the PDIV (blue), sensor signal without filtering (black), sensor signal filtered at 200 MHz (green), PD signal reconstructed by CWT with the automated choice of the mother wavelet (“coif1” in this case) (red)

### III.12 Conclusion

The digital denoising method based on continuous wavelet transform is functional and it sets all the wavelet transform configuration parameters automatically. This method has real interest with respect to high-pass filtering because human expertise is no longer required to remove noise in signals.

It is still important to note the limitations of this technique. First, to be functional, it is necessary for the signal to be discretized with a large sampling frequency in order to represent fast signals.

Another important point is that the amplitude of the signal reconstructed by the method has a very significant error. Indeed, frequency band overlap corresponding to each level of decomposition induces a very significant error. However, error is also induced with the use of a high-pass filter because all frequency components below the cutoff frequency are removed.

Some work is now needed to automate choice levels for reconstruction to denoise all the noise induced by switching.

With the development of this denoising tool associated with the detection method it is possible to carry out tests in order to detect the presence of PDs on real devices on industrial test benches.

This study is presented in the next chapter.





## **Chapter IV. Investigations on electric motor test benches**



The purpose of investigating industrial test benches is to check the validity of the detection method, particularly the sensor used. This sensor was tested in a laboratory environment but a few tests were also carried out on industrial test benches. In these tests, Thibaut Billard and Benjamin Cella worked on motors test benches respectively from Renault and Liebherr [35], [64].

Currently, to our knowledge there are no paper in the literature on on-line and non-intrusive partial discharge detection in type 1 motors supplied by PWM voltage. The work presented in this chapter highlights the ability of the developed method to detect partial discharges on equipment currently embarked in aircrafts.

From an industrial point of view, the interest of the PDs detection method comes from the need to qualify their equipment and then to certify them. To do this, it is necessary to have a robust method capable of functioning under any test conditions. The only way to make the developed method robust is to carry out numerous tests on different test benches.

For confidentiality reasons, the names of the companies and technical details of the systems tested are not mentioned. We only go into details regarding the analysis and observations made while using the detection method. Moreover, for whole of the results presented below, the temporal data have been normalized in order to represent only the period of the voltage signals observed (which is also a method to keep the confidentiality of the results).

We performed numerous tests on about ten different benches. Five specific cases are developed below to highlight the difficulty of detecting partial discharges under normal operating conditions. In particular, those cases address:

- the difficulty of removing noise
- a new issue of overvoltage induced by power electronics
- the need to perform a complete analysis to confirm the presence or absence of partial discharges
- a low voltage case where the method is functional and for which we observed partial discharges
- a high voltage case where the method proves its validity

It is important to point out that a lot of other tests on engine benches were carried out at low pressure, on different machines and different conditions, nevertheless for reasons brevity and of confidentiality these studies will not be detailed below. Moreover, this study gives only a few additional observations compared to the different cases presented.

## IV.1 Filtering

Before investigating the presence of partial discharges, it is also necessary to determine the optimal cutoff frequency for the high-pass filters to use. The procedure is to perform a preliminary test using a filter with a low cutoff frequency, then to observe the signals that coincide temporally with voltage edges. If recurring signals for each voltage front are still present, it is necessary to repeat the procedure by gradually increasing the cutoff frequency of the filter used until the disappearance of these recurring signals, while hoping the filtering has not removed also the signal due to PD.

An example of this procedure in a real case is presented below.

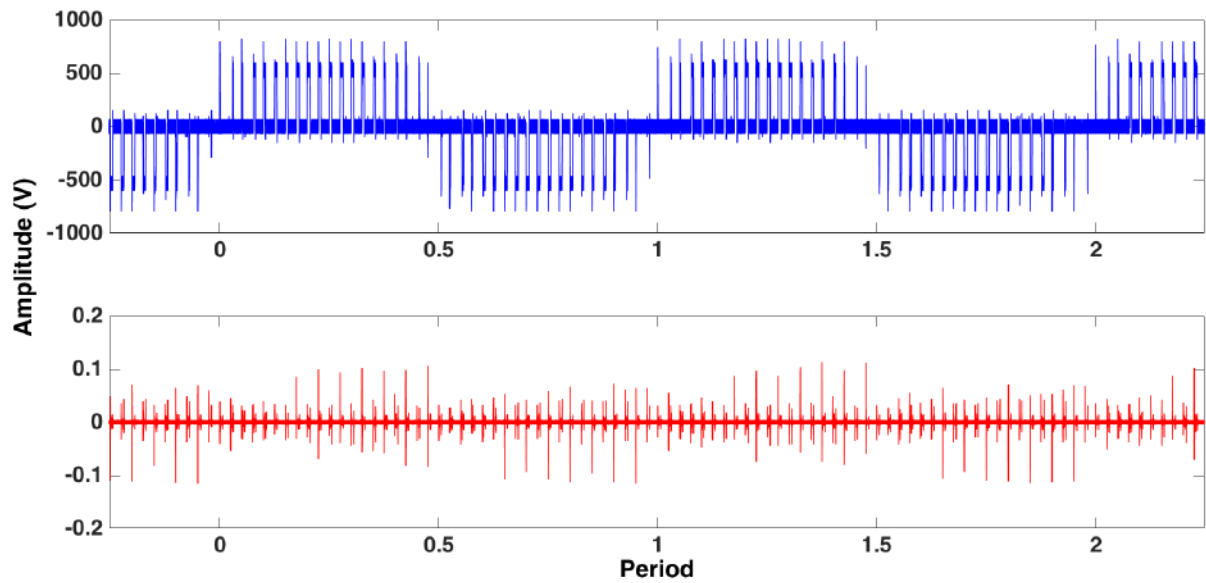


**Figure IV.1: Phase to phase voltage (blue), sensor signal on 1 of this 2 phases without filtering (red)**

As it can be seen, recurring signals occur at each voltage edge without filtering. The amplitude of the recurring signal is about 100 mV, making it impossible to observe partial discharge signals if there are any.

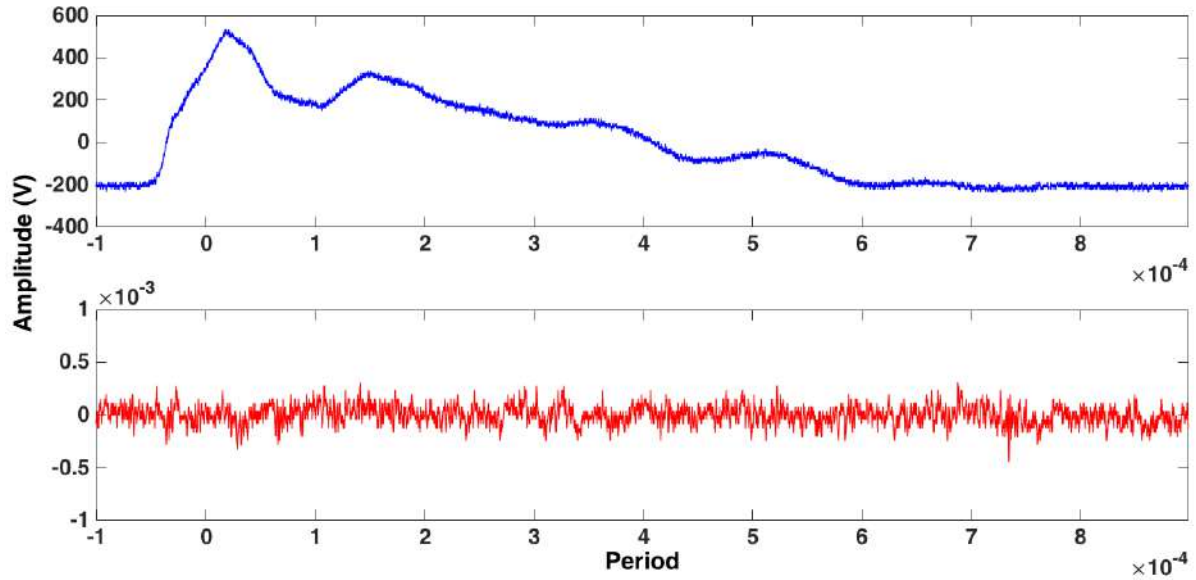


**Figure IV.2: Zoom on the  $dV/dt$  of the phase to phase voltage (blue), sensor signal on 1 of this 2 phases with filtering (red)**

In the Figure IV.2, the recurrent noise has been completely removed using filters with a 200 MHz cutoff frequency. It is important to note that the value of the cutoff frequency depends on the system being studied. Indeed, the frequency range over which the noise spans depends on the voltage edge, and more particularly on the  $di/dt$  induced. It will therefore be necessary to perform this procedure for each test set-up, preventing automatic filter choice. It is worth stressing that the filter choice depends on the expertise of the operator performing the test, and that the quality of results are highly dependent on this preliminary choice.

## IV.2 Partial discharge investigations on motor test benches

Once the filter choice achieved, the analysis of the presence of partial discharges may be performed. Generally, the simplest method is to vary the voltage and observe the ignition or extinction of particular signals coinciding temporally with the maximum voltages and voltage edges. However, during industrial tests, reality is often far more complex. Indeed, industrial benches on which tests were performed, were not designed for partial discharge tests. It is therefore often impossible to vary the voltage magnitude, even if just over a relatively small range. This prevents the observation of ignition or extinction of signals that could be related to partial discharges. It is therefore necessary to conduct a thorough analysis of the observed signals. It is not possible to propose an universal method for analyzing these signals, because any such method depends on experimental parameters that can be varied.

The five cases below represent an overview of the tests conducted with the industrial partners:

- The first case highlights the difficulty of filtering that may be encountered in some cases, and thus prevents PD detection.



- The second case focuses on the presence of surges that are not dependent of phenomena usually documented in literature, and may increase the risk of partial discharge occurrence.
- The third case emphasizes the need to perform a complete analysis to confirm the presence or absence of partial discharges.
- The fourth case puts forward the ability of our system to detect partial discharges on an equivalent electromechanical chain to those on-board of certain aircraft.
- The last case puts forward the ability of our system to detect partial discharges on systems supplied by IGBT inverters with higher voltage level or by SiC inverter.

### IV.2.1 Experimental set-up

The diagram in Figure IV.3 represents the generic set-up used for measurement. During tests, the number of differential probes or sensors may vary, as well as the cutoff frequency of the filters used. However, an important issue concerns the acquisition system. In some cases, the use of two oscilloscopes is necessary for acquiring all voltages and to search for PDs on all phases. The oscilloscope trigger is defined on an oscilloscope to observe all phenomena at the same time. This oscilloscope (oscilloscope master) then sends a synchronization signal to trigger the second oscilloscope (slave oscilloscope) at the same moment.

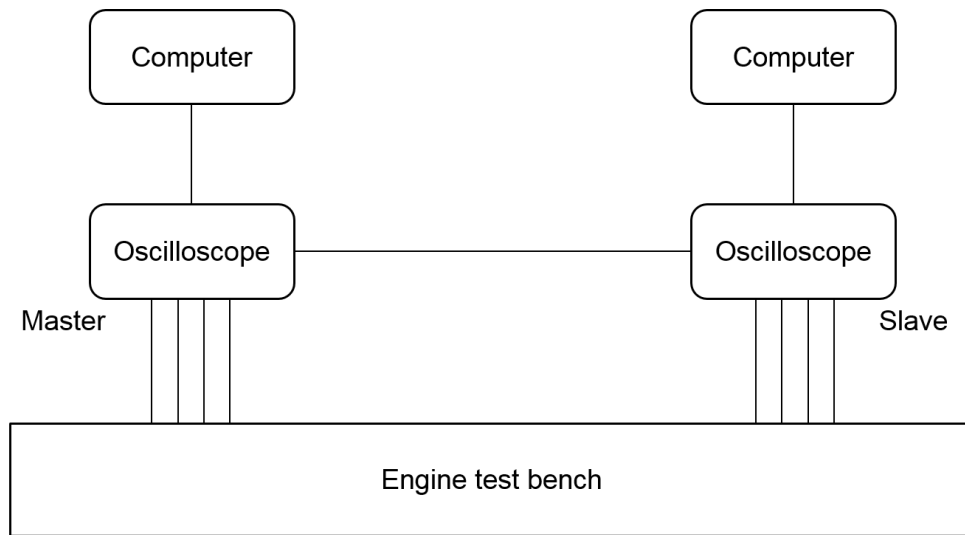


Figure IV.3 : Generic experimental set-up

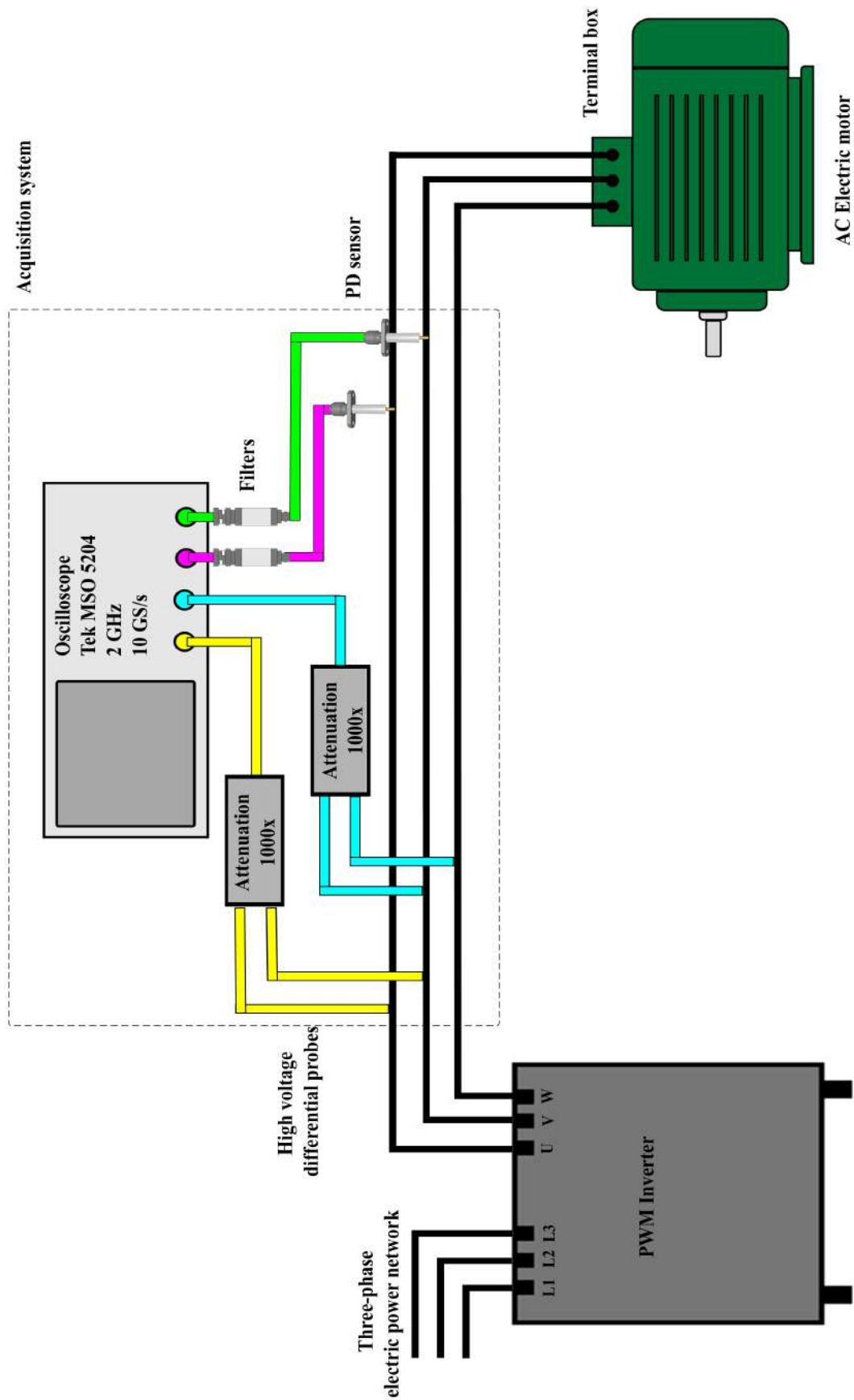
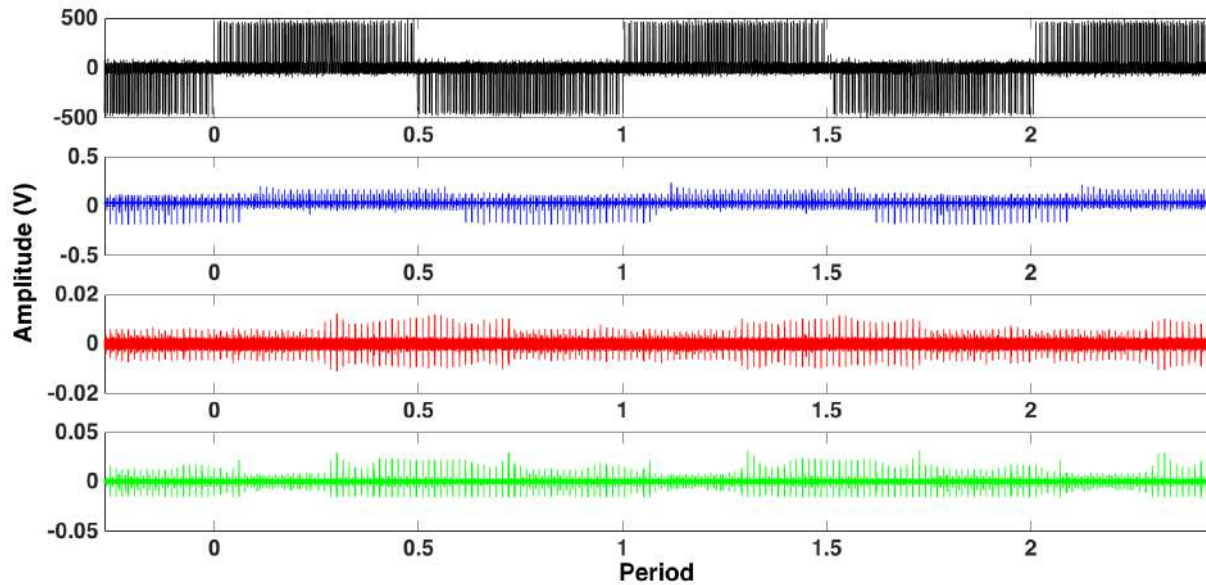


Figure IV.4: Example of a specific experimental set-up

## IV.2.2 Case 1: Filtering difficulties

First, a test was conducted with a DC bus voltage of 388 V and a speed of 2000 rpm on an Actia industrial test bench. This test was intended to adjust the oscilloscope calibers and to optimize the input filter choice for the scope. This test also allowed us to determine the amplitude of the voltage across the machine. The curves representing the voltage at the machine terminals and the output signals from the different sensors are plotted below.



**Figure IV.5:** Phase to phase voltage VW(black), sensor signal filtered at 200 MHz phase V (blue), sensor signal filtered at 400 MHz phase W (red), sensor signal filtered at 400 MHz phase U (green)

First of all, it can be seen in the Figure IV.5 that no surge is present at the converter output. It is possible to conclude that the 200 MHz cutoff frequency is not suitable because noise is not suppressed enough and reaches amplitudes on the order of hundreds of mV, which prevents searching for possible PDs.

Filters with a cutoff frequency of 400 MHz were used to optimize filtering. Noise is decreased significantly in this case, however, it is still not filtered enough. Indeed, the amplitude of sensor output noise for these filters reaches an amplitude on the order of tens of mV.

In the following, the rising edges are defined by the voltage variation from 0 V to  $\pm V$ , and falling edges by the voltage variation from  $\pm V$  to 0V

To better understand the presence of this noise, we observed the front measured during testing. Figure IV.6 shows that the  $dV/dt$  of the falling edge is about 3 kV/ $\mu s$ .

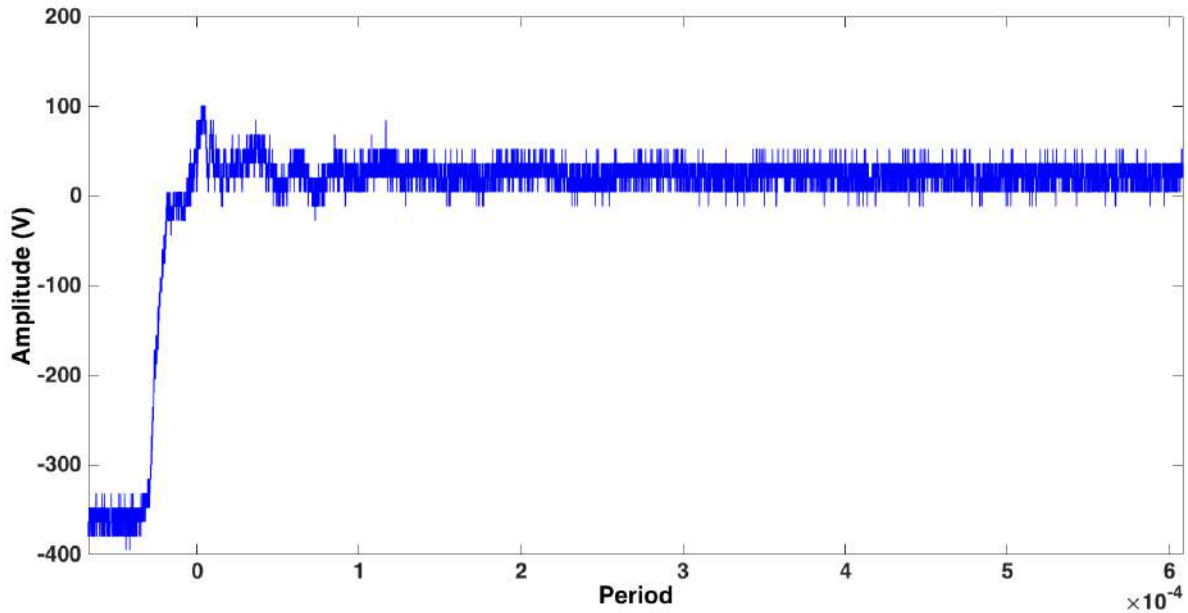


Figure IV.6: Rising edge of the voltage

For these amplitudes of  $dV/dt$ , the noise can not be beyond the cutoff frequencies of the filters used. It can therefore be deduced that the amplitude of noise, in this case, is not directly connected to the  $dV/dt$ . First, it is possible that the magnitude of the current is very large when switching. Another important point to be noted is that during these tests none of the systems are shielded and electromagnetic interference (EMI) may exist and can radiate.

#### IV.2.2.1 Comparison of the signal vs the sensor position

For these tests, the set-up test was modified to observe the influence of sensor position on the signal.

Two sensors were placed on phase W. The first is located close to the inverter, while the second is positioned near the machine terminals. The signal is filtered for the two sensors using a high-pass filter with a 400 MHz cutoff frequency. The DC bus voltage was 388 V and the machine speed was approximately 2000 rpm. The purpose of this test is to observe whether the noise disappears further away from the converter.

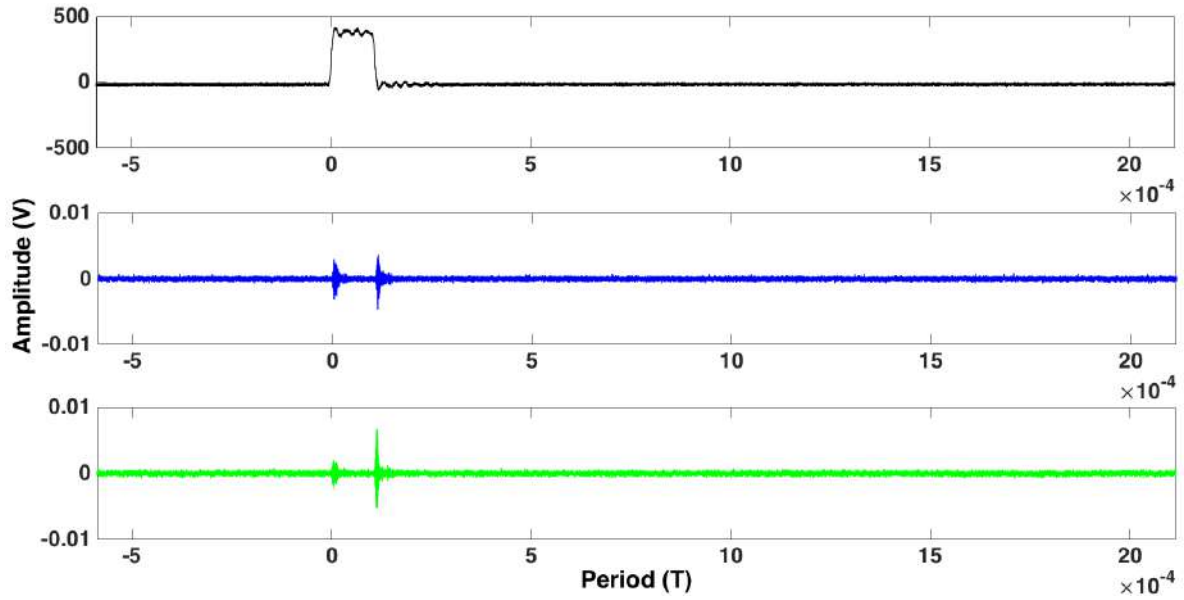


**Figure IV.7: Phase to phase voltage UW (black), sensor signal phase U close to the motor (blue), sensor signal phase U close to the inverter (green)**

Figure IV.7 shows that the sensor position has an influence on the amplitude of the observed signal. However, the sensor position does not suppress the observed noise and it does not allow the detection of PDs. The noise amplitude coinciding temporally to the falling edge is divided by two close to the motor, in comparison to the signal measured close to the converter. For noise coinciding to the rising edge, little influence of the position was observed on noise amplitude. The change in the amplitude of the noise coinciding with the falling edge between the two positions of the sensor can be explained by the filtering. The falling edge is slower than the rising edge and its spectrum therefore extends over a lower frequency range than the one associated with the rising edge. It is possible that in this case the filtering removes a large part of the energy components and induces this modification.

#### IV.2.2.2 Influence of the Current

The experimental setup remains the same in this test. The DC bus voltage was raised to 400 V with an increase in the effective current up to 350 A. The motor speed was about 2850 rpm.

The purpose of these tests is to observe the influence of the value of the current on the voltage and signal measured by the sensors.

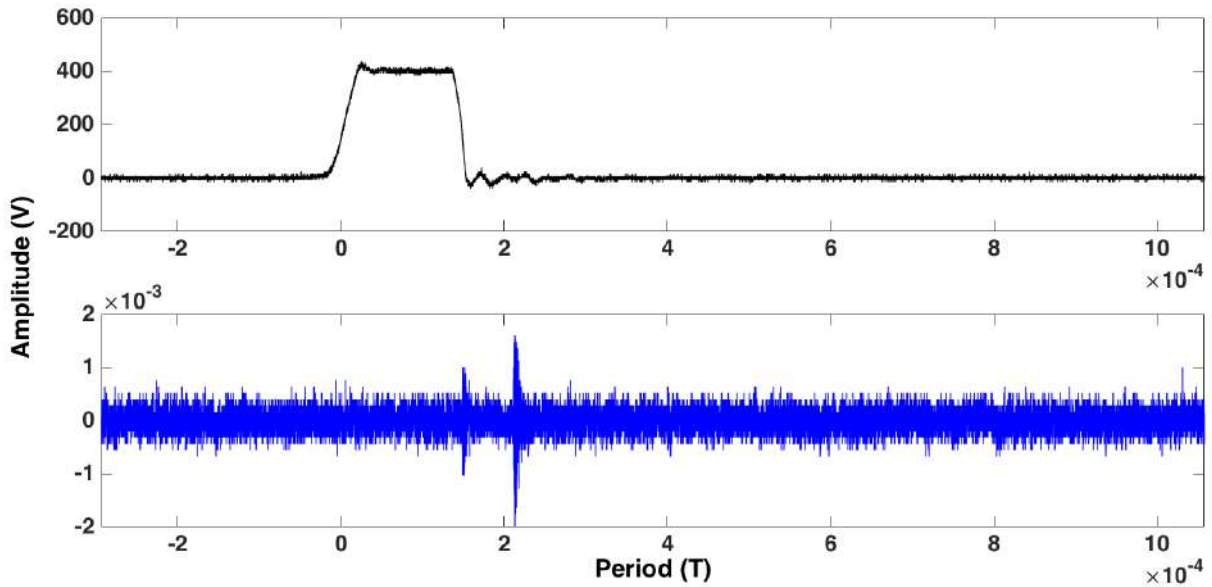


Figure IV.8: Phase to phase voltage UW (black), sensor signal on phase U close to the motor (blue)

Figure IV.8 shows that the noise associated with the rising edge has completely disappeared. This is explained by the fact that the  $dV/dt$  of the rising edge decreased with increasing current and filtering thus removes all noise. The  $dV/dt$  of the front has a magnitude of about  $1.4 \text{ kV}/\mu\text{s}$ . We can also see that there is very little noise at the falling edge. Another noise signal is present, but there is no temporal coincidence with an edge observed when measuring. This noise is most likely induced by further switching.

It is therefore impossible to reach a conclusion regarding the presence or absence of discharge for the equipment studied. However, given the test conditions, there is little risk of observing PDs, as this system does not induce overvoltage across the machine. Voltage does not exceed 420V, which is a too low level for initiating a partial discharge at atmospheric pressure.

This test shows that noise extends over a too large frequency range to be able to filter noise with the available filters. In addition, since the frequency content of a partial discharge for these  $dV/dt$  does not extend beyond a few hundred MHz, it would probably be impossible to detect partial discharges if a filter with a higher cutoff frequency was used.

This case offers a good example of the problem of noise completely preventing PD detection.

### IV.2.3 Case 2: Abnormal presence of surges

The PWM voltage was not modifiable in this test. Only the voltage of the AC source and the speed are the parameters that could be changed. In this part, when referring to the supply voltage (voltage between 180 and 260 V), reference is made to the line voltage of the AC power supply.

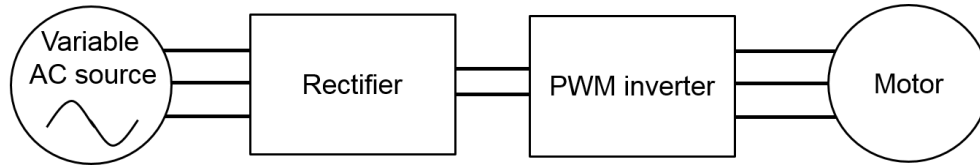


Figure IV.9 Diagram of motor test bench

We observed that increasing speed beyond a certain range affects the quality of the voltage signal. As it was not possible to control the voltage signal directly, speed was modified to modify voltage indirectly. This change induces power surges for the appearance of PDs. The nominal operating motor voltage level was 540 V, with a very short cable length connecting the actuator to the inverter (about ten cm). There was theoretically little risk that surges would initiate PDs.

Machine temperature was monitored during testing, varying between 46 °C and 52 °C. As this variation is small, it does not seem to influence the development of PDs.

#### IV.2.3.1 The influence of rotation speed

First, we paid attention to the influence of rotational speed on the voltage waveform. The figures below show the shape of voltage between phases for different speeds.

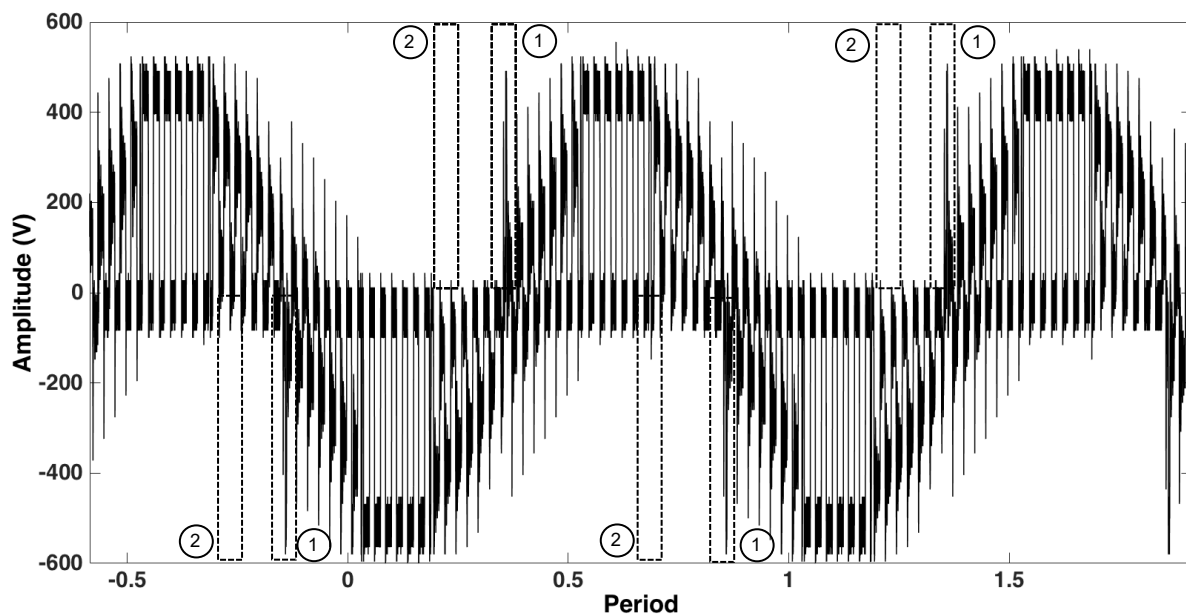


Figure IV.10: Voltage between phases for lowest rotation speed



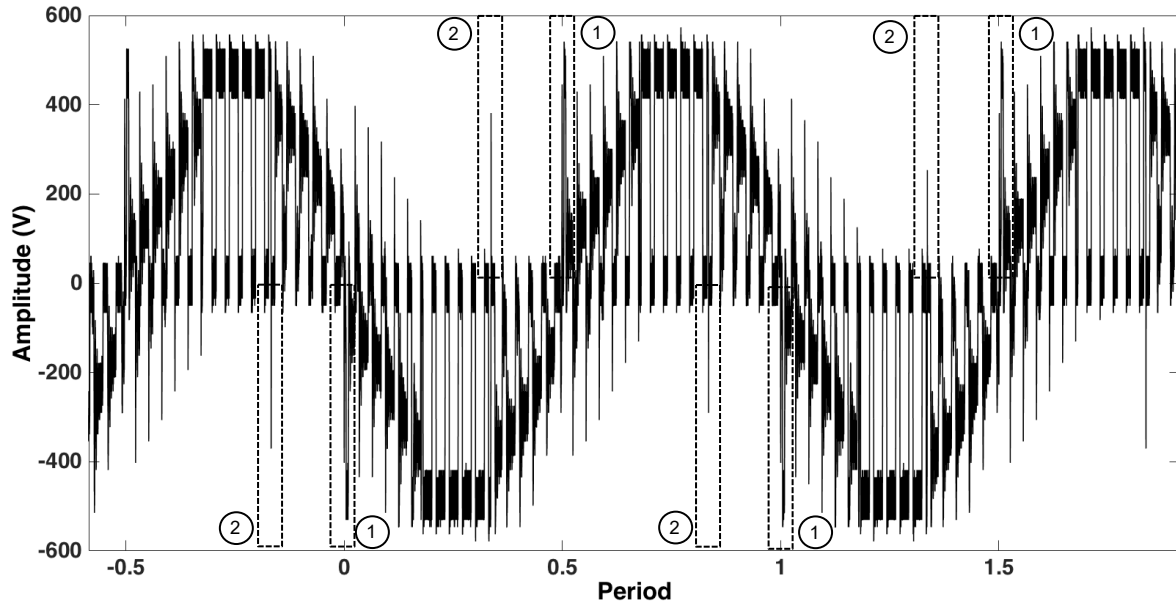


Figure IV.11: Voltage between phases for medium rotation speed

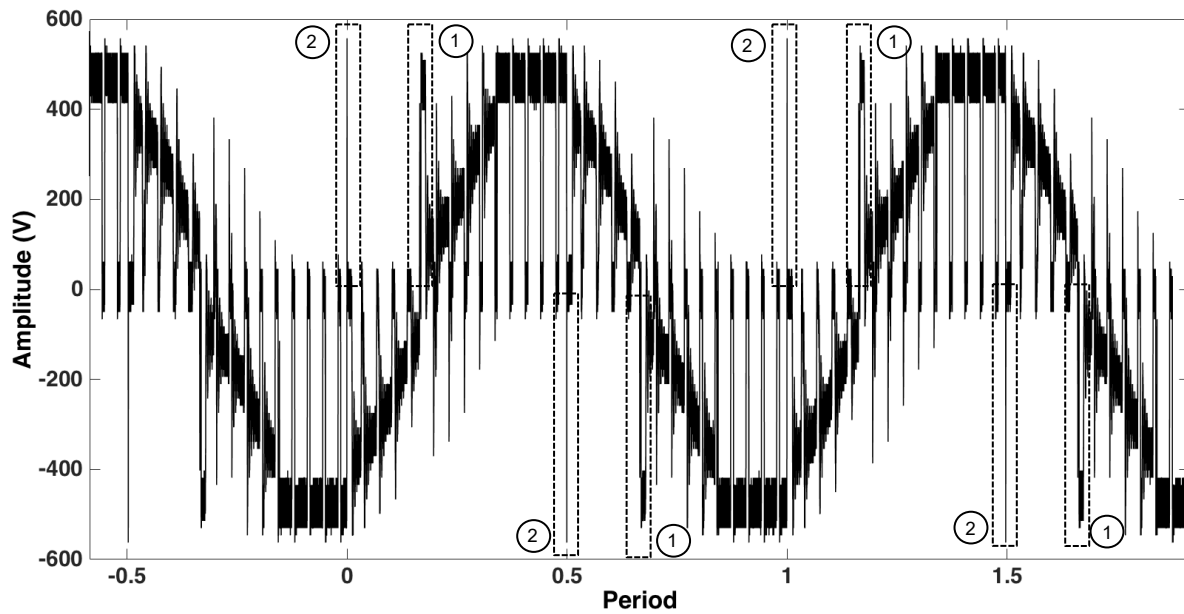


Figure IV.12: Voltage between phases for fastest rotation speed

Two surges can be observed. The first one (no. 1) occurs during the polarity change whatever the speed, while the other (no. 2) appears gradually, coinciding with a change of polarity on one of the other power phases. Speed does not seem to have an effect on the first amplitude surge but only on that of the second. For a speed of 10,000 rpm, there is no overvoltage. The overvoltage can be observed only from 12,000 rpm. For a speed of 12,000 rpm and a source amplitude of 200 V, the overvoltage has “peak to peak” amplitude of about 900V. For a speed of 14,000 rpm, the overvoltage has “peak to peak” amplitude of about 1.1kV. Analyzing the influence of the speed highlighted the fact that the command induces very high overvoltages. The cable length is very short in our case, but we can imagine that a

combination of this command and a significantly longer cable length could increase the observed overvoltage significantly.

It is possible for PDs to appear, given the magnitude of these surges. It is important to note that surges were observed when the sinusoidal voltage source provided a voltage of 200V. It is therefore necessary to study the influence of this voltage on the amplitude of the induced voltages.

#### IV.2.3.2 The influence of voltage magnitude

The table below gives the amplitude of overvoltages associated with the machine speed at the largest speed and for different values of the AC supply voltage. Overvoltage amplitude is greatest for this rotation speed.

**Table IV.1: Overvoltage amplitude with supply voltage**

AC Supply voltage (Volts)	“Peak to Peak” magnitude of overvoltage (Volts)
180	930
200	1070
220	1170
240	1280
260	1360

It can be seen that the amplitude of the overvoltage increases almost linearly with the amplitude of the voltage. We can also observe that the largest surges can reach 1.4 kV. These very high surge values are liable to induce PDs.

#### IV.2.3.3 Partial discharge detection

With tests performed on industrial test benches, it can be complex to distinguish the presence of PD noise. Having parameters whose variation range is low (such as the voltage amplitude variation) further complicates the analysis:

- The voltage may be insufficient to initiate PDs, in which case it is impossible to search the PDIV.
- Or, the applied voltage may exceed the partial discharge inception voltage (PDIV), in which case it is impossible to sufficiently reduce the voltage amplitude to reach the partial discharge extinction voltage (PDEV).

As already mentioned with a PWM power supply, the main problem regarding PD detection is the electromagnetic noise induced by switching, which is directly related to  $dV/dt$ . Also, according to the state of art, when the voltage reaches the PDIV, PDs appear during the  $dV/dt$ . They are buried in noise. In order to observe them, “low frequency” components must be filtered because the frequency spectrum of a PD generally extends over a larger frequency range than the noise associated with semiconductor switching

Thus, for a 260V supply voltage and the fastest speed of the machine, output signals of the sensor that could be PDs are observed (Figure IV.13). The high-pass filter has a cutoff frequency of 200 MHz.

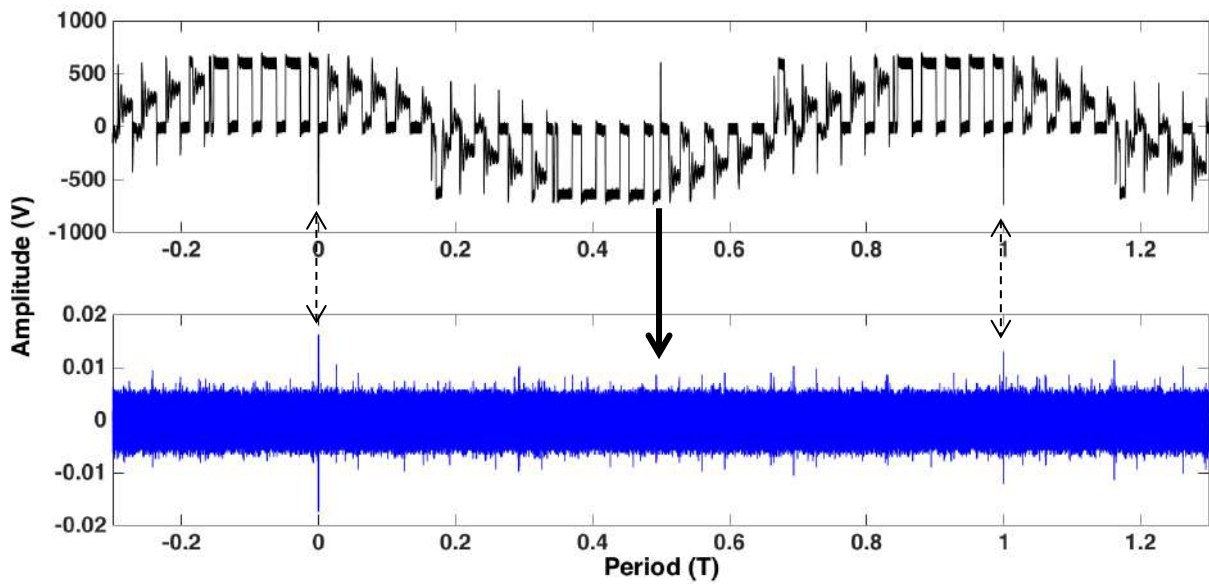


Figure IV.13: Phase to phase voltage UW (black), sensor signal on U and filtered at 200 MHz (blue)

Figure IV.13 shows that:

- These signals coincide temporally with the phase to phase voltage surges (dashed arrows)
- Their amplitude varies (which is a feature of the stochastic nature of PDs).
- For overvoltage, there is no associated signal output from the sensor (continuous arrow).

#### IV.2.3.4 Studying $dV/dt$

To verify that the signals observed by the sensor are not due to the noise associated with switching, it is important to observe the different voltage. For this, zooming on the peak signals at the sensor output enables us to observe  $dV/dt$  for the associated surge. This zoom makes it possible to measure the rise time of the PWM voltage.

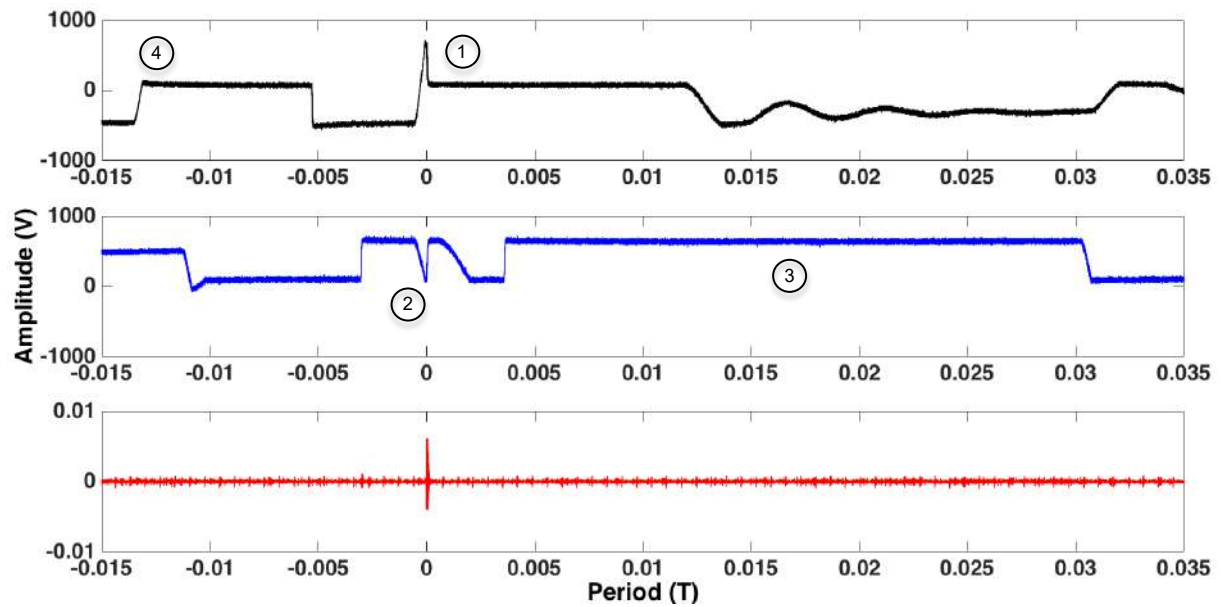
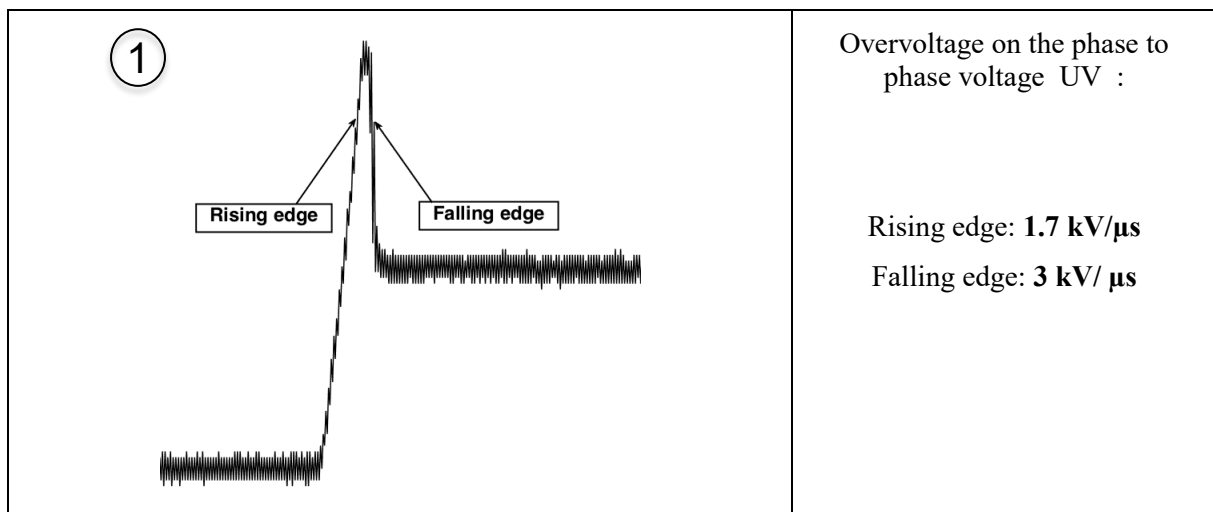


Figure IV.14: Phase to phase voltage UV (black), phase to phase voltage VW (blue), sensor signal filtered at 200 MHz (red)

The list of studied  $dV/dt$  and associated rise times are given below. In the following, the rising edges are defined by the voltage variation from 0 V to  $\pm V$ , and falling edges by the voltage variation from  $\pm V$  to 0V. In the case of overvoltage, the rising edge is the transition from one polarity to the other, and the falling edge is the return to 0V. The edges below were recorded for a 260 V power supply.



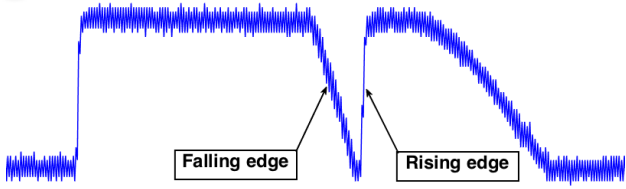
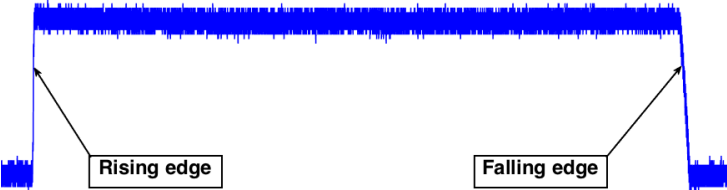
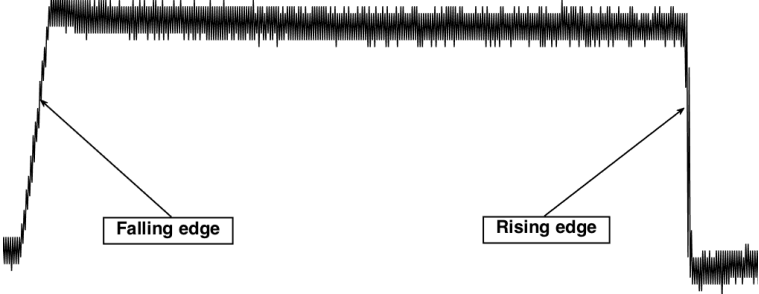
<p>②</p> 	<p>Voltage shape of the phase to phase voltage VW associated with the overvoltage on the phase to phase voltage UV:</p> <p>Rising edge: <b>4.5 kV/μs</b> Falling edge: <b>890 V/μs</b></p>
<p>③</p> 	<p>Voltage shape of one pulse of phase to phase voltage VW (positive polarity):</p> <p>Rising edge: <b>6.24 kV/μs</b> Falling edge: <b>1 kV/μs</b></p>
<p>④</p> 	<p>Voltage shape of one pulse of the phase to phase voltage UV (positive polarity):</p> <p>Rising edge: <b>6.4 kV/μs</b> Falling edge: <b>1.1 kV/μs</b></p>

Table IV.2: Voltage edges shape and their associated dV/dt

The fastest edges correspond to the rising edges of the pulse of the PWM voltage. An electromagnetic noise extending to higher frequencies will be associated with these fronts, but as it may be noted no singular peak is observed on the filtered output signal from the sensor.

The filter cutoff frequency used here is sufficient to suppress noise induced by switching. The peak observed at the sensor output corresponds to slower fronts. This peak is not due to electromagnetic noise from switching and could be associated with PD. Before validating this assumption, it is necessary to ensure that this signal is not related to another phenomenon.

### IV.2.3.5 Signal analysis

First, the signal was observed over many periods to estimate its recurrence (Figure IV.15).

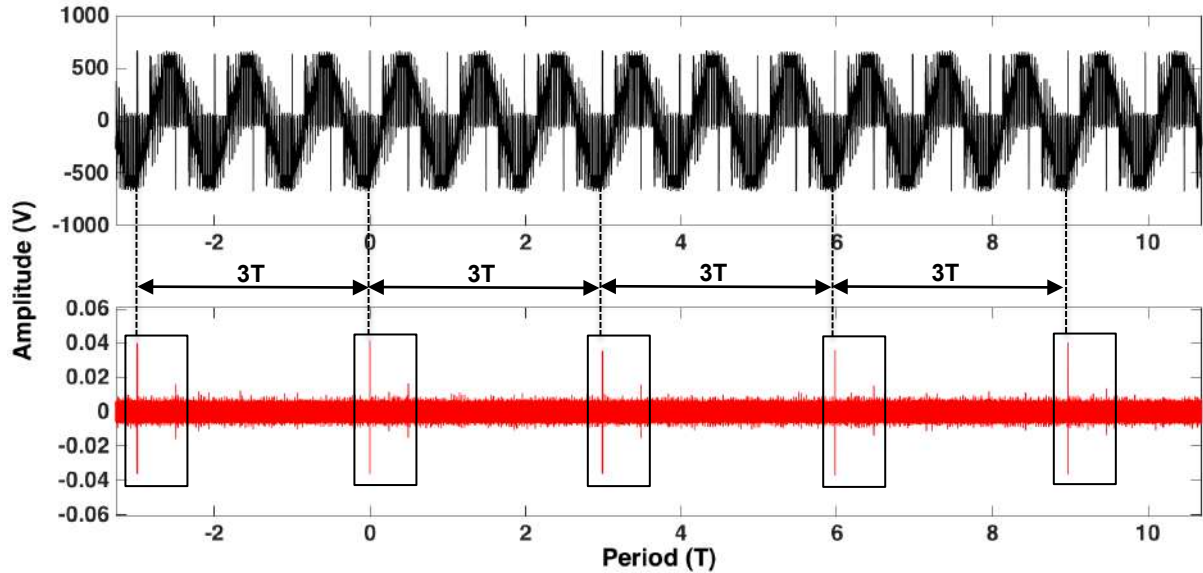


Figure IV.15: Acquisition for analyzing recurrence

Two groups of peaks were observed:

- The first, corresponding to high amplitude peaks coinciding with the surge that starts in the negative polarity and ends in the positive polarity.
- The second, consisting of lower amplitude peaks coinciding with the surge that starts in the positive polarity and ends in the negative polarity.

We can also notice that the latter behavior recurs in all three periods. This type of phenomenon is not characteristic of PDs. Indeed, an appearance in each period would be more likely. The present state of our knowledge does not allow us to propose a valid origin to explain the observed behavior.

We then analyzed the signal using a filter with a lower cutoff frequency (100 MHz). The signal below was observed (Figure IV.16):

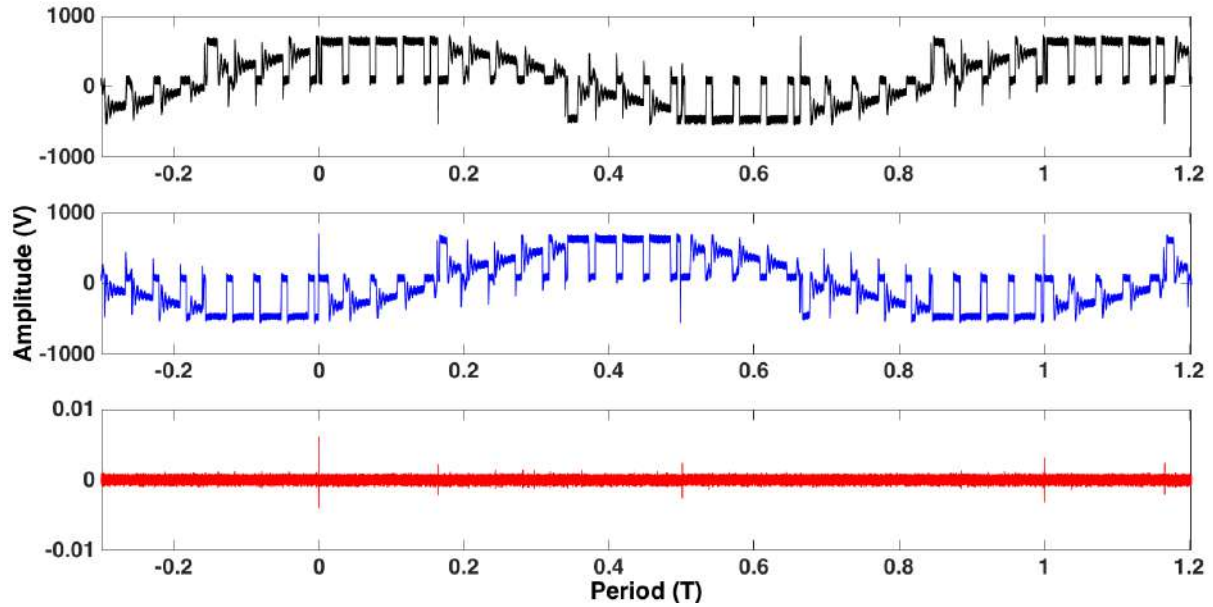


**Figure IV.16: Phase to phase voltage UV (black), phase to phase voltage VW (blue), sensor signal filtered at 100 MHz (red)**

The peaks appearing for surges starting in the positive polarity and ending in negative polarity of the phase to phase voltage UV (black curve) are observed consistently. However, additional peaks of smaller amplitude, coinciding with the surge observed of the phase to phase voltage VW (blue curve) appear. Reducing the cutoff frequency of the filter leads to the detection of phenomena that can be noise associated to switching occurrences, on other non-instrumented phases, and not PDs.

Given the presence of surges, PD appearance may not be excluded. The presence of overvoltages induced by the type of command had not been observed to date. In addition, the magnitude of these surges is directly related to the machine's rotation speed. When the surge is sufficient, the sensor detects some signals, but it is currently not possible to rule on the nature of the detected peaks. The characteristics of the peaks that may be associated with PDs are as follows:

- Their position in the phase must coincide with surges.
- They are not related to electromagnetic noise-induced by switching since they do not occur for fronts with the highest  $dV/dt$ .

Nevertheless, their recurrence rate does not match with that usually observed for PDs. Another assumption is that they could be related to a certain type of discharge but more fundamental works are still necessary before being able to conclude

This case helped highlight the emergence of surges depending on speed and induced by the command. This behavior had not been documented previously. Also, it can be seen that, in some cases it is possible to observe signals that can be related to partial discharges, though some features do not

correspond to PDs. In some case, it may be impossible to rule on the presence of PDs even if noise is completely removed.



### IV.2.4 Case 3: Necessity of a deep analysis

The nominal operating motor voltage level in this case was 540V and the cable length connecting the actuator to the inverter was significantly long. There is theoretically a risk to obtained surges, which may initiate PDs. However, it was not possible to carry out voltage measurements at the motor terminals for this configuration because the test bench was in a tank and all the measurements were made on a connexion box outside of this tank.

After determining the appropriate cutoff frequency filters, acquisition was carried out to observe the sensor output signals.

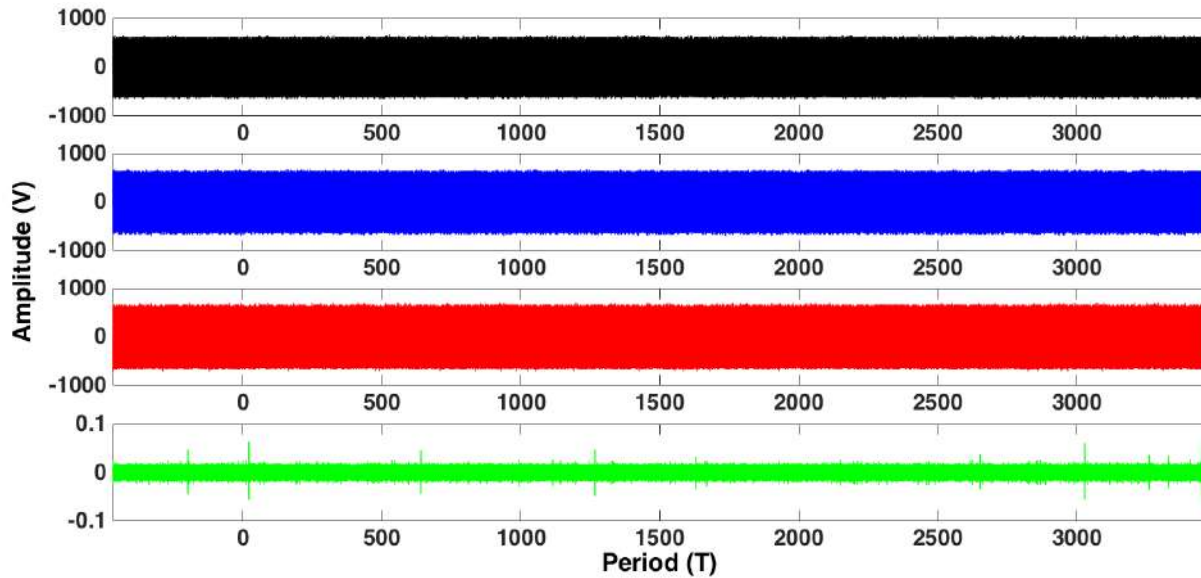


Figure IV.17. Phase to phase voltage UV (black), phase to phase voltage VW (blue), phase to phase voltage WU (red), sensor signal on phase U1 filtered at 150 MHz (green) on a large time

First of all, it can be seen in Figure IV.17 that the noise is fully filtered. Then, it may be observed that the sensor output signals may be similar to partial discharges. The amplitude of the signal varies significantly from one case to another. In addition, the phenomenon is not periodic suggesting that the phenomenon is not related to noise. To further investigate the signals, acquisitions were performed in a shorter time.

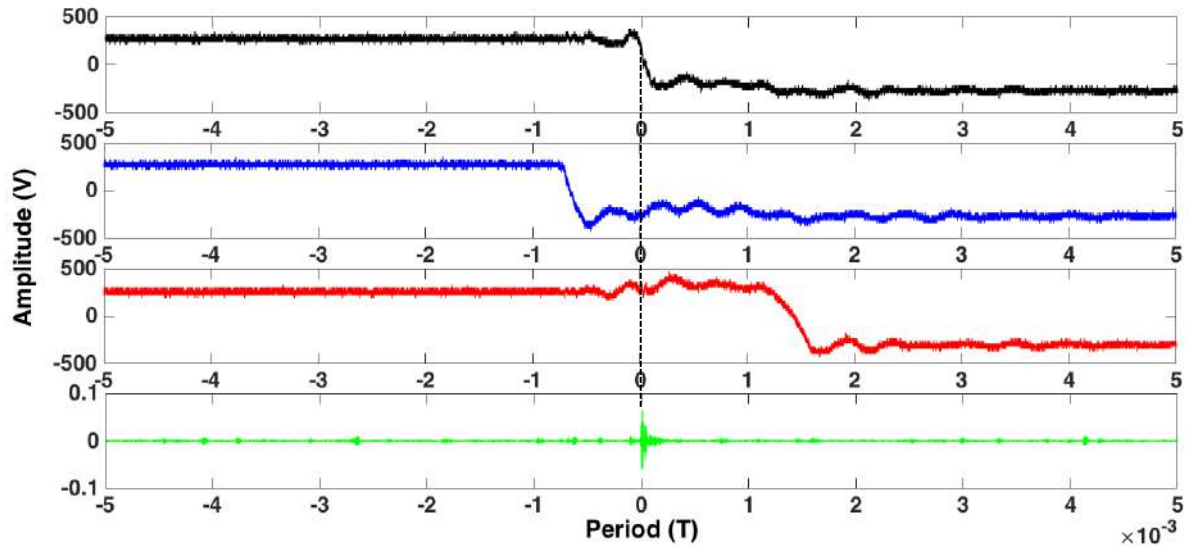


Figure IV.18: Phase to ground voltage U (black), phase to ground voltage V (blue), phase to ground voltage W (red), sensor signal on phase U filtered at 150 MHz (green)

Figure IV.18 shows that the sensor output signal appears during the switching of phase to ground voltage U. A slight time difference can be seen between the maximum value of the phase to ground voltage, which can be explained by signal wave propagation time. However, this glitch does not match the peak temporally after the change in polarity, but rather to a ripple just before the change in polarity. Moreover, a maximum voltage oscillation of 375V is observed. If the sensor signal output corresponds to a PD, then it is not located in the slot because the voltage is too low compared to the values usually measured during the initial off-line partial discharge tests.

A study of the phase to phase voltage is needed to know whether the PDs are initiated or not.

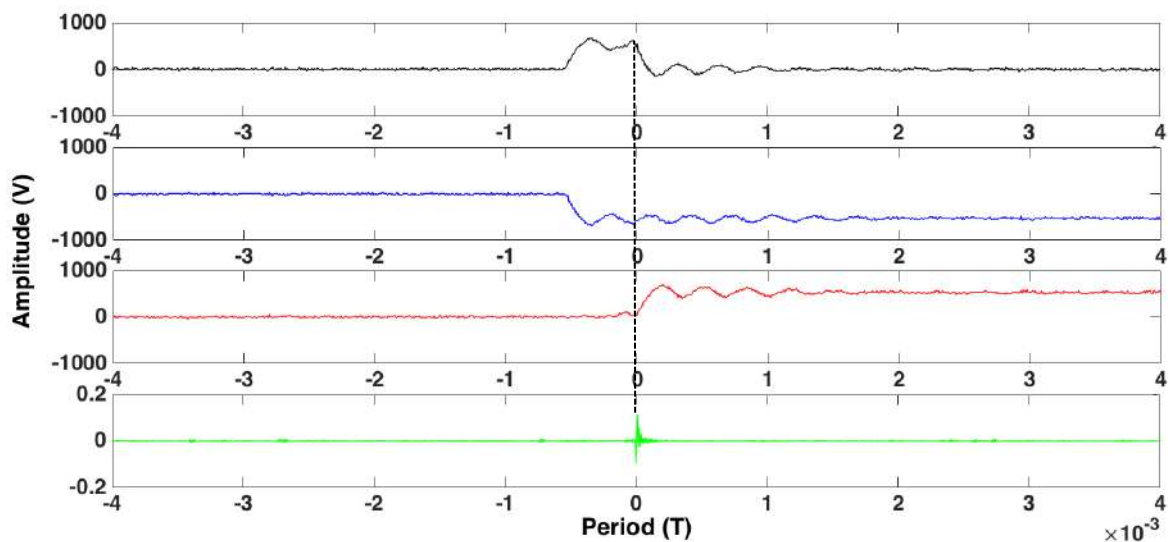
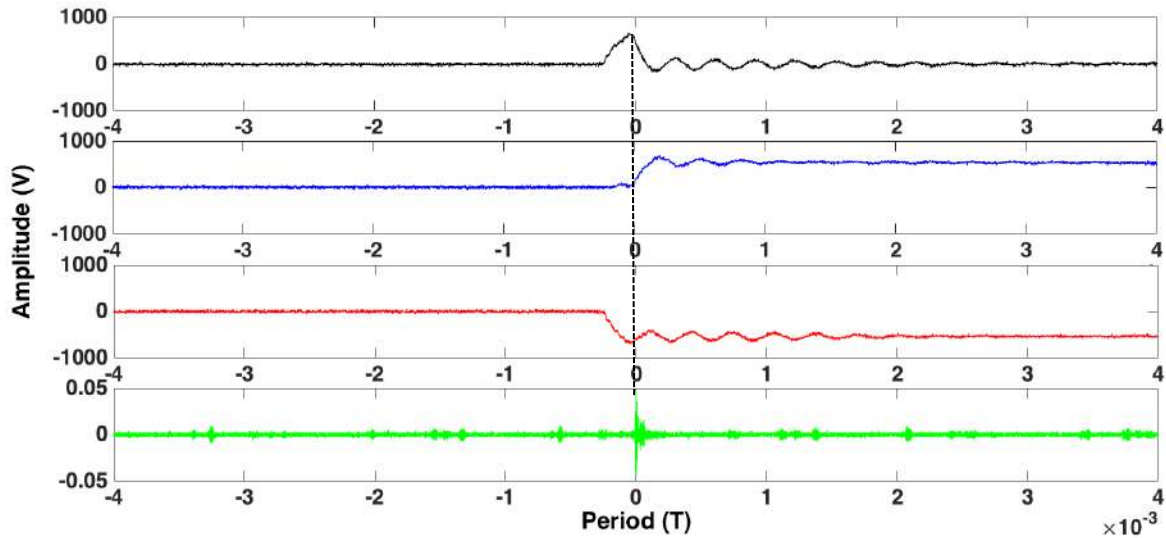


Figure IV.19: Phase to phase voltage UV (black), phase to phase voltage VW (blue), phase to phase voltage WU (red), sensor signal on phase U filtered at 150 MHz (green), zoom on sensor signal

Figure IV.19 shows that the output signal does not match the maximum of the first oscillation of the phase to phase voltage UV, but rather the maximum of the second oscillation. The maximum voltage of the second oscillation is 633V, whereas the maximum voltage of the first oscillation is 660V. If the signal is a partial discharge, it would be surprising that this signal coincides with the second oscillation, as the maximum voltage is located in the first oscillation.

Other acquisitions were performed to observe whether this phenomenon repeats itself or not.



**Figure IV.20: Phase to phase voltage UV (black), phase to phase voltage VW (blue), phase to phase voltage WU (red), sensor signal on phase U filtered at 150 MHz (green), zoom on sensor signal**

Figure IV.20 shows that the signal coincides with a maximum phase to phase voltage UV. In that case, the maximum voltage value is 700V.

In the three Figures above, we can see that the sensor output signals appear to coincide for voltages of square waves having the lowest duty cycle. A signal was investigated over ten periods and, then the temporal position of the sensor output signals was studied.

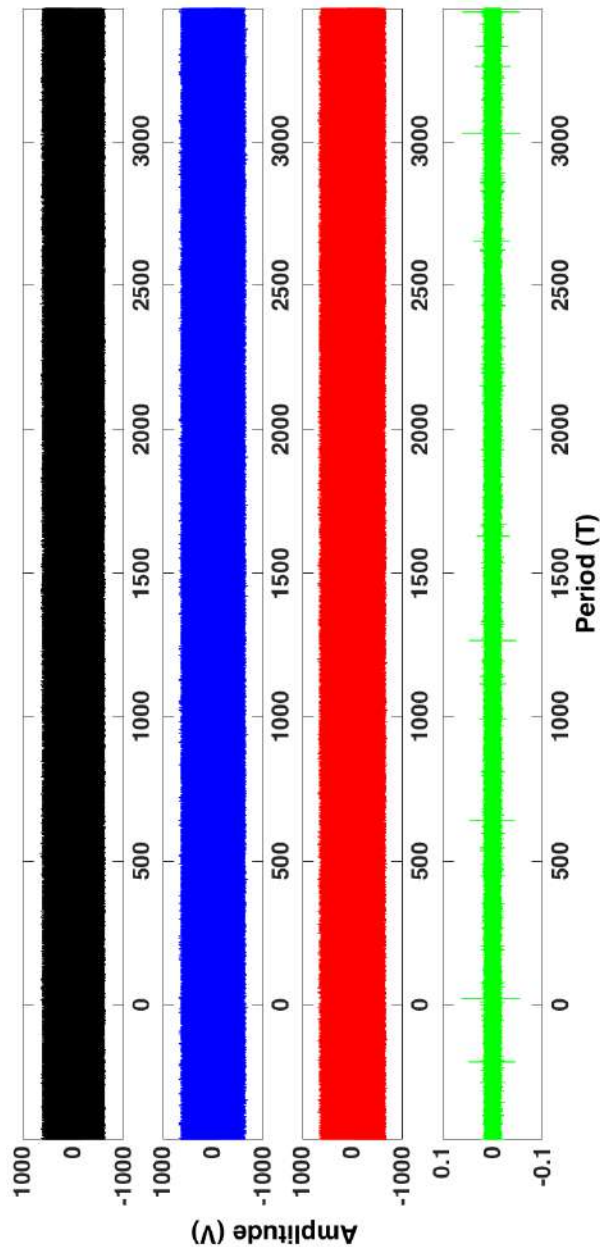


Figure IV.21: Phase to phase voltage UV (black), phase to phase voltage VW (blue), phase to phase voltage WU (red), sensor signal on phase U filtered at 150 MHz (green) on a large time

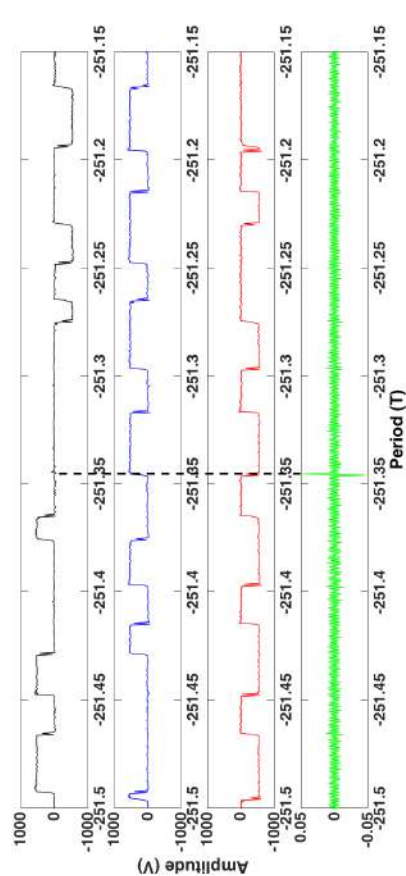


Figure IV.23: Zoom on phase to phase voltage UV (black), phase to phase voltage VW (blue), phase to phase voltage WU (red), sensor signal on phase U filtered at 150 MHz (green)

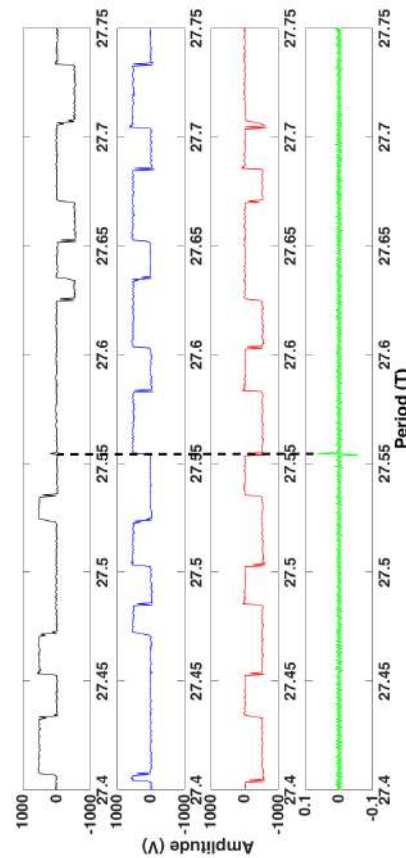


Figure IV.22: Zoom on phase to phase voltage UV (black), phase to phase voltage VW (blue), phase to phase voltage WU (red), sensor signal on phase U filtered at 150 MHz (green)

Two zooms on interesting signals are shown in Figure IV.22 and Figure IV.23. For these two signals, it can be seen that the signal coincides temporally with the last pulse of the positive polarity of the phase to phase voltage UV. It is nevertheless difficult to see these voltage pulses because their duration is less than 1  $\mu$ s. Also, it can be seen that these nearly square waves have low voltage amplitude: the pulse of Figure IV.23 has a peak amplitude of 86 V, while the pulse of Figure IV.22 has a peak amplitude of 186 V. It can be claimed with certainty that the signals observed in these cases are not PDs.

Given the results obtained, the observed signals do not correspond to partial discharge. During the steady state, these signals still appear at the last pulse of the polarity for which the voltage can be very low. However, other parameters such as low occurrence and the fact that the signal appears for the maximum voltage of a pulse can be misleading. Indeed, these parameters are generally associated with PD signals. It is therefore important to pay attention to these false positives, and it would be impossible to rule on these signals if they had not appeared for very low voltages (<100V ).

A switch aborted by the command could cause these voltage pulses of very short duration and sometimes very low amplitude. It is actually uncommon for all branches of the inverter to switch so close to each other, and commutations are generally operated in pairs in a standard PWM strategy. Updating the duty cycles for the command controlling the machine may, in some cases, involve this kind of switching, later aborted by control and safety devices. The proximity of these events with polarity changes in the steady state and during the starting phase would indicate a borderline case for calculating duty cycles from the desired operating point.

### IV.2.5 Case 4: “Simple” PD detection

For this test, it was possible to vary the speed and bus voltage over a wide range.

First, a test with a DC bus voltage of 554V was conducted. This test was intended to adjust oscilloscope calibers and optimize selection of the filters. The diagram below shows the curves representing the voltage at the machine terminals and the output signals from the different sensors.

Connection to the oscilloscope, channel:

1. W phase to ground voltage measurement
2. UW phase to phase voltage measurement
3. Jack-SMA sensor on U phase – No filtering
4. Jack-SMA sensor on W phase – No filtering

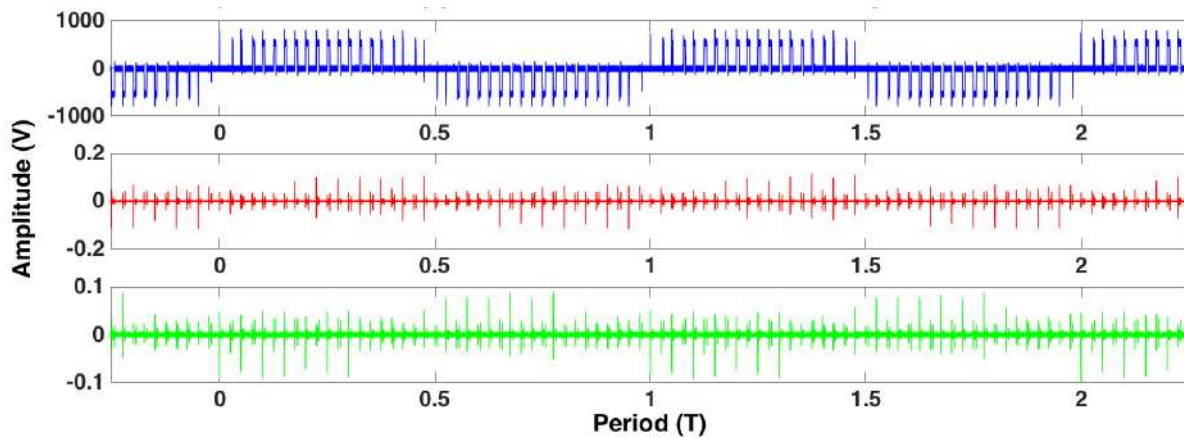


**Figure IV.24: Phase to phase voltage UW (blue), sensor signal on U without filtering (red), sensor signal on W without filtering (green)**

Overvoltages can be observed on the phase to phase voltage measurement. These surges have a maximum amplitude of 770V peak. It can then be seen that the sensors are saturated by switching, and further tests are necessary using high-pass filters to suppress electromagnetic noise.

For this test, the previous set-up has been used, but high-pass filters with cutoff frequency of 200 MHz were added.

The figure below shows that the use of these filters removes all the output signals from the sensors, particularly noise-induced voltage edges (Figure IV.24).

Connection to the oscilloscope, channel:

1. UW phase to phase voltage measurement
2. Jack-SMA sensor on U phase – 200 MHz high-pass filtering
3. Jack-SMA sensor on W phase – 200 MHz high-pass filtering



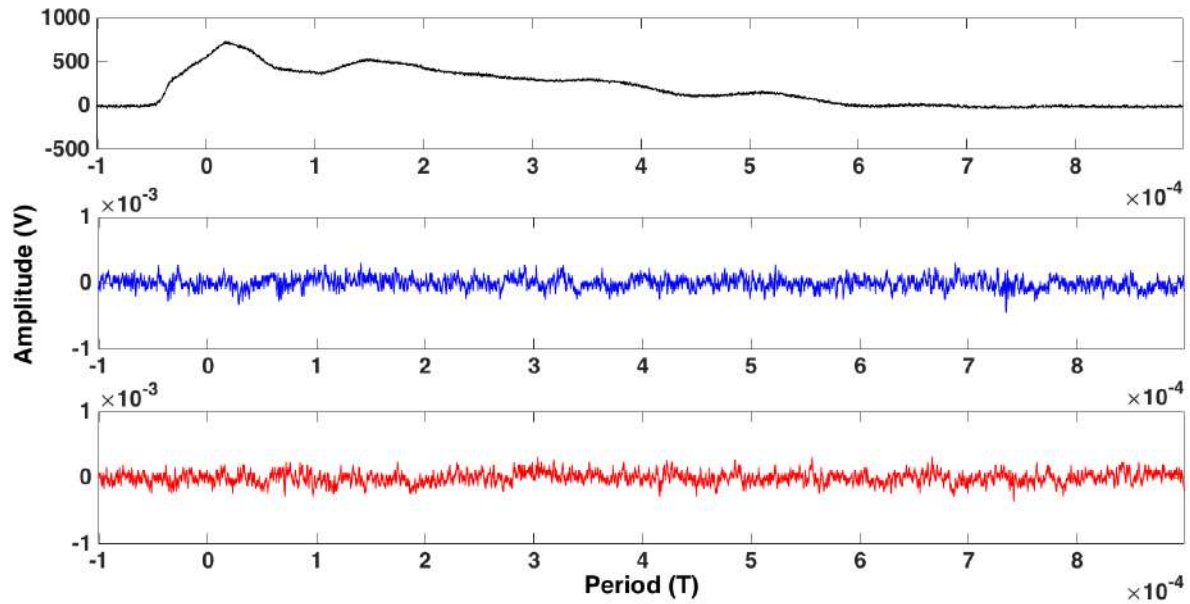


Figure IV.25: Phase to phase voltage UW (black), sensor signal on U filtered at 200 MHz (blue), sensor signal on W filtered at 200 MHz (red)

#### IV.2.5.1 Study on the winding

In the case below, the filters were replaced by filters with a lower cutoff frequency (100 MHz). A signal similar to a PD signal can be seen in the Figure IV.26 for the two sensors. The noise induced by switching is completely filtered.

The parameters, which confirm the hypothesis of the presence of discharges, are:

- Low recurrence
- PD signal seem to coincide temporally with peak voltages
- Consecutive signals at different voltage polarities
- And, last but not least, signals appearing from the same voltage as the PDIV measured under AC supply voltage in a previous test

Various acquisitions were performed for different times in Figure IV.26.

Connection to the oscilloscope, channel:

1. UW phase to phase voltage measurement
2. Jack-SMA sensor on U phase – 100 MHz high-pass filtering
3. Jack-SMA sensor on W phase – 100 MHz high-pass filtering

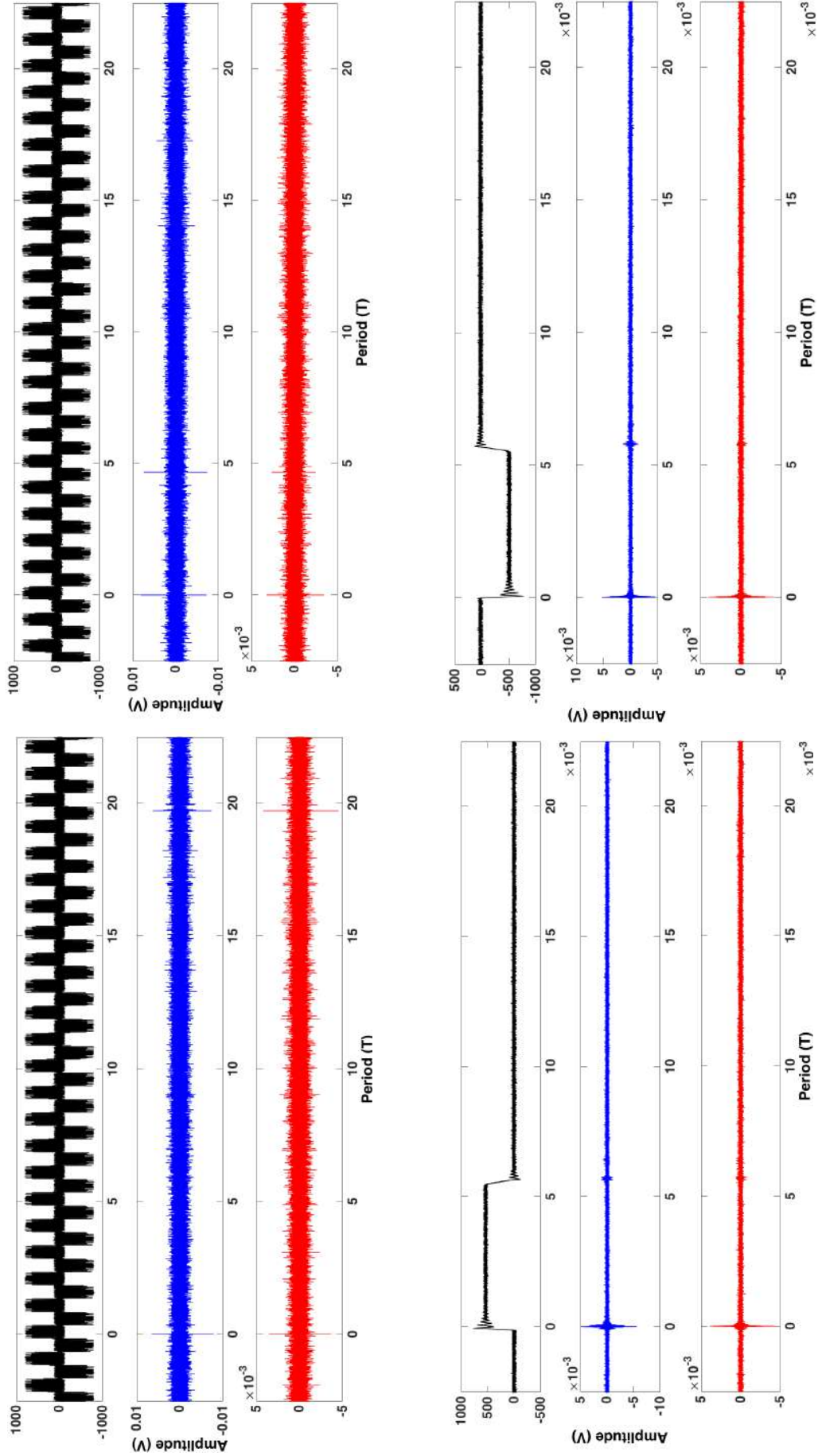
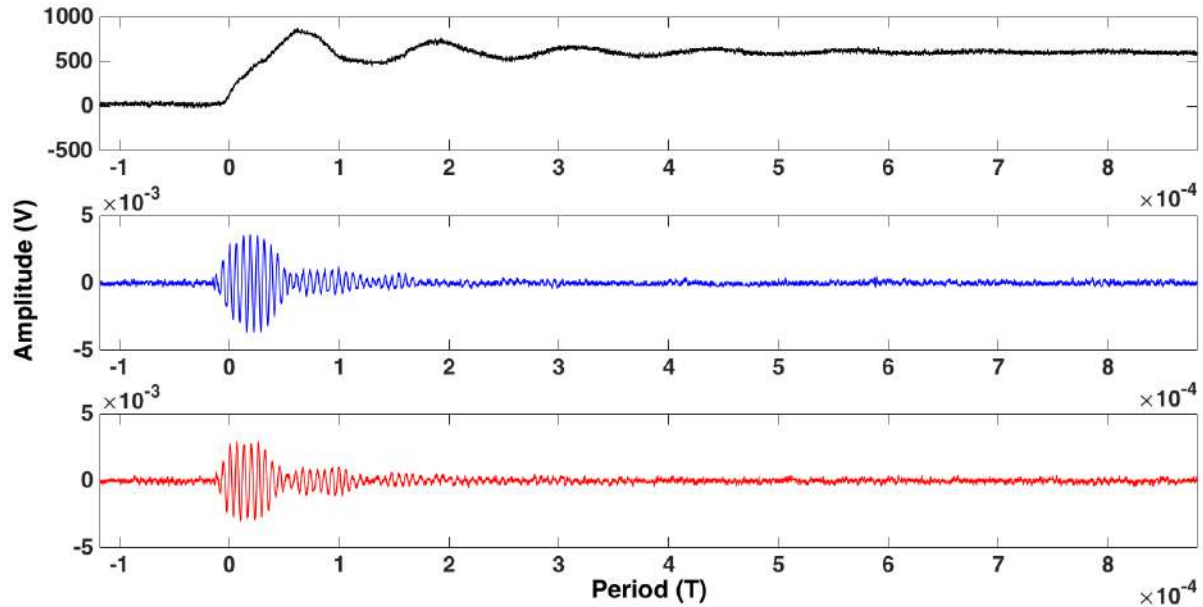


Figure IV.26: Phase to phase voltage UW (black) sensor signal on phase U filtered at 100 MHz (blue), sensor signal on phase W filtered at 100 MHz (red) for different time scales



The temporal position of the signal was observed to compare it to the maximum voltage in order to confirm the assumption that these signals correspond to discharges.

Nevertheless, Figure IV.27 shows that the characteristic signals appear in advance from the maximum voltage, so it is necessary to measure the other phase to phase voltages to ensure that these signals appear at a maximum voltage.



**Figure IV.27: Phase to phase voltage UW (black), sensor signal on phase U filtered at 100 MHz (blue), sensor signal on phase W filtered at 100 MHz (red), comparison between sensor signal and maximum voltage time position**

Following the previous tests, we decided to measure all the voltage between phases.

Connection to the oscilloscope, channel:

1. UV phase to phase voltage measurement
2. UW phase to phase voltage measurement
3. VW phase to phase voltage measurement
4. Jack-SMA sensor on U phase – 100 MHz high-pass filtering

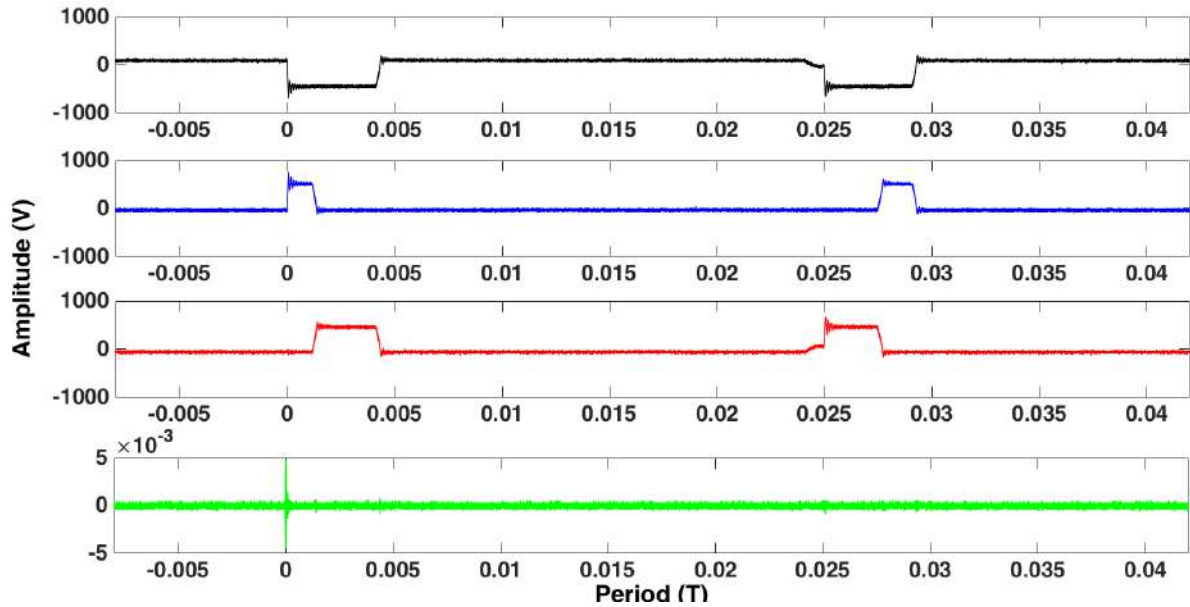


Figure IV.28: Phase to phase voltage UV (black), phase to phase voltage UW (blue), phase to phase voltage VW (red), sensor signal on phase U filtered at 100 MHz (red), time position comparison between sensor signal and all the maximum voltage

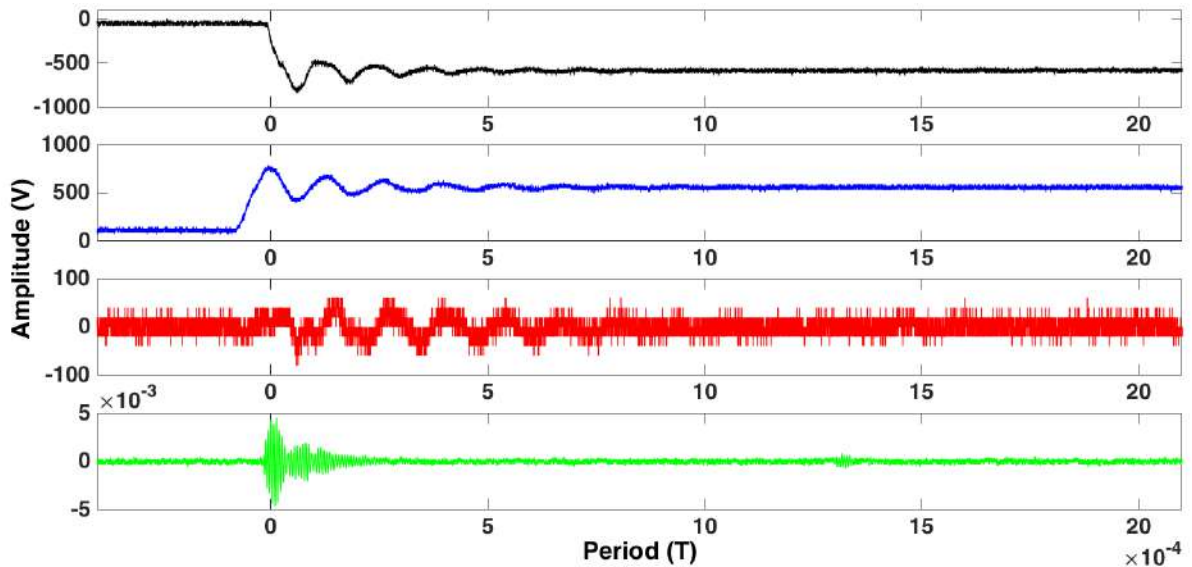


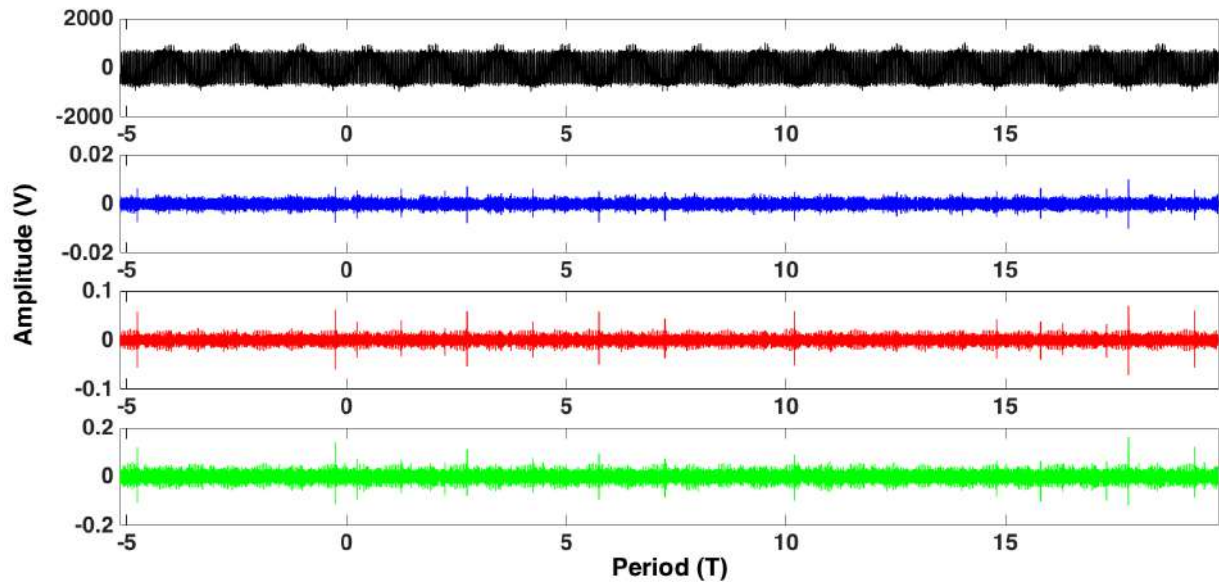
Figure IV.29: Phase to phase voltage UV (black), phase to phase voltage UW (blue), phase to phase voltage VW (red), sensor signal on phase U filtered at 100 MHz (green), Zoom of the sensor signal and all the maximum voltage

Figure IV.29 shows that the sensor signal appears at the maximum value of the phase to phase voltage UW.

To improve the detection, we decided to try to increase the capacitive effect of the sensor using copper tape. At the same time, we placed an inductive sensor.

Connection to the oscilloscope, channel:

- UV phase to phase voltage measurement.
- Jack-SMA Sensor located on U + High Pass filter 100 MHz.
- Inductive sensor located on U + High Pass filter 100 MHz
- Jack-SMA Sensor located on U + additional capacitive effect (Scotch tape) + High Pass filter 100 MHz
- 



**Figure IV.30: Phase to phase voltage UV (black), sensor (jack SMA) signal on phase U filtered at 100 MHz (blue), sensor (inductive) signal on phase U filtered at 100 MHz (red), sensor (jack SMA + additional capacitive effect) signal on phase U filtered at 100 MHz (green)**

First of all, Figure IV.30 shows that the amplitude of discharges on the sensor, which is improved with the capacitive effect, is much larger than that on the single sensor.

It can also be observed that the inductive sensor detects PD. However, the signal amplitude is lower than the one measured by the sensor with the improved capacitive effect.

Another important point is that all the sensors detect the same signal. This suggests that our detection system is functional and able to detect and locate all discharge phenomena

These tests detect signals similar to partial discharges on representative equipment operated under normal conditions. These signals have all the features of partial discharges:

- Low recurrence
- PD signal temporally coinciding with peak voltages
- Consecutive signals at different voltage polarities.
- Signals appearing from the same voltage as the PDIV measured under AC supply voltage

We can therefore consider that the detection system is functional. The increase in the sensor's coupling capacitance can increase the magnitude of the measured signals significantly. Ten times greater amplitude can be seen compared to the “single” sensor. Twice greater amplitude was observed relative to the inductive sensor.

#### IV.2.5.2 Denoising by CWT method

The denoising method based on wavelet decomposition, detailed in Chapter III, has only been validated on on laboratory samples. It is therefore particularly interesting to apply under real constraints in an industrial environment.

The results of the denoising method applied to the previous case are given in Figure IV.31.

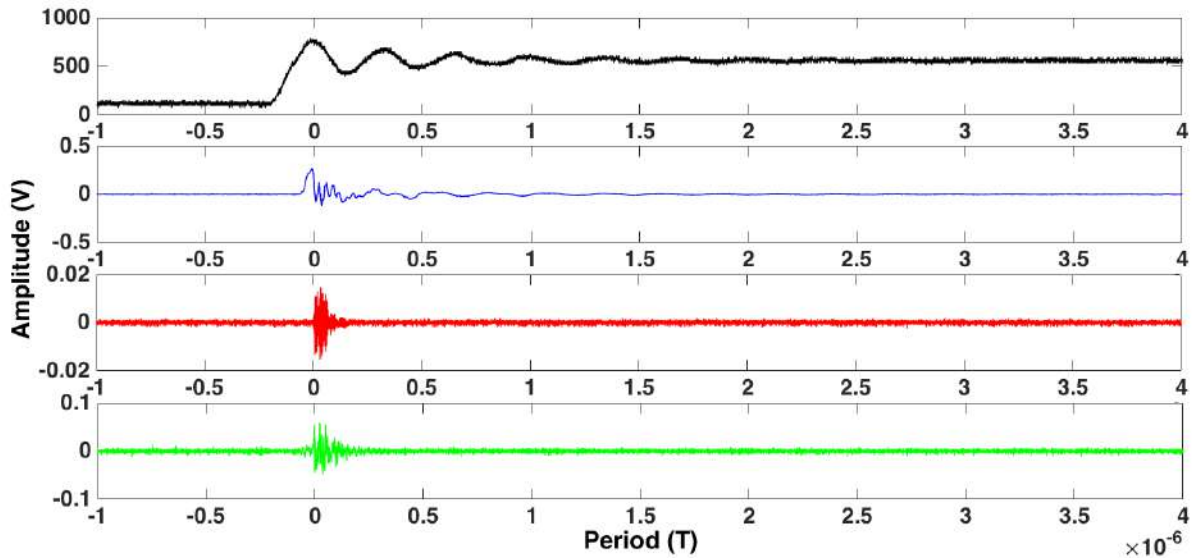


**Figure IV.31: Phase to phase voltage UW (black), sensor signal on phase U without filtering (blue), sensor signal on phase U filtered at 100 MHz (red), sensor signal reconstructed by CWT (green) (note the scale changes)**

Our method allows suppressing the noise (blue curve) and leads to a good reconstruction of the PD signal. Moreover, the amplitude of the signal reconstructed thanks to the numerical method is five times greater than the signal filtered analogically. In the case under study here, there was few doubts regarding the presence of discharges, but in other cases, not shown here, the proposed method improves the denoising.

## IV.2.6 Case 5: PD detection in machines fed by SiC inverter

With the concept of “more electric aircraft”, higher voltage levels and changing electrical architectures (notably the increased use of converters) was observed. Future projects related to hybrid propulsion for e.g. are considering a further increase in voltage levels. In a relatively near future (20 years), voltage up to several kilovolts may be envisioned. In addition, silicon carbide-based (SiC) electronic power components will probably replace the current silicon-based components in some high efficiencies and high power density applications. The use of high voltage will increase the risk of partial discharge occurrence, while the evolution of electronic components will result in an increase in switching speed and consequently an increase in the noise frequency spectrum.

In this context, it is important to determine whether the detection method detailed in this thesis will always be functional, given this development. Currently, many domains use voltages on the order of kilovolts and are studying converters using SiC components. Some tests were carried out on an industrial bench using on SiC converters supplied by a DC bus of a few hundred volts. All tests were carried out on prototype motors with an important length of cabling.

The brief description of the results obtained with the detection method during these tests is provided below, allowing a clear demonstration of the ability of the method to detect PDs.

### IV.2.6.1 PD detection

Tests were performed with a SiC converter supplied by a DC bus at 750 V and the distance between the inverter and the motor was about ten meters.

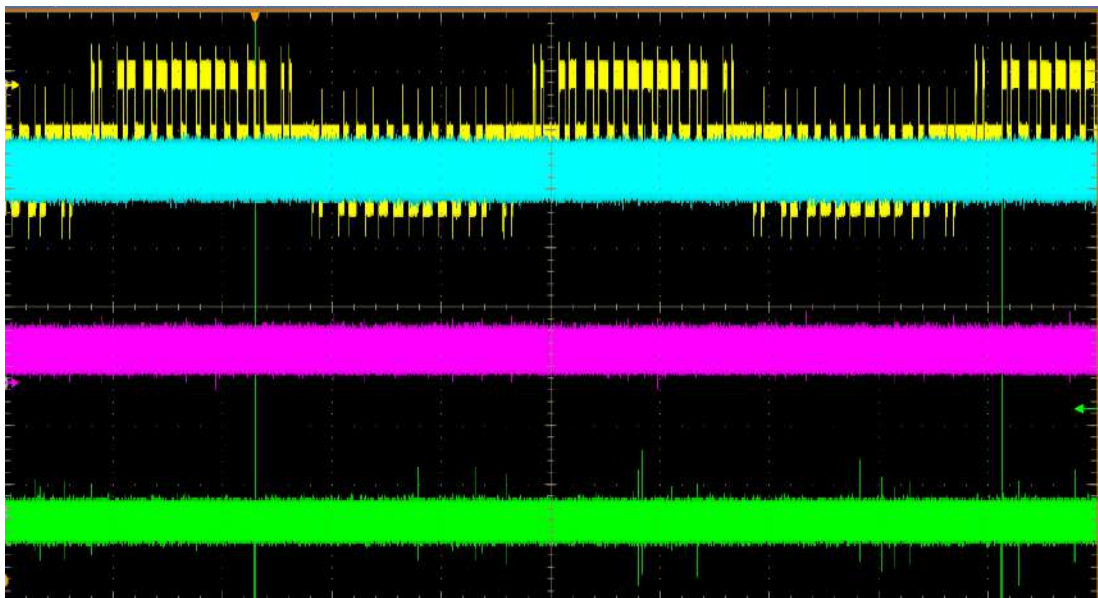
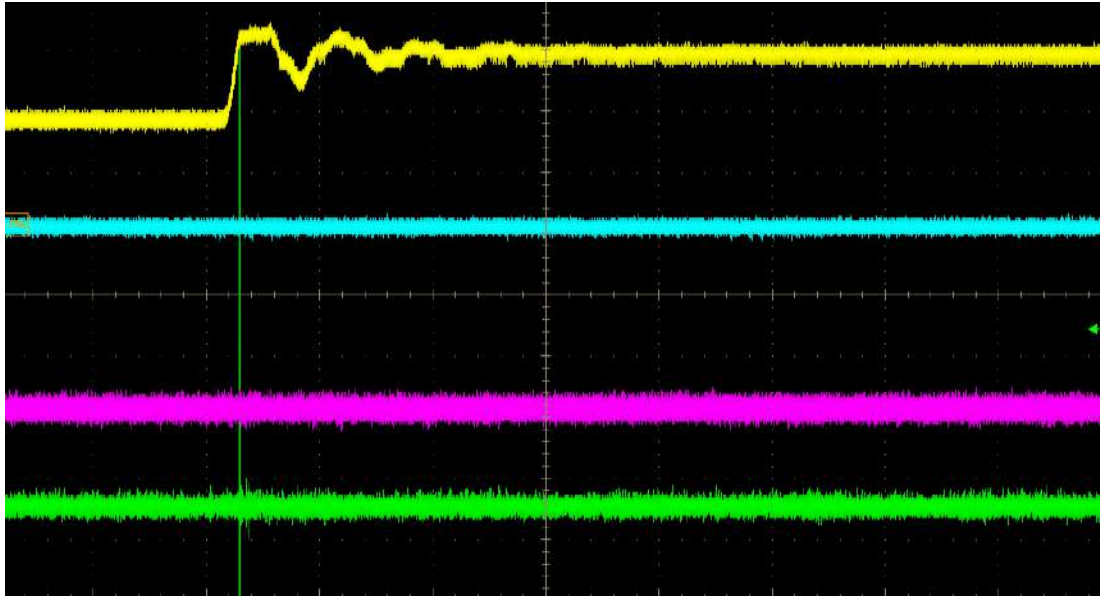


Figure IV.32: PD research on a motor supplied by a SiC converter





**Figure IV.33: Zoom on a partial discharge for a 1 kV overvoltage**

Under such conditions, the overvoltages amplitude is about 1100 V and the  $dV / dt$  have a value of 10 kV/ $\mu$ s. To eliminate the noise induced by these voltage fronts, it was necessary to use high pass filters having a cut-off frequency of 500 MHz.

There are no characteristic signals that coincide temporally with all fronts, indicating that the filter is adequate for removing noise-induced switching.

The observed signals have many characteristics of the presence of discharges:

- Low recurrence
- Signals seem to coincide temporally with peak voltages

The Jack-SMA sensors optimized with a 5 cm copper tape were used for the observation of PDs, but the signals detected after filtering had a too large amplitude ( $> 10$  V). It was not necessary to enhance the sensor to detect the PD in this case. Discharges were therefore very energetic.

Another interesting result of this study concerns the ability of detecting PDs despite the use of filters having a high cut-off frequency. It has been observed in Chapter II that the amplitude of the frequency components of PDs, appearing under PWM for 3 kV /  $\mu$ s edges, is very low beyond 300 MHz. In this case, despite of the use of filters having a cutoff frequency of 500 MHz, signals of PDs have been detected, which proves that in this case the frequency spectrum of the PDs spreads over a higher frequency range than for 3 kV /  $\mu$ s edges. The  $dV / dt$  thus appears to have an influence on the frequency spectrum of the PDs.

The method is functional and the characteristic signals of PDs coincide temporally to overvoltage occurrences. Additionally, the variable distribution of the amplitude of the sensor signals corresponds to the stochasticity of partial discharge.

#### IV.2.6.2 Temporal position of PDs

All the studies presented up to now have been focused on low-voltage motors working at voltage levels generally lower than the PDIV and it is only the overvoltage induced by the electromechanical chain that lead to PDs ignition. This is why discharges appear during the voltage edge and why denoising is such a big problem.

During these tests, the rating coltage was high compared to the PDIV. It seemed therefore particularly interesting to study the distribution in time of the PDs.

Hence Figure IV.34 and Figure IV.35 clearly illustrate that PDs appear not only during the voltage front but also during the plateau part of the voltage. Such a behavior corresponds to the PDs pattern observed and reported in the literature for motors operating at high voltage. The detection during the continuous part (plateau) of the voltage being much simpler because there is no need to filter the signals.

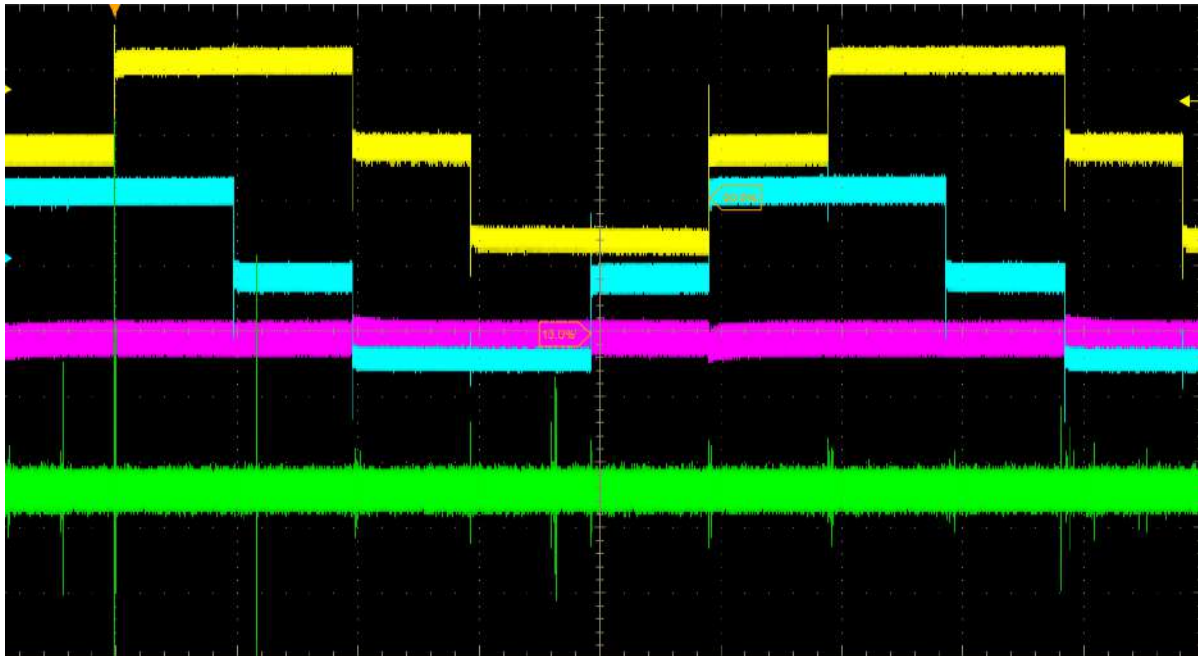


Figure IV.34: Temporal position of PDs on two periods

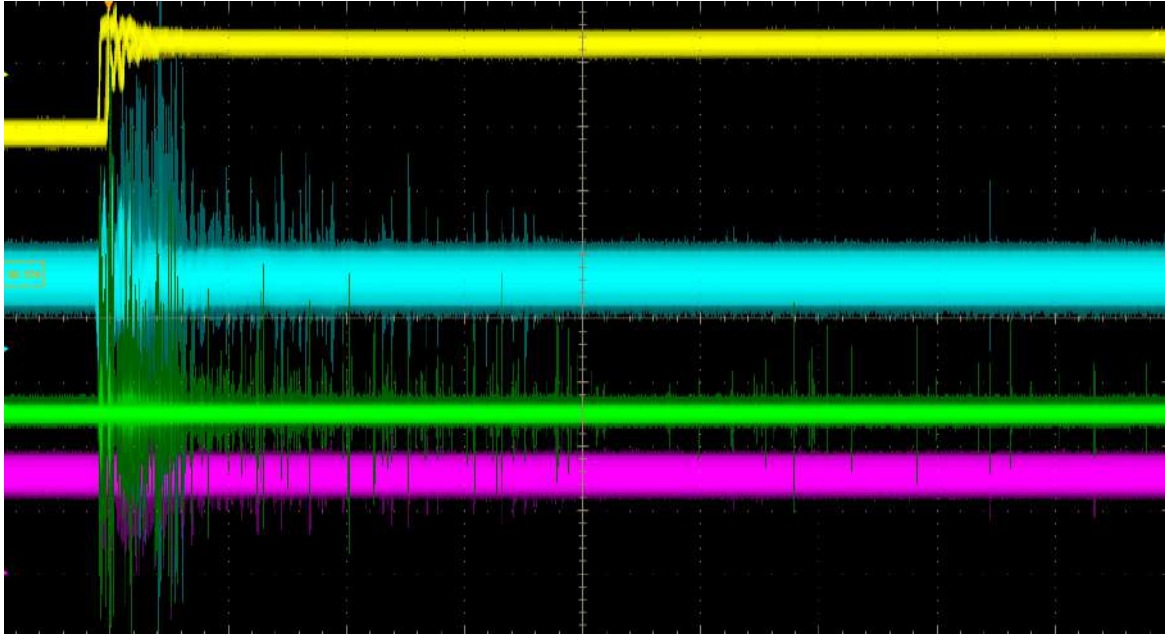


Figure IV.35: Zoom and persistence on a voltage edge to observe temporal position of PDs

As another fact, In the case of motors operating at higher voltages, the PDs not only appear during the front but also on the continuous part of the square waveform (Figure IV.36). The appearance of PDs in this type of machines is much more studied [65], [66].

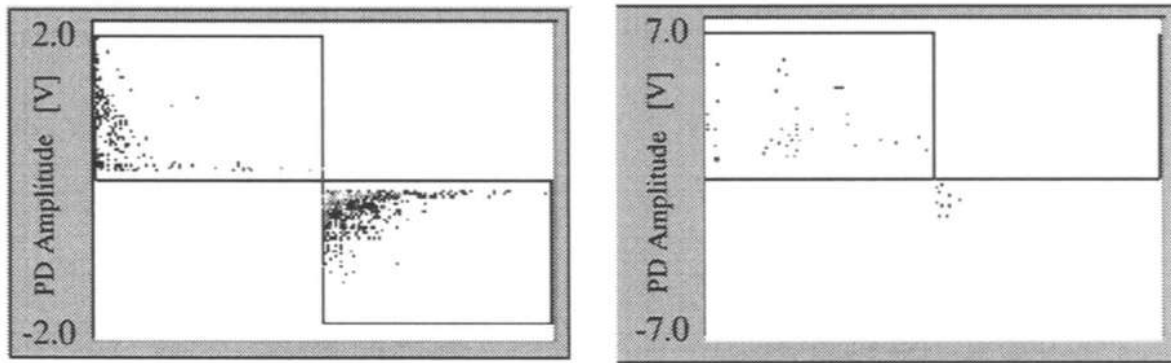


Figure IV.36: PD patterns at 1.8 kV (peak value) with bipolar and unipolar square waveforms [67]

The results presented in Figure IV.34 and Figure IV.35 look like the ones of the Figure IV.36.

We can therefore state that our method also works for detecting discharges in motors powered by SiC inverters and high voltages. Further tests must now be performed to ensure the validity of these preliminary conclusions.





## **Conclusion**



Given the current state of the art, the concept of “more electric aircraft” has led to the possible occurrence of partial discharges in on-board electrical equipments. This phenomenon was not known in the aeronautical field until recently, yet it could result in accelerated failure of these equipments

Increase in the magnitude of the voltage due to the replacement of some other energy vectors, the increased use of converters, and the use of Type I motors are factors that induce the probability of occurrence of partial discharges. PWM voltage causes the inhomogeneity of voltage distribution in the coil as well as significant surges to the motor terminals. It is therefore mandatory to assess the insulation systems of the various equipment from a partial discharge perspective. To do this, we must be able to detect partial discharges, particularly in an online and non-intrusive manner to obtain an accurate representation of the phenomena’s occurrence, studied under nominal equipment operating conditions.

For that reason, the aim of this work was to develop such a detection method.

To fulfill this goal, we had first to understand the phenomena leading to the occurrence of partial discharges, along with existing detection methods. The state of the art helped highlight the Type I motors used in aircraft and supplied by PWM, where partial discharges could be obtained. Methods for detecting these phenomena are well-known under AC and DC voltage, but under PWM, detection methods are less mastered. Additionally, for the operating voltage under study close to (or lower than) the PDIV, it has been observed that partial discharges occur mainly in the voltage edge and are thus embedded in the electromagnetic noise created by the switching. Analog high-pass filtering proved its ability to remove noise and retrieve partial discharge signals.

It seemed necessary to first drive an analysis of the sensor used for detecting partial discharges in order to optimize its operation. This sensor is based on capacitive coupling, and it was demonstrated that increasing the value of the induced capacity is sufficient to increase the performance of the sensor. In the aeronautics field, variations in pressure and temperature can have a major influence on equipment operations, specifically on the appearance of partial discharges. It is well known that the partial discharge inception voltage depends on these two parameters. However, it has been observed that, under low-pressure, sensors based on detecting electrical phenomena can no longer detect the real inception or even the presence of partial discharges. To explain this, we completed a study on the influence of pressure on partial discharge. This study highlights the modification of the partial discharge frequency spectrum depending on pressure. The decrease in pressure causes a reduction in the amplitude of high-frequency components, while increasing the amplitude of the low-frequency ones. This effect is detrimental to the detection under PWM because the association of this phenomenon with high-pass filtering can lead to an inability to detect partial discharge or with a significant error. Another observation concerns the frequency range over which the partial discharges extend, depending on the shape of the supply voltage. It was observed that the frequency range over which partial discharges extend is much higher for twisted pairs supplied by PWM voltage than by AC voltage. It would be thus

interesting to conduct a study on spectrum evolution according to  $dV/dt$  values to see if there is a relationship.

The second issue is to filter the noise induced by switching. While being a crucial point for detection, testing showed that implementing effective filtering is not a trivial task. Furthermore, there is no predefined methodology for choosing the cutoff frequency for removing noise while maintaining the signals associated with partial discharge. This choice can only be made during the test because it is directly related to the equipment tested. The presence of an expert is therefore always required to achieve good detection, however, the quality of filtering depends strongly on the experimenter, which can cause a wide disparity in results. To avoid this problem, we developed a digital processing method based on wavelet decomposition to remove the noise in signals. To further avoid the requirement for human expertise, we developed a detection algorithm. This method of digital noise removal demonstrated its effectiveness during laboratory tests on twisted pair supplied by PWM.

The method proved its efficiency through tests on different motor test benches and enabled us to highlight various phenomena that can lead to false positives to take into account when analyzing results. In addition to the detection of partial discharges, this method can be versatile and flexible regardless of the equipment under test. In industrial scenarios, partial discharge tests must be superimposed on other tests, which means that it is important not to disturb the existing set-up and testing. Our method fulfilled all these requirements.

Following this work, many opportunities may be proposed to improve our ability to detect partial discharges and improve understanding of these phenomena in the aeronautical environment. These perspectives can be divided into two main axes:

First of all from an application point of view, using the combination of the experimental set-up and the digital processing tool described can lead to a mobile platform for detecting partial discharge. However, this platform is based on scientific equipment and is therefore more suited to laboratory tests, rather than testing in industrial environments. It would be interesting to create test equipment based on this detection method, but more adapted to the industrial environment. In addition, a denoising program based on wavelet transform has been developed (Appendix 1). From a general point of view, the detection system can be transposed to other areas than aeronautics. The method has already been tested in the field of railway and automobile for nearly equivalent voltage levels. Moreover, the current trend is an increase of voltage magnitude for future aircrafts. The method has demonstrated its ability to detect PDs in the case of motors operating at high voltage and will therefore be transposable to future equipments that will operate with these new voltage levels. Nevertheless, in view of the concerns with the current voltage levels, it can be said with certainty that the systems will be submitted to the PDs for higher voltage levels.

Secondly, it has been shown that the pressure has an influence on the nature of the discharge and consequently on the ability of the sensors to detect them. A study focusing on PDs phenomenology would be important to better understand these variations. Moreover, it would allow to better understand the influence of the pressure on the aging induced by the PDs.



## **Appendix**





## V Digital processing tool

As discussed in Chapter III, a method of partial discharge noise suppression was developed along with an algorithm to automate the selection of the method's input parameters. Developed with MATLAB®, this method is functional in laboratory testing. However, the use of MATLAB® is less widespread in the industrial field than in the laboratory and it therefore seemed interesting to develop a digital tool in an executable format so that any industrial partner could use it and share their experience of its operation with us. The developed tool is described below.

### V.1 User interface

The interface associated with the digital tool is shown below. A brief description of the different interface elements are presented afterwards as an example of applying the method.

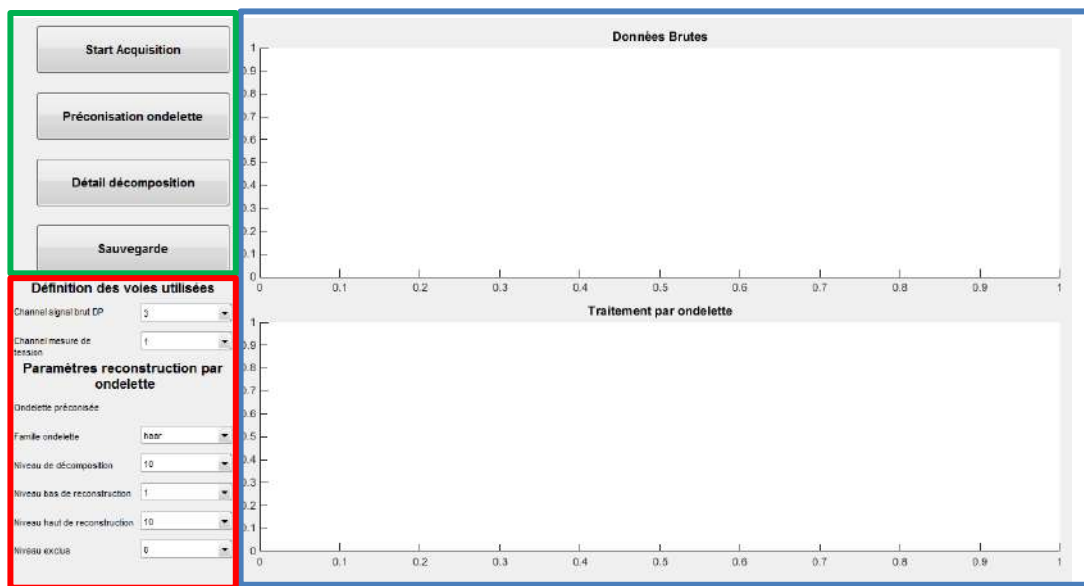


Figure V.1: Three parts of the interface: graphical area (blue), configuration area (red), and control area (green)

#### V.1.1 Graphical area

The first graph, named “Données brutes” (“raw data”), displays the voltage and the sensor signal that corresponds to the signal that will be processed by the wavelet method. These two curves are the same as those displayed by the acquisition system.

The second graph, named “Traitement par ondelette” (“wavelet processing”) is used to display the sensor signal denoised by the treatment method. This will display the signal processed by wavelet, and optionally the presence of discharges.

### V.1.2 Control area

This section consists of 4 buttons:

- **“Start acquisition”**: This button launches acquisition and digital processing or stops it if it is running. Once acquisition is initiated, the name of the button changes to **“Stop acquisition”**.
- **“Préconisation ondelette” (“Wavelet recommendation”)**: This button automatically determines the most appropriate wavelet for extracting PD signals. This button is used before starting acquisition. As soon as the button is pressed and calculation is performed, a frame with the name of the recommended wavelet appears in the configuration area to the right of “Ondelette préconisée” (“recommended wavelet”).
- **“Détail décomposition” (“Detailed decomposition”)**: This button opens an interface that shows different levels of decomposition after wavelet treatment. This makes it possible to refine method configuration.
- **“Sauvegarde” (“Save”)**: This button opens a backup window to save the various displayed curves in “.xlsx” or “.csv” format.

### V.1.3 Configuration area

In this area, there are two configuration zones. First, **“Définition des voies utilisées”** (“Setting channels used”), and **“Paramètres reconstruction par ondelettes”** (“Wavelet reconstruction settings”). The description of the various parameters of these zones is given below:

#### Setting channels used:

- **“Channel Signal brut PD” (“Raw PD Signal Channel”)**: This drop-down menu allows the user to choose the channel number used for acquiring the PD sensor signal to be processed digitally.
- **“Channel Mesure de voltage” (“Voltage Measurement Channel”)**: This drop-down menu allows the user to choose the channel used for acquiring the voltage signal.

#### Wavelet reconstruction parameters:

- **“Ondelette préconisée” (“Recommended wavelet”)**: When the wavelet recommendation button has been switched, a framework specifying the recommended wavelet is displayed.
- **“Famille ondelette” (“Wavelet family”)**: This drop-down menu allows the user to select the wavelet that will be used for digital processing. It is recommended to select the recommended wavelet, though the user has the option to choose others.
- **“Niveau de décomposition” (“Decomposition level”)**: This drop-down menu allows the user to select the decomposition depth of the digital processing method. It is recommended to leaving this level at 10 for the first acquisition. After observing the detailed decomposition, it the level may be lowered.
- **“Niveau bas de reconstruction” (“Low reconstruction level”)**: This drop-down menu lets the user choose the level of decomposition from which the method will start reconstruction of the final signal.
- **“Niveau haut de reconstruction” (“High reconstruction level”)**: This drop-down menu lets the user choose the level of decomposition from which the method will finish the reconstruction of the final signal.
- **“Niveau Exclus” (“Level excluded”)**: This drop-down menu lets the user delete a decomposition level between the high and low reconstruction levels. This function is useful when noise is present on one of the decomposition levels. In order to not exclude any signal, the default value for this parameter is 0. As long as the setting is at this value, the processing tool does not take it into account for reconstruction.

## V.2 Acquisition results

An example of denoising partial discharges for testing on a twisted pair at low pressure is shown below:

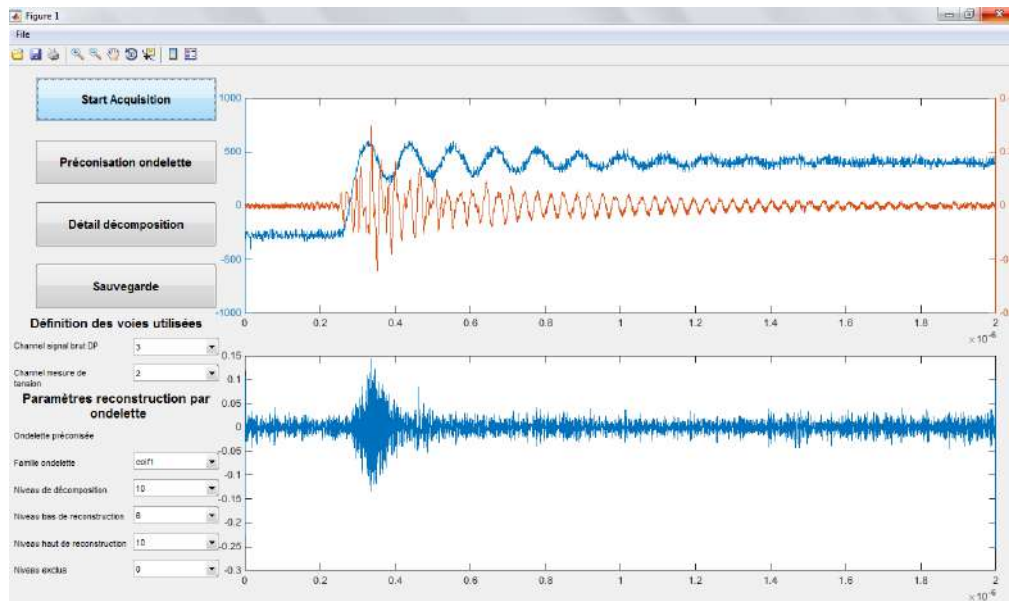


**Figure V.2: Example of denoising using the digital numerical tool**

This tool performs “online” processing virtually. In reality, processing time is limited by the speed of data transfer between the acquisition system and the computer on which the tool is running. As an example, the refresh time on a desktop laptop computer is on the order of one second.





## References





- 
- [1] X. Roboam, “New trends and challenges of electrical networks embedded in more electrical aircraft” in *2011 IEEE International Symposium on Industrial Electronics*, 2011, pp. 26–31.
  - [2] J. S. Cloyd, “A status of the United States Air Force’s More Electric Aircraft initiative,” in *IECEC-97 Proceedings of the Thirty-Second Intersociety Energy Conversion Engineering Conference (Cat. No.97CH6203)*, 1997, vol. 1, pp. 681–686 vol.1.
  - [3] I. Cotton, A. Nelms, and M. Husband, “Higher voltage aircraft power systems,” *IEEE Aerosp. Electron. Syst. Mag.*, vol. 23, no. 2, pp. 25–32, Feb. 2008.
  - [4] CENELEC, “NF EN 60270 Technique des essais à haute tension - Mesure des décharges partielles.” UTE, 2001.
  - [5] P. H. F. Morshuis, “Degradation of solid dielectrics due to internal partial discharge: some thoughts on progress made and where to go now,” *IEEE Trans. Dielectr. Electr. Insul.*, vol. 12, no. 5, pp. 905–913, Oct. 2005.
  - [6] R. Bartnikas and E. McMahon, Eds., *Engineering Dielectrics Volume I Corona Measurement and Interpretation*. 100 Barr Harbor Drive, PO Box C700, West Conshohocken, PA 19428-2959: ASTM International, 1979.
  - [7] J. S. Townsend, *Electricity in gases*. Oxford : Clarendon Press, 1915.
  - [8] “F. Paschen, Sur la différence de potentiel nécessaire à la formation d’arc électrique dans de l’air, de l’hydrogène et du gaz carbonique sous différentes pressions (trad. Über die zum Funkenübergang in Luft, Wasserstoff and Kohlensäure bei verschiedenen Drücken erforderliche Potentialdifferenz), Wied. Annales de physique, Vol.37, pages 69-96, 1889.” *Wied Ann. Phys.*, vol. 37, pp. 69–96, 1889.
  - [9] H. . Wittenberg, “Gas tube design,” in *Electron Tube Design*, RCA Electron Tube Division, 1962, pp. 792–817.
  - [10] W. G. Dunbar and J. W. Seabrook, “High Voltage Design Guide for Airborne Equipment,” Jun. 1976.
  - [11] W. G. Dunbar, “High Voltage Design Guide. Volume V. Spacecraft,” 1983.
  - [12] “Rotating electrical machines - Part 18-41: Partial discharge free electrical insulation systems (Type I) used in rotating electrical machines fed from voltage converters - Qualification and quality control tests,” IEC 60034-18-41:2014, 2014.
  - [13] M. Chapman, N. Frost, and R. Bruetsch, “Insulation Systems for Rotating Low-Voltage Machines,” in *Conference Record of the 2008 IEEE International Symposium on Electrical Insulation, 2008. ISEI 2008*, 2008, pp. 257–260.
  - [14] N. Frost, M. Chapman, and R. Bruetsch, “Considerations for Rotating Low-Voltage

- Machine Insulation Designs,” in *Conference Record of the 2008 IEEE International Symposium on Electrical Insulation, 2008. ISEI 2008*, 2008, pp. 571–574.
- [15] G. C. Stone, I. M. Culbert, and B. A. Lloyd, “Stator insulation problems associated with low voltage and medium voltage PWM drives,” in *IEEE Cement Industry Technical Conference Record, 2007*, 2007, pp. 187–192.
- [16] E. Persson, “Transient effects in application of PWM inverters to induction motors,” *IEEE Trans. Ind. Appl.*, vol. 28, no. 5, pp. 1095–1101, Sep. 1992.
- [17] H. Foch, F. Forest, and T. Meynard, “Onduleurs de tension Mise en œuvre,” *Tech. Ing. Convert. Électr. Appl.*, vol. base documentaire : TIB253DUO., no. ref. article : d3177, 2000.
- [18] J. Holtz, “Pulsewidth modulation for electronic power conversion,” *Proc. IEEE*, vol. 82, no. 8, pp. 1194–1214, Aug. 1994.
- [19] H. Foch, F. Forest, and T. Meynard, “Onduleurs de tension Structures. Principes. Applications,” *Tech. Ing. Convert. Électr. Appl.*, vol. base documentaire : TIB253DUO., no. ref. article : d3176, 1998.
- [20] A. Mbaye, F. Grigorescu, T. Lebey, and B. Ai, “Existence of partial discharges in low-voltage induction machines supplied by PWM drives,” *IEEE Trans. Dielectr. Electr. Insul.*, vol. 3, no. 4, pp. 554–560, Aug. 1996.
- [21] M. Kaufhold, “Failure mechanism of the interturn insulation of low voltage electric machines fed by pulse controlled inverters,” in *Conference on Electrical Insulation and Dielectric Phenomena, 1995. Annual Report*, 1995, pp. 254–257.
- [22] M. Fenger, G. C. Stone, and B. A. Lloyd, “The impact of humidity on PD inception voltage as a function of rise-time in random wound motors of different designs,” in *2002 Annual Report Conference on Electrical Insulation and Dielectric Phenomena*, 2002, pp. 501–505.
- [23] P. Bidan, T. Lebey, G. Montseny, and J. Saint-Michel, “Transient voltage distribution in inverter fed motor windings: Experimental study and modeling,” *Power Electron. IEEE Trans. On*, vol. 16, no. 1, pp. 92–100, 2001.
- [24] P. Bidan, T. Lebey, and C. Neacsu, “Development of a new off-line test procedure for low voltage rotating machines fed by adjustable speed drives (ASD),” *IEEE Trans. Dielectr. Electr. Insul.*, vol. 10, no. 1, pp. 168–175, Feb. 2003.
- [25] M. J. Melfi, “Low-Voltage PWM inverter-fed motor insulation issues,” *IEEE Trans. Ind. Appl.*, vol. 42, no. 1, pp. 128–133, Jan. 2006.
- [26] M. Tozzi, A. Cavallini, and G. C. Montanari, “Monitoring off-line and on-line PD under

- impulsive voltage on induction motors - part 1: standard procedure,” *IEEE Electr. Insul. Mag.*, vol. 26, no. 4, pp. 16–26, Jul. 2010.
- [27] A. von Jouanne, P. Enjeti, and W. Gray, “The effect of long motor leads on PWM inverter fed AC motor drive systems,” in *Applied Power Electronics Conference and Exposition, 1995. APEC '95. Conference Proceedings 1995., Tenth Annual, 1995*, pp. 592–597 vol.2.
- [28] D. Fabiani, “Accelerated Degradation of AC-Motor winding insulation due to voltage waveforms generated by adjustable speed drives,” University of Bologna, 2003.
- [29] M. Melfi, J. Sung, S. Bell, and G. Skibinski, “Effect of surge voltage risetime on the insulation of low voltage machines fed by PWM converters,” in *Conference Record of the 1997 IEEE Industry Applications Conference, 1997. Thirty-Second IAS Annual Meeting, IAS '97, 1997*, vol. 1, pp. 239–246 vol.1.
- [30] “IEEE Guide to the Measurement of Partial Discharges in Rotating Machinery,” *IEEE Std 1434-2000*, pp. 1–64, Aug. 2000.
- [31] F. H. Kreuger, *Partial discharge detection in high-voltage equipment*. Butterworths, 1989.
- [32] F. Guastavino, A. Dardano, and E. Torello, “Measuring partial discharges under pulsed voltage conditions,” *IEEE Trans. Dielectr. Electr. Insul.*, vol. 15, no. 6, pp. 1640–1648, Dec. 2008.
- [33] R. Giussani, I. Cotton, and R. Sloan, “Detection of corona with RF methods and spectra analysis,” in *Conference Record of the 2012 IEEE International Symposium on Electrical Insulation (ISEI), 2012*, pp. 132–136.
- [34] T. Billard, T. Lebey, and F. Fresnet, “Partial discharge in electric motor fed by a PWM inverter: off-line and on-line detection,” *IEEE Trans. Dielectr. Electr. Insul.*, vol. 21, no. 3, pp. 1235–1242, Jun. 2014.
- [35] T. Billard, “Off-line and on-line partial discharges detection in low voltage motors of electric vehicle fed by a PWM inverter using non-intrusive sensor,” phd, Université de Toulouse, Université Toulouse III - Paul Sabatier, 2014.
- [36] B. Cella, T. Lebey, and C. Abadie, “Partial discharges measurements at the constituents’ level of aerospace power electronics converters,” in *2015 IEEE Electrical Insulation Conference (EIC), 2015*, pp. 274–277.
- [37] M. Tozzi, G. C. Montanari, D. Fabiani, A. Cavallini, and G. Gao, “Off-line and on-line pd measurements on induction motors fed by power electronic impulses,” in *2009 IEEE Electrical Insulation Conference, 2009*, pp. 420–424.

- [38] R. Bartnikas, "Some observations on the character of corona discharges in short gap spaces," *Electr. Insul. IEEE Trans. On*, no. 2, pp. 63–75, 1971.
- [39] R. Rui and I. Cotton, "Impact of low pressure aerospace environment on machine winding insulation," in *Conference Record of the 2010 IEEE International Symposium on Electrical Insulation (ISEI)*, 2010, pp. 1–5.
- [40] P. Wang, P. L. Lewin, and S. J. Sutton, "Calibration of capacitive couplers for online PD detection in HV cables," *IEEE Electr. Insul. Mag.*, vol. 21, no. 3, pp. 28–39, May 2005.
- [41] R. Morin, R. Bartnikas, and G. Lessard, "In-service location of partial discharge sites in polymeric distribution cables using capacitive and inductive probes," in *1999 IEEE Transmission and Distribution Conference*, 1999, vol. 1, pp. 120–127 vol.1.
- [42] Y. Tian, P. L. Lewin, A. E. Davies, S. J. Sutton, and S. G. Swingler, "Partial discharge detection in cables using VHF capacitive couplers," *IEEE Trans. Dielectr. Electr. Insul.*, vol. 10, no. 2, pp. 343–353, Apr. 2003.
- [43] G. Wei, Y. Deng, and J. Tang, "The Design of a Sensor for Monitoring Partial Discharge within a Joint of Power Cable," in *Power and Energy Engineering Conference (APPEEC), 2012 Asia-Pacific*, 2012, pp. 1–5.
- [44] BSI, "IEC 60851:2008 Winding wires - Test methods." 2008.
- [45] R. Bartnikas, "Partial discharges. Their mechanism, detection and measurement," *IEEE Trans. Dielectr. Electr. Insul.*, vol. 9, no. 5, pp. 763–808, Oct. 2002.
- [46] G. Robles, M. Sánchez-Fernández, R. A. Sánchez, M. V. Rojas-Moreno, E. Rajo-Iglesias, and J. M. Martínez-Tarifa, "Antenna Parametrization for the Detection of Partial Discharges," *IEEE Trans. Instrum. Meas.*, vol. 62, no. 5, pp. 932–941, May 2013.
- [47] B. Vigneshwaran, R. V. Maheswari, and P. Subburaj, "An improved threshold estimation technique for partial discharge signal denoising using Wavelet Transform," in *2013 International Conference on Circuits, Power and Computing Technologies (ICCPCT)*, 2013, pp. 300–305.
- [48] L. Satish and B. Nazneen, "Wavelet-based denoising of partial discharge signals buried in excessive noise and interference," *IEEE Trans. Dielectr. Electr. Insul.*, vol. 10, no. 2, pp. 354–367, Apr. 2003.
- [49] G. Sharmila, R. V. Maheswari, and P. Subburaj, "Partial discharge signal denoising using wavelet techniques-on site measurements," in *2013 International Conference on Circuits, Power and Computing Technologies (ICCPCT)*, 2013, pp. 673–678.
- [50] S. Sriram, S. Nitin, K. M. M. Prabhu, and M. J. Bastiaans, "Signal denoising techniques

- for partial discharge measurements,” *IEEE Trans. Dielectr. Electr. Insul.*, vol. 12, no. 6, pp. 1182–1191, Dec. 2005.
- [51] A. Contin, A. Cavallini, G. C. Montanari, G. Pasini, and F. Puletti, “Digital detection and fuzzy classification of partial discharge signals,” *IEEE Trans. Dielectr. Electr. Insul.*, vol. 9, no. 3, pp. 335–348, Jun. 2002.
- [52] J. M. Martínez-Tarifa, M. Rojas, G. Robles, B. MacPherson, P. Moore, and I. Portugués, “Partial discharges and noise separation in high frequency signals using inductive sensors,” in *Instrumentation and Measurement Technology Conference (I2MTC), 2012 IEEE International*, 2012, pp. 1607–1611.
- [53] P. Wang, A. Cavallini, and G. C. Montanari, “The influence of square voltage rise time on partial discharge spectra,” in *2012 Annual Report Conference on Electrical Insulation and Dielectric Phenomena (CEIDP)*, 2012, pp. 129–132.
- [54] C. S. Burrus, R. A. Gopinath, and H. Guo, *Introduction to Wavelets and Wavelet Transforms: A Primer*, 1st ed. Upper Saddle River, N.J: Prentice Hall, 1997.
- [55] H. Zhang, T. R. Blackburn, B. T. Phung, and D. Sen, “A novel wavelet transform technique for on-line partial discharge measurements. 1. WT de-noising algorithm,” *IEEE Trans. Dielectr. Electr. Insul.*, vol. 14, no. 1, pp. 3–14, Feb. 2007.
- [56] J. Seo, H. Ma, and T. Saha, “Probabilistic wavelet transform for partial discharge measurement of transformer,” *IEEE Trans. Dielectr. Electr. Insul.*, vol. 22, no. 2, pp. 1105–1117, Apr. 2015.
- [57] O. Altay and O. Kalenderli, “Wavelet base selection for de-noising and extraction of partial discharge pulses in noisy environment,” *IET Sci. Meas. Technol.*, vol. 9, no. 3, pp. 276–284, 2015.
- [58] X. Ma, C. Zhou, and I. J. Kemp, “Interpretation of wavelet analysis and its application in partial discharge detection,” *IEEE Trans. Dielectr. Electr. Insul.*, vol. 9, no. 3, pp. 446–457, Jun. 2002.
- [59] C. Valens, *A Really Friendly Guide to Wavelets*. 1999.
- [60] X. Zhou, C. Zhou, and I. J. Kemp, “An improved methodology for application of wavelet transform to partial discharge measurement denoising,” *IEEE Trans. Dielectr. Electr. Insul.*, vol. 12, no. 3, pp. 586–594, Jun. 2005.
- [61] D. Evagorou, A. Kyprianou, P. L. Lewin, A. Stavrou, V. Efthymiou, and G. E. Georghiou, “Evaluation of Partial Discharge Denoising using the Wavelet Packets Transform as a Preprocessing Step for Classification,” in *2008 Annual Report Conference on Electrical Insulation and Dielectric Phenomena*, 2008, pp. 387–390.

- [62] E. C. T. Macedo *et al.*, “Wavelet transform processing applied to partial discharge evaluation,” *J. Phys. Conf. Ser.*, vol. 364, no. 1, p. 12054, 2012.
- [63] *MATLAB and Wavelet Toolbox*. Natick, Massachusetts, United States: The Mathworks, Inc.
- [64] B. Cella, “On-line partial discharges detection in conversion systems used in aeronautics,” phd, Université de Toulouse, Université Toulouse III - Paul Sabatier, 2015.
- [65] G. C. Stone, H. G. Sedding, and C. Chan, “Experience with on-line partial discharge measurement in high voltage inverter fed motors,” in *2016 Petroleum and Chemical Industry Technical Conference (PCIC)*, 2016, pp. 1–7.
- [66] D. Fabiani, G. C. Montanari, A. Cavallini, and G. Mazzanti, “Relation between space charge accumulation and partial discharge activity in enameled wires under PWM-like voltage waveforms,” *Dielectr. Electr. Insul. IEEE Trans. On*, vol. 11, no. 3, pp. 393–405, 2004.
- [67] D. Fabiani, G. C. Montanari, A. Cavallini, and G. Mazzanti, “Relation between space charge accumulation and partial discharge activity in enameled wires under PWM-like voltage waveforms,” *IEEE Trans. Dielectr. Electr. Insul.*, vol. 11, no. 3, pp. 393–405, Jun. 2004.